U.S. DEPARTMENT OF THE INTERIOR

U.S. GEOLOGICAL SURVEY

IMPLICATIONS OF FLUID-INCLUSION RELATIONS IN THE ELDER CREEK PORPHYRY COPPER SYSTEM, BATTLE MOUNTAIN MINING DISTRICT, NEVADA

by

Natalya Gostyayeva, Ted G. Theodore, and Jacob B. Lowenstern

Menlo Park, California 94025

Open-File Report 96–268

1996

IMPLICATIONS OF FLUID-INCLUSION RELATIONS IN THE ELDER CREEK PORPHYRY COPPER SYSTEM, BATTLE MOUNTAIN MINING DISTRICT, NEVADA

by

Natalya Gostyayeva, Ted G. Theodore, Jacob B. Lowenstern
U.S. Geological Survey
Menlo Park, 94025

ABSTRACT

The porphyritic monzogranite of Elder Creek was emplaced during the late Eocene or early Oligocene into upper plate rocks of the Roberts Mountains allochthon near the northeast edge of the Battle Mountain Mining District. Synchronously with emplacement of the porphyritic monzogranite at approximately 38 Ma, hydrothermal alteration affected rocks belonging to the porphyry copper system in an area approximately 5-km wide that has a widespread aureole of biotite hornfels which contains hydrothermal pyrite±pyrrhotite. No commercial concentrations of base and precious metals are currently (1996) known at Elder Creek, although polymetallic veins surrounding the system have small amounts of past production. The compact 2- to 3-km-wide core of the system contains wallrocks and small bodies of porphyritic monzogranite of Elder Creek that are veined intensely by generally sulfide-mineral poor, quartz stockwork veins associated with K-silicate alteration. Large and abundant fluid inclusions are present throughout the quartz stockworks, and they are unusually well-suited to fluid-inclusion studies because of their optical clarity. The quartz-stockwork core of the system was associated with boiling, chemically complex, highly saline fluids—some estimated to be as saline as 50 weight percent NaCl equivalent and containing significant amounts of potassium, calcium, and iron, as well as carbon dioxide and methane and other minor metals—that, in parts of the core, circulated at temperatures as high as 500 °C during vein emplacement. The fluids have been categorized, roughly in order of their circulation in the system, as (1) complex NaCl–KCl–$CaCl_2$–($FeCl_3$)–(CO_2)–H_2O saline to hypersaline brines enriched with various base metals (including copper, lead, and zinc), as well as barium and other minor anions; (2) $CaCl_2$–(NaCl)–(KCl)–H_2O moderate salinity brines; (3) NaCl–KCl–$CaCl_2$–H_2O moderate salinity brines; and (4) NaCl–(KCl)–H_2O–CO_2 relatively low salinity fluids. The saline and hypersaline fluids represented by fluid inclusions probably are fluids that exsolved directly from an associated magma into a two phase environment near the top of the system where phase separation was occurring at pressures of approximately 300–350 bars, equivalent to lithostatic paleodepths of about 1–1.3 km.

Some of the hottest and most saline fluids found in the system were present in the general area of the Morning Star Mine—a small polymetallic vein occurrence in the northeast part of the quartz stockworks, where recorded production has uncommonly low silver/gold ratios. In addition, from west to east in the quartz stockworks, there appears to be a general increase in salinities and homogenization temperatures toward the area of the Morning Star Mine implying that an apophysis of the igneous phase of the porphyry system, which is genetically responsible for the stockworks, may be close to the surface near the mine. East of, and near the margin of the quartz stockworks, narrow quartz-arsenopyrite veins at approximately 1,000-ft depths probably are related to 35-Ma granodiorite porphyry emplaced along an extensive north-south trending zone of faults and fractures that cuts this part of the porphyry system. However, geothermometry, on the basis of microprobe analyses of arsenopyrite, suggests unreasonably high temperatures compared to fluid-inclusion data from the same samples, confirming that analyses of arsenopyrite in a low pressure hydrothermal environment are inappropriate for geothermometric determinations. Although fluids associated with the Elder Creek system are quite similar to those present in many other large productive porphyry copper-molybdenum deposits, there are no known economic copper deposits at Elder Creek. Further, any remaining exploration target for gold in quartz stockworks near the Morning Star Mine must be mesothermal, and must be related to fluids having a significant magmatic component.

INTRODUCTION

The Tertiary Elder Creek porphyry copper system is located in the northeast part of the Battle Mountain Mining District (fig. 1). Historically, the Battle Mountain Mining District has been a site of significant base- and precious-metal production since the late 1860s (Roberts and Arnold, 1965; Doebrich and others, 1995; Doebrich and Theodore, 1996). Copper, gold, silver, and lead-zinc ores have been produced from the porphyry systems at Copper Canyon (Roberts and Arnold, 1965; Theodore and Blake, 1975; 1978) and at Copper Basin (Theodore and others, 1992), as well as copper and gold at the Buffalo Valley gold deposit (Seedorff and others, 1991)—between 1924 and 1941 the latter deposit produced 4,367 kg Cu (Roberts and Arnold, 1965), and exploration for gold was continuing during early 1996 (Fairmile

Acquisitions Inc., press release, January, 1996). The mining district was noted primarily for its base-metal production up until 1978, at which time large-scale mining in the Copper Canyon area was converted largely to production of precious metals. The Copper Canyon area of the mining district, which to date (1996) is the most productive part of the mining district and which has an age of mineralization of approximately 37–39 Ma (Theodore and others, 1973), probably will achieve a cumulative geologic resource of approximately 5.5 million oz Au by the time all near-surface ore bodies have been exploited there in the early 2000s (P.R. Wotruba, oral commun., 1996). Of this amount, eventual gold recovery will be about 4.9 million oz Au, with approximately 1.9 million oz Au credited to production from the Fortitude gold skarn deposit (Wotruba and others, 1986; P.R. Wotruba, oral commun., 1994; Myers, 1994).

The 38–Ma porphyry copper system at Elder Creek is situated along the range front, where it lies astride part of the linear, northwest-trending flank of the range in the northeast part of the mining district (fig. 1). As such, the system is present at the intersection of two broad mineralized trends, a northwesterly one along the range front, and defined, in part, by a large number of Tertiary plutons, and a north-south trend defined mostly by a concentration of a large number of normal faults and similarly trending dikes (Doebrich and Theodore, 1996). The system is emplaced into mostly feldspathic arenite of the Upper Cambrian Harmony Formation, one of the regionally extensive and distinctive units that compose the upper plate of the Roberts Mountains allochthon in the mining district (Roberts, 1964; T.G. Theodore, unpub. data, 1996). The Elder Creek porphyry system is one of seven porphyry copper and stockwork molybdenum systems in the mining district, of which three stockwork molybdenum systems, including the Buckingham deposit, are Late Cretaceous in age (Theodore and others, 1992), and the remaining porphyry copper systems are late Eocene or early Oligocene (Doebrich and others, 1995; Doebrich and Theodore, 1996). The secondarily-enriched copper ore bodies at Copper Basin (fig. 1), on the east end of the Buckingham stockwork molybdenum system, are part of a copper-enriched shell that surrounds the Buckingham stockwork molybdenum system (Blake, 1992; see also, Ivosevic and Theodore [1996] for discussion of the superposition of Tertiary mineralized rocks onto distal gold-silver zones of the Buckingham system). All seven porphyry systems are exposed in bedrock areas of the mining district, and, quite significantly, all seven crop out south of the Miocene Oyarbide fault (fig. 1), a major post-mineral oblique-slip fault that has had its northwest block downdropped approximately 800 m relative to its footwall (Roberts, 1964; T.G. Theodore, unpub. data, 1996). This fault also apparently includes approximately 1 km of right-lateral separation. The Oyarbide fault, in addition, has roughly the same strike as the trend of the Miocene Midas trough, approximately 30 km to the northeast of Elder Creek, which is inferred to have recorded its major displacements sometime during the last 17 m.y., possibly even in the last 9 m.y. (Wallace, 1991; see also, Doebrich and Theodore, 1996).

North of the Oyarbide fault, several gold deposits have been discovered in recent years. These deposits, including those (8–South,Top Zone, Red Rock, and East Hill/UNR) in the general area of the Old Marigold Mine (Graney and Wallace, 1988; Graney and McGibbon, 1991) and at Lone Tree (Bloomstein and others, 1991; 1993), probably represent the tops of deep-seated porphyry systems (Howe and Theodore, 1993; Doebrich and others, 1995; Doebrich and Theodore, 1996; T.G. Theodore, unpub. data, 1996). Sulfur isotopic ratios in hydrothermal barites in several of these deposits suggest involvement of a significant magmatic component in the ore-generating fluids. Lone Tree is approximately 10 km north-northwest of the 8–South deposit, and provides one of the anchors along the north-south, intensely metallized, Twin Creeks-Marigold trend (T.G. Theodore, unpub. data, 1996). Geologic resources at least 1 million oz Au and approximately 5 million oz Au, respectively, were present at the Marigold and Lone Tree clusters of deposits prior to start up of mining operations (Doebrich and others, 1995; Doebrich and Theodore, 1996; Santa Fe Pacific Gold Corp., press release, January 30, 1996). Recently, Santa Fe Pacific Gold Corp. announced the presence of economic concentrations of gold at its Trenton Canyon Project—including as much as 590,000 oz Au in 18 million tonnes ore (Santa Fe Pacific Gold Corp., press release, January 30, 1996). This project involves mining operations at three widely separate deposits, which are being prepared currently (1996) for eventual production in 1997. The major concentration of gold in the Trenton Canyon Project is present in a deposit south of the Oyarbide fault (fig. 1). In addition, primarily because of the apparent large component of magmatic fluid associated with mineralization at the Marigold deposits and the presence of extremely saline, high-temperature, and boiling fluids at the Lone Tree deposit, all these gold deposits should probably best be classified as distal-disseminated silver-gold deposits (Cox and Singer, 1990) rather than Carlin-type systems (Doebrich and others, 1995; Howe and others, 1995; T.G. Theodore, unpub. data, 1996). Some fluid inclusions in vein quartz from mineralized veins at the Lone Tree deposit contain as many as seven translucent daughter minerals. These veins

also contain coexisting large numbers of obviously high temperature vapor-rich and moderately saline fluid inclusions—all suggestive of a porphyry copper environment (D. A. John, oral commun., 1996).

The Elder Creek porphyry system is marked by an approximately 5-km-diameter zone of hydrothermal alteration that surrounds several small bodies of porphyritic monzogranite, which are probably apophyses derived from a much larger intrusive body at depth (fig. 2). The pattern of alteration in the system—a central K-silicate zone, partly mantled by a propylitic zone, as well as the absence of a strongly developed phyllic zone—suggests that the system, as currently exposed, is relatively deep, and that the top of the system has either been eroded or faulted off. The latter does not seem likely because of the absence of a fault, or set of faults, in the bedrock areas of the system to account for such a relation. The iron-sulfide halo that surrounds the system is not conspicuous. Compared to the other major Tertiary hydrothermal systems in the Battle Mountain Mining District, the paleodepth of the Elder Creek system is probably deeper than the Copper Canyon system, which is, in turn, deeper than the Buffalo Valley system. The Elder Creek system also is probably at about the same level of erosion as the nearby Upper Paiute Canyon system (Ivosevic and Theodore, 1996). The porphyry sytem at Elder Creek, furthermore, is cut by a young north-northeast striking fault, the Elder Creek fault (fig. 2), which may include some Quaternary or Holocene scissors-type displacement along its trace. This fault shows significant separations of the outer limit of quartz stockworks that crop out widely in the center of the porphyry system. If the quartz stockworks define an essentially inward dipping zone at the exposed top of the system—the map pattern of the quartz stockworks suggests this (Theodore, 1994)—then the pattern of these separations of quartz stockworks across the Elder Creek fault suggests that the west block of the fault (including the bulk of the exposed core of the porphyry system itself) has been downdropped. The geologic block including the Morning Star Mine may have been uplifted again by subsequent offsets along a northwest-striking fault (fig. 2). Both of these faults, the Elder Creek fault and the northwest-striking fault, apparently are quite young because they have displaced unconsolidated gravels.

The primary purposes of this report are to describe briefly some salient features of the currently non-economic Elder Creek porphyry copper system, and to summarize the results of comprehensive fluid-inclusion studies from exposures of quartz stockworks in the core of this largely undisturbed system. Furthermore, the optical clarity of these veins provide an unusual opportunity to gather an excellent suite of data from an admittedly "weakly" developed porphyry system—though "weakly" only in an economic sense— and to compare the implications of these data with those of highly productive porphyry systems elsewhere. In addition, a large number of microprobe analyses of arsenopyrite from a select quartz vein in drill core were obtained in order to evaluate the validity of arsenopyrite compositions from this magmatic-hydrothermal environment as geothermometers independent from measured fluid-inclusion data. The sections below entitled "History of exploration at Elder Creek," "Porphyritic monzogranite of Elder Creek," and "Granodiorite porphyry" are modified slightly from Theodore (1996).

HISTORY OF EXPLORATION AT ELDER CREEK

The Elder Creek area has a long history of exploration activity primarily because of the abundance of secondary copper minerals present near the core of the system, and the location of the system close to some of the major emigrant trails followed since the late 1840s to the goldfields of central California. Although it was not tested as a porphyry target until the middle 1960s, many prominent concentrations of mineralized veins and mineralized faults in the Elder Creek porphyry copper system had already attracted significant exploration activity at a time when some of the earliest exploration targets in the mining district were first being assessed in the late 1800s and early 1900s (Roberts and Arnold, 1965). In this system, many polymetallic veins and mineralized faults (such as those at the Morning Star, Big Pay, Gracie, and Ridge Mines) show minor amounts of gold in their production records. The total recorded base-metal production of several mines are: Morning Star Mine approximately 8,182 kg Cu; the Big Pay Mine 2,364 kg Cu and 2,727 kg Pb; the Gracie Mine approximately 53,636 kg Cu; and the Ridge Mine approximately 9,091 kg Cu and 222 kg Pb (Roberts and Arnold, 1965). After these early attempts to develop base- and precious-metal vein occurrences, the area received little exploration until 1965 when Duval Corporation became the first company to test the Elder Creek area as a porphyry copper target by drilling three core holes near the west border of sec. 6, T. 32 N., R. 44 E. These three core holes were placed on the eastern margins of the system, because of the land situation at the time (Joe Lamanna, written commun., 1994). In addition, the three holes formed part of a much broader regional copper exploration program that was being conducted about the same time that the extent of the copper deposits at Copper Canyon and Copper Basin was

being delineated by Duval Corporation (Sayers and others, 1968).

Rocky Mountain Energy, formerly a subsidiary company of Union Pacific, apparently was the next company to test the porphyry copper target in the Elder Creek area by drilling eight holes during 1968 (P.R. Wotruba, written commun., 1994). Six of the holes were located in W 1/2 sec. 1, T. 32 N., R. 43 E., another hole was drilled in the south-central part of sec. 36, T. 33 N., R. 43 E., and the last hole was drilled in NW 1/4 sec. 6, T. 32 N., R. 44 E. Subsequently in the middle 1970s, AMOCO conducted some geophysical exploration in the gravel-covered pediment portions of the Elder Creek area (S.W. Ivosevic, written commun., 1995).

Battle Mountain Gold Co. then drilled another 40 holes in the Elder Creek area after they staked additional claims there in 1985 (Joe Lamanna, written commun., 1994). However, all drilling by Battle Mountain Gold Co. was targeted toward discovery of economic gold mineralization peripheral to the porphyritic monzogranite of Elder Creek. The 40 drill holes were spread throughout secs. 1, 2, 11, and 12 of T. 32 N., R. 43 E.; and sec. 36 of T. 33 N., R. 43 E. Of the 40 holes, seven were drilled in sec. 36, five in sec. 2, six in sec. 11, 13 in sec. 1, and nine in sec. 12.

Late in 1994 and early in 1995, Western Mining Corporation (U.S.A.) drilled an additional 19 holes in the northeastern and eastern parts of the Elder Creek porphyry copper system (Tom Gray, written commun., 1995). The deepest hole is approximately 500 m. Most holes were collared in unconsolidated gravels on the pediment areas of the system, and they were targeted to explore the precious-metal potential of the donut-shaped positive aeromagnetic anomalies that mantle the quartz stockwork-enriched core of the system. Approximately 30 intercepts of roughly 3–m thicknesses were penetrated that have in excess of 100 ppb Au in 11 of the holes. Most elevated concentrations of gold appear to be associated with arsenopyrite that is present at depth in the eastern part of the system. Small grains of argentian tetrahedrite are present in some polished thin sections of these arsenopyrite-rich rocks. However, significant concentrations of chalcopyrite also were encountered sporadically in various holes, in places amounting to approximately 10 to 20 volume percent chalcopyrite across short intercepts of drill core. The most impressive intercept visually consists of hornfels of the Harmony Formation that has been bleached by widespread, fine-grained white mica and impregnated with abundant chalcopyrite at a depth of approximately 220 m in one of the drill holes at locality 10 (fig. 2). At this depth, chalcopyrite is associated with pyrite, sphalerite (trace), sulfosalt minerals, vein quartz, and carbonate minerals, as well as minor amounts of chlorite and traces of sphene—all suggestive of a propylitic assemblage. In addition, along this particular approximately 0.3–m-long chalcopyrite-rich intercept, there were only 26 ppb Au in an approximately 2–m-long drill core that brackets the intercept. There are, as well, 4 ppm Pb, 12 ppm Zn, and 23 ppm As in the 2–m-long drill core.

All of these efforts at Elder Creek during the last 30 years have yet to result in discovery of a commercial concentration of copper or gold in the system up to early 1996.

GEOLOGY OF THE ELDER CREEK AREA

Harmony Formation

Rocks of the Upper Cambrian Harmony Formation (Roberts, 1964) weather to smooth-rounded slopes, and they commonly are poorly exposed in many places around the Elder Creek porphyry copper system, especially on sides of hills. The formation consists of mostly olive gray-green feldspathic arenite where unmetamorphosed and unaltered. Minor amounts of calcareous shaly hornfels are present locally, and some of these sequences, where well within the outer alteration aureole of the porphyry copper system, show metasomatic replacement by diopside- and garnet-bearing assemblages. However, large tracts of this unit have been converted to variably sulfidized biotite hornfels around the Elder Creek porphyry copper system. Where metamorphosed to biotite hornfels, rocks of the formation are various shades of drab gray brown, and, in places, they are subsequently bleached yellowish white largely as a function of the amount of iron sulfide minerals introduced during development of the biotite hornfels. In the southwest part of the system, biotite hornfels is succeeded outwards by two narrow chlorite-dominant zones of propylitic alteration (fig. 2). Locally close to the trace of the Dewitt thrust, rocks of the Harmony Formation are intensely sheared, and they have fabrics almost phyllonitic in appearance.

Lamprophyre

An approximately 2– to 3–m-wide, brownish-black fine-grained lamprophyre dike emplaced into thermally metamorphosed rocks of the Upper Cambrian Harmony Formation crops out in SW 1/4 sec. 36, T. 33 N., R. 43 E. (fig. 2). The lamprophyre is probably Tertiary in age and is cut by quartz-stockwork veins associated with the Oligocene or Eocene Elder Creek system, and, therefore, is older than the porphyry system. In thin section, lamprophyre is composed essentially

of euhedral blue-green (optic Z–axis) hornblende (average grain size 0.1 mm), clouded plagioclase (approximately An_{60}), and dark brown (optic Z–axis) primary biotite—listed in order of declining abundance. Hornblende probably makes up about 60 volume percent of the lamprophyre dike. Biotite includes 10– to 20–μm-wide anhedral blebs of ilmenite, confirmed by scanning electron microscope (SEM), which, in turn, are mantled by thin rims of sphene (fig. 3). Biotite also includes some small grains of zircon, approximately 0.2 μm wide. Extremely sparse K–feldspar in lamprophyre is associated with late-stage hornblende-quartz veins. The lamprophyre falls into the calc-alkaline branch of the lamprophyre clan of Rock (1991), and should best be termed spessartite according to his classification scheme. The lamprophyre dike is assumed to be Tertiary in age on the basis of lithologic similarity with some of the potassium-argon-dated Tertiary biotite and hornblende-biotite lamprophyres present in general area of Hancock Canyon in the Shoshone Range, approximately 25 km to the southeast (E.H. McKee, oral commun., 1994)

Porphyritic monzogranite of Elder Creek

Many small, generally K–silicate altered (Beane, 1982) intrusive bodies are clustered in the general area of Elder Creek are associated genetically with development of the Elder Creek porphyry copper system. The broad core of this system is probably centered approximately in NW 1/4 sec. 1, T. 32 N., R. 43 E. (fig. 2), where the largest exposures of porphyritic monzogranite of Elder Creek are present within the area of outcrop of quartz stockwork veins (fig. 4). The porphyritic monzogranite of Elder Creek includes hornblende-biotite and biotite-only phases, both showing highly variable concentrations of bipyramidal quartz phenocrysts (Theodore, 1994). Presence of numerous pendants of the Harmony Formation in the porphyritic monzogranite suggests that the current level of exposure probably is near its roof. Locally abundant secondary copper minerals are present in many outcrops, and locally intense quartz flooding and stockwork quartz veining result in almost complete obliteration of igneous texture of the rocks. Quartz stockworks in some places, such as near the portal to the Morning Star Mine, define well-developed "stars" (steeply dipping planar sets of variably striking quartz veins that roughly intersect along a common line) in outcrops, and are interpreted to have formed close to the center of the porphyry system. Many outcrops, also in the general area of the center of the system, show abundant concentrations of secondary copper minerals, including chrysocolla and copper oxides. However, the quartz stockworks are generally poor in sulfide minerals. Some outcrops of brecciated rock contain slickensides on secondary-copper-bearing fractures indicative of post-mineral movement along prominent N. 45° W.–striking fractures cutting porphyritic monzogranite. These slickensides are probably related to displacements along some of the post-mineral faults in the area such as the Elder Creek fault (fig. 2). In addition, some exposures of brecciated rock include well-rounded fragments of biotite hornfels derived from the Harmony Formation, and these brecciated rocks are cemented by porphyritic monzogranite and subsequently veined by copper-stained quartz veins. These relations suggest that some brecciation near the core of the porphyry system preceeded circulation of some hydrothermal fluids of the porphyry system.

Igneous biotite from the porphyritic monzogranite has been dated radiometrically, and a number of samples from these intrusive rocks also have been analyzed chemically. A sample of igneous biotite from porphyritic monzogranite collected from NE 1/4 sec. 2, T. 32 N., R. 43 E., yields a 38.3±0.7–Ma age (recalculated) by the potassium-argon method (Theodore and others, 1973). Two whole-rock chemical analyses of porphyritic monzogranite (Theodore and others, 1973) have compositions that vary relatively widely from a granodiorite to a monzogranite protolith that has undergone moderate potassium metasomatism. Both of these analyzed samples contain less MgO than the altered granodiorite of the Copper Canyon area—3.0 and 1.5 weight percent MgO versus 4.15 weight percent MgO (see also, Myers, 1994). In addition, 10 samples of porphyritic monzogranite collected generally from the core of the porphyry system at Elder Creek have Cu concentrations in the 200– to 1,000–ppm range, and Mo concentrations in the <5– to 50–ppm range. Silver, in the 1– to 5–ppm range, was detected in every sample analyzed, and gold was detected at concentrations of 20 ppb in four of 10 porphyritic monzogranite samples analyzed by Theodore and others (1973). These metal values emphasize the overall mineralized and hydrothermally altered character of much of the exposed porphyritic monzogranite in the core of the porphyry system.

Petrographic examination of approximately 20 samples of porphyritic monzogranite indicate an aplitic groundmass (average grain size in the range 0.06 to 0.12 mm) throughout the unit, where the groundmass includes mostly quartz and K–feldspar, and minor amounts of biotite and hornblende (fig. 5*A*, *B*). Plagioclase ($An_{35–45}$) is exclusively phenocrystic (generally 1 to 3 mm wide), and K–feldspar is almost entirely confined to the groundmass. These relations suggest that the bulk of the quenching—as well as the accompanying exsolution of a magmatic

aqueous fluid from melt near the current exposure levels of porphyritic monzogranite—occurred just before the chemical composition of the magma(s) associated with the system reached the cotectic between plagioclase solid solution and K–feldspar solid solution. Those samples examined containing phenocrystic K–feldspar show the K–feldspar to be approximately one-third to one-tenth the size of the plagioclase phenocrysts and also show a corresponding decrease in the amount of K–feldspar present in the groundmass. However, other samples having comparatively small volumes of groundmass (roughly 10 volume percent) do not have an added presence of phenocrystic K–feldspar. Crystallization of primary biotite appears to have preceded that of hornblende except in those rocks having relatively high concentrations of hornblende, and, in places, hornblende and biotite continued to crystallize synchronously with development of groundmass (fig. 5*B*). Porphyritic monzogranite containing abundant modal hornblende has multiple generations of amphibole, including some that crystallized prior to crystallization of igneous biotite phenocrysts and some secondary actinolite (?) along veins that cut the igneous fabric of the rocks. All of these textures in the porphyritic monzogranite at Elder Creek are remarkably similar to many of the other Tertiary stocks in the Battle Mountain Mining District, including the altered granodiorite of the Copper Canyon area (Roberts , 1964; Theodore and others, 1973; Theodore and Blake, 1975).

Typical indications of potassic alteration are reflected in prevalence of K–feldspar-stable alteration assemblages characterized by (1) secondary biotite replacing primary hornblende and primary biotite, (2) quartz-K–feldspar±biotite±amphibole±sphene in veins cross-cutting igneous fabric of porphyritic monzogranite, and (3) widespread presence of K–feldspar in alteration selvages along margins of quartz±K–feldspar±sulfide mineral veins. Minor accessory minerals include sphene (primary and secondary), apatite, and traces of allanite. Overall intensity of potassic alteration (mostly evident as replacement of hornblende by "shreddy"-textured secondary biotite) is less in narrow dikes of porphyritic monzogranite near the outer limit of quartz stockwork veins than the intensity of potassic alteration in the central core of the system. Late-stage chlorite, primarily as a marginal alteration of primary and secondary biotite is generally sparse, although some rocks have complete replacement of primary biotite by chlorite, and a few other samples of porphyritic monzogranite contain chlorite+K–feldspar+epidote+sphene veins. Overall, in the porphyritic monzogranite, the effects of intermediate argillic alteration plus minor weakly developed phyllic alteration (white mica+clay alteration of plagioclase and stable K–feldspar) appear to be confined to areas close to some of the major post-mineral faults that cut the porphyry system, such as the Elder Creek fault (fig. 2).

Granodiorite porphyry

Approximately 0.3 km south-southwest of the Ridge Mine, the outer limit of pyrite alteration within biotite hornfels surrounding the Elder Creek porphyry copper system seems to be a function partly of intensely phyllic-altered and quartz-pyrite-veined Oligocene granodiorite porphyry (fig. 2). Granodiorite porphyry may have intruded rocks previously altered by the Elder Creek porphyry system, because elsewhere in the Battle Mountain Mining District granodiorite porphyry appears to cut porphyry-type mineralization (Ivosevic and Theodore, 1996). Granodiorite porphyry is petrographically distinct throughout the mining district primarily because of its prominent bold outcrops characterized typically by aphanitic groundmass and large euhedral phenocrysts of K–feldspar. The intrusive rocks exposed at the Gracie Mine appear to be granodiorite porphyry (fig. 2). Moreover, the secondarily enriched copper ore bodies at this mine may owe introduction of their primary copper to granodiorite porphyry, or, alternatively, to the abundant phyllic alteration providing a favorable environment. Elsewhere in the mining district, such as in the general area of the Buckingham stockwork molybdenum system, granodiorite porphyry apparently has an approximate 35–Ma age, and these intrusive rocks are associated with minor lead-zinc mineralization (Theodore and others, 1992). However, altered granodiorite porphyry approximately 0.2 km south-southwest of the Ridge Mine (not shown on figure 2 in NW 1/4 sec. 12, T. 32 N., R. 43 E.) is along a short mineralized segment of a fault that has the same strike as the 1.5–km-long mineralized structure that controls mineralization at the Ridge Mine. Several polished thin sections examined petrographically from the occurrence southwest of the Ridge Mine also have traces of disseminated chalcopyrite in groundmass of phyllic-altered granodiorite porphyry. Several shallow workings at this occurrence most likely represent prospecting for precious metals. Abundant quartz-pyrite veins cut granodiorite porphyry at this locality, and the fluid inclusions in the vein quartz lack daughter minerals and contain a wide range of liquid-vapor proportions in two-phase fluid inclusions suggestive of boiling. These fluid-inclusion relations stand in stark contrast to the halite-bearing fluid-inclusions in quartz stockworks near the core of the Elder Creek porphyry copper system to be described below, and may be a reflection of the preponderance of dilute fluids in the distal parts of the Elder Creek porphyry system. Narrow dikes of granodiorite porphyry also crop out close to

locality 10 (fig. 2), from which quartz-arsenopyrite veins were obtained at approximately 1,000–ft depths and studied for this report.

FLUID-INCLUSION STUDIES

Preliminary determination of the types of fluid inclusions in the Elder Creek porphyry copper system by standard petrographic methods—including paragenetic determinations among types and ages of fluid inclusions versus host minerals—indicates that stockwork veins in the core of the system typically contain abundant 20– to 40–μm-wide, liquid- and vapor-rich, two-phase fluid inclusions, together with abundant fluid inclusions containing halite and many other daughter minerals. However, some stockwork veins only host predominantly two-phase, liquid plus vapor fluid inclusions together with lesser abundances of CO_2–bearing fluid inclusions, which suggests that there may be some heterogeneity in space and time of fluid compositions as they evolved in a late magmatic to hydrothermal environment. As with all other porphyry systems, most samples at Elder Creek show extremely complex parageneses in their fluid inclusions involving multiple generations and complex and varied chemistries. In any one small domain of a quartz vein or quartz phenocryst, there is textural evidence that the rocks have been subjected to repeated passage of fluids as the porphyry system evolved. At room temperature, some phase proportions in three-phase CO_2–bearing fluid inclusions suggest that they are largely composed of CO_2, although subsequent freezing tests, to be described below, indicate that many also contain CH_4. In addition, there appears to be a temporal heterogeneity in composition of fluids associated with fluid inclusions in phenocrystic quartz and some of the later quartz veins that cut the igneous rocks. Some phenocrystic quartz contains much more abundant halite-bearing fluid inclusions than two-phase fluid inclusions. Also in quartz phenocrysts, some vapor-rich fluid inclusions that contain opaque daughter minerals may be fluids that exsolved directly from a magma at near-subsolidus conditions and below the P–T trajectory of the applicable critical isochore for the low density, entrapped fluid (Bodnar, 1995). The population of fluid inclusions, taken as a whole at Elder Creek, is quite analogous with the types of fluid inclusions present in many major porphyry copper deposits (Nash, 1976; Roedder, 1984; Bodnar, 1995), as well as with some other magmatic-hydrothermal systems that did not result in development of a major porphyry copper deposit (John, 1989; Campbell, 1995). The halite-bearing fluid inclusions are somewhat smaller than the two-phase fluid inclusions in many of the samples; the chemically complex halite-bearing fluid inclusions average about 15 μm in diameter. Some trapped minerals and daughter minerals from quartz veins at Elder Creek are illustrated in Theodore (1996), and the relations among minerals in fluid inclusions found during that preliminary investigation will not be repeated here—halite is present in many fluid inclusions together with sylvite as well as chalcopyrite and iron sulfide minerals. Complementary mineral relations to those shown by Theodore (1996) are, however, shown below.

Methods of study

Fairly comprehensive standard heating and freezing studies (Hollister and Crawford, 1981; Roedder, 1984; De Vivo and Frezzotti, 1994) were performed on 17 samples from 16 localities distributed widely across the system (fig. 2; table 1); data obtained from these heating and freezing tests were reduced using the MacFlinCor software package (Brown and Hagemann, 1994). Measurements were made on a Fluid Inc.-adapted U.S. Geological Survey-type gas-flow heating and freezing stage (Werre and others, 1979; Belkin, 1994), calibrated at –56.6 °C, 0.0 °C, and 374.1 °C with synthetic fluid inclusions. Accuracy of the heating and freezing measurements is estimated at ±0.1 °C at temperatures less than 25 °C, and ±5 °C for temperatures in the 400–500 °C temperature range. Measurements in the 25–400 °C temperature range probably have an accuracy somewhere between ±0.1 and ±5 °C. Fluid-inclusion heating and freezing data initially were obtained on thick doubly-polished plates by recording temperatures of first melting and final melting of frozen fluid-inclusion waters, as well as the temperatures of all phase transformations—the latter particularly applies to the CO_2– and CH_4–bearing fluid inclusions studied. Subsequently, data from the doubly polished plates were obtained at temperatures elevated incrementally during single protracted heating tests to preclude stretching of the fluid inclusions as much as possible. A scanning electron microscope (SEM) also was used extensively throughout the investigation to identify trapped minerals and daughter minerals (Roedder, 1984) hosted by the fluid inclusions. In addition, four other methods were used to evaluate the fluid inclusions: (1) a cryogenic stage attached to the SEM was used to determine qualitatively those cations detectable in fluid-inclusion ice in a small number of samples; (2) select fluid inclusions were also analyzed with the synchrotron X–ray fluorescence (SXRF) microprobe installed on beamline X26A of the National Synchrotron Light Source (NSLS) at Brookhaven National Laboratory in Uptown, New York; (3) analytical Fourier transform infrared spectroscopic techniques were used to identify CO_2 in some samples; and (4) some samples were crushed, as well, under oil at room temperature as

an additional verification of the presence of condensed CO_2 gases in fluid inclusions. In the Fourier spectroscopic techniques, the fluid inclusions were individually apertured with a Spectra Tech Analytical IR microscope attached to a Nicolet Magna 550 Fourier Transform Infrared (FTIR) spectrometer located at the U.S. Geological Survey in Menlo Park, CA. Approximately 500 scans were collected by a liquid–N_2–cooled, MCT–A detector at 4 wavenumber resolution. Finally, median filling temperatures, as well as maximum filling temperatures of certain types of fluid inclusions, were used to construct thermal isopleths across the system by means of the gridding and filtering procedures outlined in Kotlyar and others (1995).

Classification of fluid inclusions

The types of fluid inclusions at Elder Creek are classified microscopically into a number of categories primarily on the basis of their liquid and vapor phase proportions at room temperatures, and on the basis of the types daughter minerals present (see also, Roedder, 1984; Cline and Vanko, 1995). As will be described below, fluid inclusions from Elder Creek can also be classified according to the chemical systems of the trapped fluids; however, because this requires data primarily from the various heating and freezing tests performed, discussion of the predominant chemistries associated with the various categories of fluid inclusions will be deferred until after the tests are described. Nonetheless, it must be emphasized that the general fluid-inclusion population at Elder Creek should best be considered to comprise a broad spectrum of compositions that do not have sharply defined limits among them.

Type I fluid inclusions (fig. 6) are fluid inclusions that at room temperatures consist of liquid and vapor—the liquid-phase constitutes more than approximately 50 volume percent of the fluid inclusion and it is made up of mostly H_2O, although some of these fluid inclusions were shown by freezing tests and by Fourier transform infrared microspectrometry (see also, Barres and others, 1987; Brown and Vry, 1990; Pironon and Barres, 1990; Wopenka and others, 1990) to include minor amounts of CO_2 (fig. 7*A*) and possibly some CH_4. Generally, most type I fluid inclusions at Elder Creek belong to the system NaCl–KCl–H_2O±(CO_2±CH_4). Samples from localities 9 and 12 and a few others contain fluid inclusions that show critical-point phase transitions consisting of the disappearance of a solid at temperatures of about –82 to –85 °C, which is indicative of the probable presence of CH_4 in the fluid inclusions. Further, some fluid inclusions also show melting of a solid phase at temperatures less than –56.6 °C—actually to as low as about –59 °C—indicative of the probable presence of CH_4 in the fluid inclusions. A small number of these type I fluid inclusions were determined to have CO_2 densities of about 0.3g/cm^3 and to contain 0.03 mole fraction CH_4. Nonetheless, some type I fluid inclusions also include opaque, probable daughter minerals—these opaque minerals may be either a sulfide mineral or an iron titanium oxide (fig. 7*A*). Although type I fluid inclusions are ubiquitous in quartz throughout the system, they are most abundant in quartz veins just interior to the outer limit of the quartz stockworks (for example, location 2, fig. 2), and in vein quartz associated with arsenopyrite veins in drill core just outside the outer limit of the quartz stockworks (location 10, fig. 2)—they probably make up more than 90 percent of the fluid-inclusion population at these two localities. Many others have reported that type I fluid inclusions in porphyry systems probably reflect entry of meteoric fluids into the systems during their latter stages (Roedder, 1984), or type I fluid inclusions could represent early fluids trapped prior to evolution of the system to a two phase environment.

Type II fluid inclusions (fig. 8) are fluid inclusions that at room temperature consist of liquid and vapor—the vapor-phase part makes up more than approximately 50 volume percent of the fluid inclusion and it is composed mostly of H_2O, although some of these fluid inclusions were shown by freezing tests and by Fourier transform infrared microspectrometry to include minor amounts of CO_2 (fig. 7*B*). Some probably contain CH_4, as well as some probable N_2, because of phase transitions in the –120 to –126 °C temperature range. Type II fluid inclusions are co-extensive and cogenetic with the type III fluid inclusions that homogenize by vapor disappearance. Some secondary type II fluid inclusions are made up almost entirely of vapor. Liquid CO_2 in many type II fluid inclusions becomes apparent only when the fluid inclusions are cooled below room temperature and the liquid CO_2 then appears as a discrete third phase present as a thin meniscus between vapor and mostly liquid H_2O. These CO_2–bearing fluid inclusions contain highly variable amounts of CO_2 and probably form a continuum with those fluid inclusions that contain notable CO_2 as a separate phase at room temperature. As used in this report, some fluid inclusions that include extremely small opaque, probable daughter minerals, as well as high proportions of vapor (fig. 7*B*), also are referred to as type II fluid inclusions, although their evolution may entail P–T paths somewhat different from other type II fluid inclusions that lack daughter minerals. Many type II fluid inclusions appear to be preferentially concentrated in quartz

veins that cut biotite hornfels of the Harmony Formation in what subsequently was determined to be those parts of the system through which some of the hottest fluids circulated (for example, location 3, fig. 2). At this locality, "robust" appearing type II fluid inclusions commonly are 25–50 μm wide, and they predominate locally in micro domains of vein quartz suggesting that vapor must have dominated some parts of the system as it evolved. These type II fluid inclusions have pseudosecondary relations with the host vein quartz. Close to location 3, type II fluid inclusions are also common in fluid-inclusion-"crowded" quartz phenocrysts of the porphyritic monzogranite that crops out at the Morning Star Mine (fig. 2), and they have a variety of ages relative to the quartz phenocrysts. Most relatively large and "robust" type II fluid inclusions appear to be pseodosecondary, some type II fluid inclusions appear to be cogenetic with similarly-sized halite-bearing fluid inclusions along annealed microcracks, and other type II fluid inclusions are definitely secondary and smaller overall than the "robust" appearing ones. The paragenesis is important in that it appears to verify a temporal tie between type II fluid inclusions and halite-bearing ones, thereby establishing fluid immiscibility or boiling as a mechanisn for their generation. Type II fluid inclusions may or may not contain opaque, probable daughter minerals, regardless of their paragenesis relative to the host quartz phenocryst.

Type III fluid inclusions contain one or more translucent daughter minerals (fig. 9*A–D*)—the most common daughter mineral is halite, probably followed by sylvite in order of abundance, as well as a large number of other minerals that are best illustrated by scanning electron micrographs rather than standard photomicrographs. In addition, the presence of CO_2 and CH_4 in the gas phase of some type III fluid inclusions is indicated by melting of clathrates in the +1.0 to +13 °C temperature range. It is important to note that many type III fluid inclusions that will be shown below to homogenize by halite dissolution after liquid-vapor homogenization contain small amounts of CO_2 and CH_4. However, sylvite is the only daughter mineral in many type III fluid inclusions. Some sylvite crystals on broken surfaces in quartz appear as if they have fallen out of a nearby train of secondary cavities, which may have been fluid-inclusion cavities or mineral cavities, suggesting that some trapped fluids may have belonged to the system KCl–H_2O (fig. 9*C*). In other samples, rounded blebs of NaCl, individually less than 1 μm wide, appear as if they may be dessication products relict from fluid-inclusion waters that dried on the surface after the sample was broken (fig. 9*D*). Furthermore, on the basis of visual estimates of the numbers of daughter minerals and their volumetric proportions in fluid inclusions, many type III fluid inclusions could also be termed hypersaline, because of the presence in them of relatively large NaCl daughter minerals as well as a number of other translucent minerals that crowd the fluid-inclusion cavity. Examination of opened type III fluid inclusions by the X–ray microanalyzer of the SEM confirms the presence of relatively complex mineral assemblages, probably including both trapped minerals and daughter minerals, many of which are calcium bearing (fig. 9*E–F*). A calcium chloride mineral is present in some fluid inclusions together with an iron chloride mineral and sylvite (fig. 9*F*). Ilmenite, potassium iron chloride—which is probably the mineral erythrosiderite ($K_2FeCl_5 \cdot H_2O$) described previously by Wilson and others (1980) in some porphyry copper deposits in Brithish Columbia—and barite have also been detected in fluid-inclusion cavities (fig. 9*G–I*). Apatite is also present in fluid-inclusion cavities (fig. 9*J*) in 3– to 5–cm-wide veins of quartz that cut porphyritic monzogranite at location 8 (fig. 2). Commonly, the artificially broken surface of vein quartz also contains so many fluid-inclusion cavities that the surface of the quartz has a pock-marked appearance when viewed at high magnifications by SEM—many cavities host iron sulfide minerals (fig. 10). Previously, Theodore (1996) described a number of other sulfide mineral assemblages present in fluid-inclusion cavities at Elder Creek, including pyrrhotite alone; chalcopyrite, molybdenite, and pyrite; as well as chalcopyrite and K–feldspar. The presence of chalcopyrite in fluid inclusions from porphyry copper systems is recognized widely (Roedder, 1984: Mavrogenes and others, 1992). Many such occurrences may actually be daughter minerals that precipitated from the entrapped fluid-inclusion waters. The continued stability of chalcopyrite daughter minerals at elevated temperatures during experiments on the heating stage is probably the result of diffusion of hydrogen out of the fluid inclusions when they were exposed to much lower values of hydrogen fugacity during circulation of oxygenated meteoric waters into the porphyry system during its waning retrograde stages (Mavrogenes and Bodnar, 1992, 1994). The apparent stable compatability between chalcopyrite and K–feldspar in fluid inclusions at Elder Creek suggests that some primary copper in the system must have been introduced during the potassic alteration event associated with emplacement of porphyritic monzogranite. As described above, potassic alteration is approximately as widespread as the quartz stockworks (fig. 2).

The presence of apatite in fluid-inclusion cavities detected by SEM at location 8 has also been confirmed optically, and the textural relations of it to surrounding fluid-inclusion waters indicate

that the apatite must, in fact, be a daughter mineral and that calcium must have been a significant component of type III fluid inclusions at Elder Creek (fig. 11). Many of these apatite-bearing fluid inclusions also contain CO_2. As shown in figure 11*A*, a fluid inclusion containing an opaque mineral is draped partly around an elongate crystal of apatite that extends well into the surrounding vein quartz. These waters must be relict from the time of the crystallization of the apatite. Furthermore, this textural relation probably implies that many of the solid inclusions of apatite in vein quartz, such as those in figure 9*J*, partly may result from a necking down of fluid inclusions during late stages of the system. Other fluid inclusions from the same sample show apatite crystals to be confined entirely to the fluid inclusion (fig. 11*B*), and yet other textural relations record a declining amount of fluid-inclusion waters around apatite that eventually culminates in needles of apatite being completely enclosed by quartz without any fluid-inclusion waters present (fig. 11*C*). Many type III fluid inclusions that host apatite also include other translucent daughter minerals, of which halite and sylvite have been identified, indicating that the chemical composition of the fluids must have been extremely complex. Apatite is present as daughter minerals elsewhere in aqueous inclusions from a wide variety of geologic environments including (1) quartz-epidote-kyanite veins in eclogite (Selverstone and others, 1990), (2) emeralds of calcite-dolomite veins in Columbia (Giuliani and others, 1990); (3) in diamonds (Guthrie and others, 1989); and (4) in Mesozoic carbonatite-alkaline complexes in Mongolia (Samoilov and others, 1988). Apatite has also been reported by many others to be present in melt inclusions hosted by volcanic and sub-volcanic rocks.

Microthermometry

Microthermometry of the initial and final melting temperatures and final filling temperatures of type I and II fluid inclusions, as well as initial melting and final dissolution temperatures of daughter minerals of type III fluid inclusions, indicates that the fluids at Elder Creek may be categorized into the following four broad categories: (1) complex $NaCl–KCl–CaCl_2–(FeCl_3)–(CO_2)–H_2O$ saline to hypersaline brines enriched with various base metals (including copper, lead, and zinc), as well as barium and other minor anions; (2) $CaCl_2–(NaCl)–(KCl)–H_2O$ moderate salinity brines; (3) $NaCl–KCl–CaCl_2–H_2O$ moderate salinity brines; and (4) $NaCl–(KCl)–H_2O–CO_2$ relatively low salinity fluids. These fluids are listed roughly in the paragenetic order that we envision for their circulation in the system at Elder Creek. Assignment to a chemical system was attempted by observing, whenever possible, the eutectic melting temperature of the frozen aqueous brine as it warmed slowly and then referring to phase data for pertinent chloride-bearing aqueous solutions (Crawford, 1981)—this has been aided immensely by the unusual optical clarity of the samples and size of the fluid inclusions. Distribution of eutectic melting temperatures versus total filling temperatures in 445 fluid inclusions from within the area of the quartz stockworks (fig. 12*A–C*) is contrasted with similar data for 58 type I fluid inclusions (fig. 12*D*) in vein quartz associated with arsenopyrite just outside the quartz stockworks (location 10, fig. 2). Almost all fluid inclusions studied from both areas are hosted by vein and phenocrystic quartz; some are hosted by plagioclase in porphyritic monzogranite from within the area of the quartz stockworks. The modes for the eutectic melting data of the above four fluid categories respectively are approximately –70 °C (unimodal); –39 to –50 °C (multimodal); approximately –28 °C (unimodal); and approximately –23 °C (fig. 12). The eutectic melting temperature for the system $NaCl–H_2O$ is –21.2 °C (Hall and others, 1988). As a comparison, eutectic temperatures of several other chemical systems are as follows:

System	Eutectic	Source
$ZnCl_2–H_2O$	–62.0 °C	Linke (1965)
$FeCl_3—H_2O$	–55.	----do.----
$NaCl–KCl–CaCl_2–H_2O$	–55.	Yanatieva (1946)
$CaCl_2–MgCl_2–NaCl–H_2O$	–57.	Crawford (1981)
$NaCl–CaCl_2–H_2O$	–52.	----do.----
$CaCl_2–H_2O$	–49.8	---do.—
$NaCl–MgCl_2–H_2O$	–35.	----do.----
$NaCl–KCl–H_2O$	–22.9	----do.----
$KCl–H_2O$	–10.6	----do.----

Although first melting temperatures as low as –80 °C may result from metastable formation of $MgCl_2$–salt hydrates during freezing tests involving Mg–bearing fluid-inclusion waters (Davis and others, 1990), we have confirmed presence of significant concentrations of calcium in many of the fluid inclusions at Elder Creek. This confirmation involved SEM identification of Ca–bearing daughter minerals (including apatite, as described above), as well as the textural relations between the Ca–bearing minerals and the fluid-inclusion waters. Nonetheless, depressed eutectic temperatures as low as –80 °C could also be the result of the combined presence of $CaCl_2$, $FeCl_2$, and $MnCl_2$ in the fluids, commonly reflected in the presence of several daughter minerals containing these cations in type III fluid inclusions (fig. 9*B*). Many other studies in recent years have determined the presence of calcium in NaCl-

bearing fluid-inclusion waters, and these studies, including some that have described fluid-inclusions in other porphyry systems (Trudu and others, 1990; Cline and Bodnar, 1990), have shown that these types of fluid inclusions typically have first melting temperatures commonly between –45 to –60 °C (Cheilletz and others, 1994; Zwart and Touret, 1994). In addition, examination of the fluid-inclusion waters in a few select type I fluid inclusions at Elder Creek by a synchrotron X–ray fluorescence microprobe (see Lu and others [1989] and Vanko and others [1993] for descriptions of the methodology involved) indicates the presence of calcium, as well as Fe, Ti, Mn, and Cu in fluid-inclusion waters. The presence of Fe, Ti, and Mn in the fluid-inclusion waters is consistent with the identification of ilmenite in many of the fluid inclusions by SEM, and the presence of Cu is consistent with the presence of chalcopyrite in type III fluid inclusions. The presence of $FeCl_2$ in the fluid inclusion waters may result in determinations of salinity by the depression-of-freezing-point method that are somewhat elevated because of a "salting-out" effect (Roedder, 1984; see also, Cline and Vanko, 1995).

The four chemical categories of fluid inclusions at Elder Creek show median filling temperatures of approximately 350 °C, 400 °C, 325 °C, and 300 °C (fig. 12)—as a reminder, some of the latter data were obtained from vein quartz at a 1,090–ft depth at locality 10 (fig. 2). Although filling temperatures of almost all vapor-rich type II fluid inclusions from the Elder Creek system show minimum filling temperatures of 400 °C in the $CaCl_2$–(NaCl)–(KCl)–H_2O fluids and NaCl–KCl–$CaCl_2$–H_2O fluids, the abundance of this type of fluid inclusions is not well represented numerically in the tabulations of data from the experimental runs relative to visual estimates of their actual abundance in the samples. This results primarily from many of the vapor-rich fluid inclusions rupturing well prior to their being filled during heating tests despite usage of an extremely slow rate of temperature increase. All filling temperatures of type II fluid inclusions are most likely minimal ones, possibly even by a significant number of degrees Celsius, because of the difficulty in resolving precisely when the vapor bubble fills the entire fluid-inclusion cavity during a heating experiment. Roedder (1984) and Bodnar and others (1985) noted that, because of inherent optical limitations, the real filling temperature of a vapor-rich fluid inclusion may be as much as several hundred degrees Celsius higher than the apparent filling temperature recorded during a heating experiment. Nonetheless, some type II fluid inclusions, mostly those which do not contain opaque minerals, apparently are cogenetic with type III fluid inclusions and they are also cogenetic with type I fluid inclusions that belong to the system $CaCl_2$–(NaCl)–(KCl)–H_2O. However, at 1,090–ft depths just outside the quartz stockworks at locality 10, there are much less abundant type II fluid inclusions present in the quartz-arsenopyrite veins than in quartz stockworks exposed at the surface. The implications of this relation will be discussed below.

A summary plot of homogenization temperature versus salinity in weight percent NaCl equivalent for all four chemical categories of fluid inclusions in the Elder Creek system indicates that some fluids were as hot as approximately 500 °C and as saline as 45 to 50 weight percent NaCl equivalent (fig. 13*A*). Because fluid immiscibility or boiling apparently prevailed during circulation of many of the fluids, filling temperatures for most fluid inclusions do not require correction to establish their trapping temperatures (Roedder, 1984). As suggested by figure 13*A*, which includes those fluid inclusions that we referred above as being $CaCl_2$–(NaCl)–(KCl)–H_2O moderate salinity brines, there is wide-ranging spatial overlap within the quartz stockworks of fluid-inclusion types I, II, and III. The mode and the mean of the 457 filling temperatures, however, is about 340 °C. The distribution of salinities for the fluid inclusions has a major mode between 0 and 5 weight percent NaCl equivalent and the other at about 35 weight percent NaCl equivalent. Although some fluid inclusions contain high proportions of CO_2, the amount of CO_2 overall in the system is quite small and it probably does not significantly impact calculated salinities (see also, Collins, 1979; Brown and Lamb, 1989). Certainly the impact of the presence of CO_2 on calculated salinities should be much less than inherent incertitudes resulting from the chemically complex isochores at elevated temperatures and pressures. It is important to note that some low salinity fluid inclusions at Elder Creek also have have high filling temperatures—some are as high as 500 °C and many as high as 400 °C (fig. 13*A*). The coexistence of low density, vapor-rich type II fluid inclusions that homogenize by liquid disappearance at temperatures higher than 400 °C (fig. 12) suggests that fluid immiscibility may be called upon to explain type II fluid inclusions and those coexisting type III fluid inclusions whose final homogenization is characterized by disappearance of their vapor bubbles. As pointed out by Roedder (1984), the minimum temperature of homogenization for fluid inclusions that fill to vapor most likely approximates the pure end member vapor in an unmixing fluid environment. Most importantly, the overwhelming bulk of the type III fluid inclusions at Elder Creek homogenize finally by disappearance of their vapor bubble—that is, the dissolution temperatures of their halite daughter minerals is lower than the filling temperature of their vapor bubbles. It also appears likely from the

plot of homogenization temperature versus eutectic temperature for the $CaCl_2$–(NaCl)–(KCl)–H_2O moderate salinity brines that these fluids were at times boiling at minimum temperatures of about 400 °C (fig. 12*B*).

Type III fluid inclusions that homogenize by disappearance of their vapor bubbles probably represent the saline-rich fractions of immiscible fluids that were circulating as the quartz stockworks were being emplaced near the top of the Elder Creek porphyry system—initially these fluids may have been as saline as about 50 weight percent NaCl equivalent and at temperatures of about 450–500 °C (fig. 12). The 50 weight percent NaCl vapor-pressure isopleth for NaCl–H_2O fluids intersects the three phase liquid-vapor-H_2O curve at a temperature of about 450 °C (Bodnar and Vityk, 1994). Therefore, trapping temperatures along the isopleth must have been higher than 450 °C for those type III fluid inclusions that have compositions of about 50 weight percent NaCl equivalent and homogenize by vapor disappearance. Such temperatures of 450 °C or more, when compared with the approximate 400 °C apparent minimum filling temperature for type II fluid inclusions, suggest that the filling temperatures determined for the type II fluid inclusions may be as much as 50 °C too low because of optical limitations as described above. Immiscibility at 500 °C for a 50 weight percent NaCl equivalent fluid occurs at a pressures less than approximately 350 bars—at 450 °C it occurs at pressures less than approximately 300 bars (Bodnar and Vityk, 1994). Lithostatic pressures of 350 bars are equivalent to minimum paleodepths of about 1.3 km, and hydrostatic pressures of 350 bars are equivalent to maximum paleodepths of about 3.5 km.

The type III fluid inclusions at Elder Creek that homogenize finally by halite dissolution may have had a somewhat different history. Thirty four type III fluid inclusions homogenize by halite dissolution in the range 221 to 384 °C. In contrast, the overwhelming bulk of the remaining type III fluid inclusions exhibit liquid-vapor homogenization between 260 and 500 °C (fig.13*A*). As pointed out by Bodnar and Vityk (1994) and Cline and Vanko (1995), fluid inclusions that homogenize by halite dissolution may have been trapped in a vapor-free fluid environment that could be reflective of a number of different factors including trapping in a pressure environment higher than that in which other coextensive fluids subsequently unmix to liquid and vapor. Such a high pressure environment at Elder Creek could be interpreted to be reflective of *in situ* overpressurization by the magma just prior to catastrophic fracturing, or, alternatively, the type III fluid inclusions that homogenize by halite dissolution may be fluids that unmixed deep in the magmatic-hydrothermal column at Elder Creek and subsequently followed initially isobaric and then essentially isothermal paths to reach the sites in which they were eventually trapped. Some of these latter fluids could be interpreted as having exsolved directly from a magma (Cline and Vanko, 1995). If the type III fluid inclusions that homogenize by halite dissolution at Elder Creek can be represented properly by relations in the system NaCl–H_2O, then, following Cline and Vanko (1995), there is a broad pressure range—from approximately 0.25 kb to greater than 1.6 kb—over which they may have been trapped (fig. 14). However, as pointed out above, many type III fluid inclusions that homogenize finally by halite dissolution also contain CO_2 and CH_4. It does not seem reasonable to assume that the fluids in the Elder Creek system represented by type III fluid inclusions that homogenize by halite dissolution may have initially exsolved directly from magmas deep within the system and then streamed upwards to co-mingle with fluids near the top of the system that were boiling—all the while retaining their CO_2 and CH_4. It seems much more logical to assume that, if the fluids represented by these type III fluid inclusions separated from a magma deep within the porphyry sysyem, then they should not have retained any CO_2 or CH_4 . The latter two chemical components would have streamed upwards toward the top of the system. Therefore, it appears that these fluid inclusions that fill by halite dissolution must represent trapping of fluids not far removed—in a paleodepth sense—from their actual sites of exsolution from a magma. They simply may be fluids that moved more or less down the P–T path of the liquid-vapor-halite join toward lower pressures and temperatures, prior to their trapping, and after the fluids had originally formed in a liquid-vapor environment (fig. 14). Certainly the porphyry environment at Elder Creek was a dynamic one at the time the system was emplaced, and pressure fluctuations during emplacement would not be unreasonable as channelways to the nearby paleosurface repeatedly opened by fracturing and sealed by quartz deposition.

Fluid inclusions associated with approximately 2– to 2.5–cm-wide quartz-arsenopyrite veins at a 1,090–ft depth at locality 10 (fig. 2)—the deepest part of the system for which we have fluid-inclusion data—differ slightly with those associated with quartz stockworks at the surface at Elder Creek, particularly with respect to proportions of types of fluid inclusions present (fig. 13*B*). Homogenization temperatures were not obtained from any type II fluid inclusions at this locality, primarily because of their sparse numbers in the samples and their decrepitaion during heating runs. It must be emphasized, however,

that type II fluid inclusions are present in the veins, at 1,090–ft depths below the present erosion surface, and that they also include some vapor-only varieties, as well as some three-phase liquid CO_2–bearing varieties that would have undoubtedly filled to vapor during heating tests. The latter fluid inclusions also contain CH_4. Therefore, the interface between a boiling and a non-boiling environment at Elder Creek must be below the site of the veins at the time of their formation, but probably not far below, because of the relatively sparse numbers of type II fluid inclusions in the veins. Moreover, most fluid inclusions in the 1,090–ft deep quartz-arsenopyrite veins are type I low-salinity fluid inclusions that have eutectic temperatures approximately in the range –18 to –32 °C, and most of their eutectic temperatures are in the interval –24 to –29 °C (fig. 12*D*)—these fluids probably are made up of predominantly NaCl–H_2O. The mean and mode of their salinities are approximately 7 weight percent NaCl equivalent and the mean of the homogenization temperatures for these type I fluid inclusions is about 300 °C (fig. 13*B*)—as is that for some extremely sparse type III fluid inclusions. Some moderate salinity fluids may be associated with the secondary sulfosalt minerals (boulangerite and tetrahedrite), which are in places included within carbonate minerals in the quartz-arsenopyrite veins (see below). Four type III fluid inclusions from the veins at locality 10 show that their salinities cluster near 35 weight percent NaCl equivalent, and their final homogenization takes place by vapor disappearance at temperatures in the range 260 to 310 °C. These fluid inclusions most likely were trapped somewhere in P–T space along the isochore for 35 weight percent NaCl equivalent fluids. If the 35 weight percent NaCl vapor-pressure isopleth for NaCl–H_2O fluids at this locality is representative of fluids associated with early stages of emplacement of the quartz-arsenopyrite veins, then a minimum pressure of about 150 bars—approximately equivalent to paleodepths of 1.5 km if conditions were hydrostastic—would have been required at 360 °C to prevent fluid immiscibility (Bodnar and Vityk, 1994). These pressures at 1,090–ft depths are compatible with those suggested by our fluid-inclusion studies of surface samples at Elder Creek if the paleogeologic environment underwent a transition from a lithostatic to a hydrostatic regime between the time of major quartz stockworks emplacement and quartz-arsenopyrite vein emplacement at the present day 1,090–ft depths.

The quartz-arsenopyrite veins at locality 10 may have been emplaced near the margins of the 38–Ma Elder Creek system in association with 35–Ma granodiorite porphyry that was intruded into the area near the final stages of the Elder Creek system. Alteration associated with the quartz-arsenopyrite veins is propylitic, as described above, and narrow selvages of propylitic alteration around the veins cut the dominant biotitic mineral assemblages in the surrounding rocks of the Harmony Formation. Narrow granodiorite porphyry dikes crop out near locality 10, and the general area of this locality appears to be within an approximately 0.4–km-wide, north-south zone that extends as much as 2 km to the south of locality 10 (fig. 2; see also, Doebrich and Theodore, 1996). The quartz-arsenopyrite veins may have been emplaced in a pressureregime closer to hydrostatic than lithostatic. In addition, the 40– to 35–Ma time interval, approximately the time interval between emplacement of porphyritic monzogranite and granodiorite porphyry, appears to have been roughly the period of time that extensional breakup of the crust in this part of the Basin and Range began (Doebrich and Theodore, 1996). This was also a period of time during which there may have been highly accelerated erosion rates in the mining district (Theodore and Blake, 1975).

Estimates of distribution of high-temperature and high-salinity fluids

Select fluid-inclusion data from the 16 locations studied at Elder Creek were first interpolated to a square grid (using approximately a 100–m grid value) by means of a routine based on the principal of minimum curvature (Briggs, 1974) that is also described in Kotlyar and others (1995) and partly repeated here from the latter report for added clarification. These data consist of the highest temperature of filling by vapor disappearance of the most saline fluid inclusion measured from a locality (fig. 15*A*), and, for comparative purposes, the highest salinities determined from each locality (fig. 15*B*), as well as the mean temperature of all homogenization temperatures measured at each locality (fig. 15*C*). As a cautionary note, it must be emphasized that the gridding procedures employed are relatively sensitive to the density and uniformity of sampling sites in small domains. In addition, the gridded map data, which are shown in figure 15, were spatially filtered in an effort to emphasize the broad (long-wavelength) characteristics of the fluid-inclusion data by suppressing the narrow (short wavelength) components. With the specific filter used in the contouring procedure, the shorter the wavelength, the greater the suppression. The magnitude of the relative suppression between any two wavelengths is controlled in this filter by a free parameter z, which has dimensions of length. Short-wavelength characteristics of the data are more strongly attenuated by filters with large values of z. Thus, filters with large values of z are more effective in emphasizing long-wavelength characteristics of anomalies. The type of filter used in this study, when applied to gravity or

magnetic data, is known as the "upward continuation" filter (Blakely, 1994), because for a given value of z, the filtered data appear as if they had been measured on a surface that is distance z above the original data surface.

The isotherms across the Elder Creek system showing the inferred distribution of the highest filling temperature by vapor disappearance for the most saline fluid inclusion measured at the various localities appears to show quite well what we would infer generally from the data; namely, that the hottest part of the system is in the general area of the Morning Star Mine near the outer limit of the quartz stockworks (fig. 15*A*). A similar relation is also present in the contoured salinity data (fig. 15B, see following paragraph below). This relation may result from an asymmetric distribution at depth of the igneous phase of the porphyry system most closely associated genetically with generation of the quartz stockwork veins. An apophysis of this igneous phase may be close to the surface in the general area of the Morning Star Mine. There appears to be a saddle in the isotherms south of the Morning Star Mine, more or less coincident with the trace of the Elder Creek fault (fig. 15*A*). In addition, the isotherms intersect the northern outer limit of quartz stockworks at high angles—many of the intersections are at angles of approximately 90 ° to the west-northwest of the Morning Star Mine. At first appearance, the geometry of these appears to be geologically unreasonable because we would expect overall temperatures to decline near the outer limit of the stockworks. The geometry of these relations, however, may be an artifact of the locations of the fluid-inclusion sampling points in combination with the contouring procedures used, as well as the relatively small number of locations from which the fluid-inclusion data have been obtained. Alternatively, a northeast-striking normal fault, or system of faults, may be present under the unconsolidated alluvial deposits northwest of the Morning Star Mine, and this fault or system of faults may have uplifted its southeastern block—the block containing the Morning Star Mine (fig. 15*A*).

A plot showing distribution of the highest values of salinity in weight percent NaCl equivalent determined across the system by the same contouring method reveals a pattern that is a generally similar to the one for the highest temperature of homogenization by vapor disappearance for the most saline fluid inclusion at each of the localities examined (fig. 15*B*). The highest salinities at each of the localities also seem to show a broad increase in their values toward the Morning Star Mine and toward an area along the southern trace of the Elder Creek fault. In addition, the same saddle appears to be present in the salinity data south of the Morning Star Mine. From the apparent coincidence of this saddle with the trace of the Elder Creek fault, we infer that the Elder Creek fault, or its predecessor fault or faults, may have been active prior to or contemporaneous with circulation of the highest salinity fluids in the system, and may thereby have channeled some of the hottest and most saline fluids along it. If this sequence of fluid flow is generally correct, then the Elder Creek fault must have been reactivated because the last movements along the Elder Creek fault are quite young owing to unconsolidated gravels having been affected by movements along it also.

Finally, the distribution of mean temperatures of total homogenization, regardless of type of fluid inclusion and regardless of the type of total homogenization (homogenization to liquid and vapor were considered alike), across the Elder Creek system was also prepared using the same gridding and filtering procedures as above (fig. 15*C*). The numbers of fluid inclusions involved in the calculation of the means at each of the sites varies from 28 to 47. Although absolute values of the temperature distribution using mean temperatures (fig. 15*C*) are somewhat less than those determined from the distribution of the temperature of homogenization by vapor disappearance of the most saline fluid inclusion in each sample (fig. 15*A*), the overall pattern of the isotherms across the system is roughly the same as the latter—that is, there is a broad increase in temperatures from west to east across the exposed parts of the system. However, the hottest fluids by this method appear to have been present east of the Elder Creek fault in what would be some parts of the system uplifted by displacements along the Elder Creek fault system. The fact that the mean values of homogenization are quite a bit lower than the temperatures of the hottest and most saline fluid inclusions is primarily a function of the presence in the vein samples of late fluids that entered the system probably during its retrograde, meteoric-water dominated stages, although we do not have any isotopic data in support of this inference.

MICROPROBE ANALYSES OF ARSENOPYRITE

Arsenopyrite compositions were examined by electron microprobe in an attempt to corroborate the fluid-inclusion homogenization data by some other method. A number of individual crystals of arsenopyrite from the veins at locality 10 (fig. 2) that appear to have quite uniform compositions when examined by the back-scattered mode of the SEM, and that commonly include equant and elongate blebs of galena as much as 400 μm long (fig.16), were analyzed by

electron microprobe for 12 elements (Fe, Co, Ni, Sb, Bi, Au, As, S, Ag, Cu, Zn, and Pb). The veins also include pyrite and some sulfosalts, including argentiferous tetrahedrite that is paragenetically younger than boulangerite (fig. 17*A*), as well as small crystals of boulangerite and stibnite that are present in calcite on the fringes of the quartz-arsenopyrite veins (fig. 17*B*). Pyrite and arsenopyrite appear to be in equilibrium with each other. Compositions of arsenopyrite in one polished thin section (95TT002) was studied using a Jeol electron microprobe, model JXA 8800, equipped with five wavelength dispersive spectrometers. Analysis conditions for standards and unknowns were 20kV accelerating voltage and 20nA beam current. Chemically analyzed, synthetically prepared sulfide minerals or pure metals were used as standards: analyzed arsenopyrite (ASP 200) for iron, arsenic, and sulfur; synthetic Co_3S_4 for cobalt; bismuth metal, native gold, and copper metal for bismuth, gold, and copper; sphalerite for zinc; and galena for lead. Background measurements were made off peak for each analysis. Matrix corrections were made using Jeol-supplied ZAF software. Detection limits in arsenopyrite for the major elements iron, arsenic, and sulfur are typically 0.1 weight percent. In the first part of the study by microprobe, three to eight points were analyzed on each of three representative clots of arsenopyrite; these points were chosen to characterize both rim and core domains of the analyzed arsenopyrite, which, overall, is in the range 1 to 2 mm in long dimension. In the second part of the microprobe study, 14, 21, and 23 points were analyzed along three traverses across three arsenopyrite crystals that appear to show weakly developed zoning when viewed by microprobe and SEM using back-scattered electrons; and, finally, 13 and 16 points were analyzed respectively along each of two traverse lines across two pyrite crystals. Approximately 10–μm distances were present between most points analyzed along the traverses. In addition, qualitative distribution of cobalt and copper in an arsenopyrite crystal and a pyrite crystal from one of the samples of quartz-arsenopyrite vein, which was studied quantitatively above by microprobe (95TT001), was determined by preparation of elemental X–ray intensity maps also using the microprobe. Figure 18 shows distribution of Fe, Co, As, Cu, and S in the arsenopyrite crystal, and figure 19 shows distribution of those same five elements in the pyrite. The X–ray intensity maps reveal, for all intents, essentially no preferred concentration of either cobalt or copper in the two crystals analyzed with the exception of an extremely slight elevated concentration of cobalt locally near the margin of the pyrite grain in the general area where some small crystals of arsenopyrite are present in the pyrite.

All 82 analyses of arsenopyrite in the quartz-arsenopyrite vein plot in an apparently tight cluster in the Fe–As–S ternary diagram (fig. 20). The only substantial elements present in the arsenopyrite analyses are iron, arsenic, and sulfur. The element most abundant in arsenopyrite as a minor constituent is bismuth, which makes up, at most, 0.12 weight percent Bi of one analysis. Most analyses of arsenopyrite contain 0.04 to 0.06 weight percent Bi. In addition, the three arsenopyrite crystals along which microprobe analyses were determined along traverses show no detectable differences in chemical composition between rim- and core-domains of individual crystals. Representative analyses of arsenopyrite are listed in table 2. Although the analyses by microprobe are somewhat low, the atomic stoichiometry of the calculated formulas for arsenopyrite from these analyses is quite satisfactory. The range of the arsenopyrite analyses, excluding three analyses with poor totals resulting from surface defects, is 31.6 to 33.9 atomic percent As, a relatively broad range of compositions when considered from the standpoint of geothermometry—these compositions respectively correspond to temperatures of about 400 to 475 °C along the arsenopyrite-pyrite+liquid binary join in the T–X diagrams of Kretschmar and Scott (1976) and Sharp and others (1985). These temperatures are quite a bit higher than the homogenization temperatures measured from the fluid inclusions inside vein quartz in the quartz-arsenopyrite veins—type I fluid inclusions have a major mode approximately at 300 °C and type III fluid inclusions have a mode for their homogenization by vapor disappearance of 360 °C (fig. 13*B*). Type II vapor-rich fluid inclusions coexist with both of these types of fluid inclusion in the quartz-arsenopyrite veins. However, Sharp and others (1985) have pointed out, from their examination of a number of natural occurrences, that the arsenopyrite geothermometer should be applied only to rocks that have been subjected to regional metamorphic conditions of greenschist and amphibolite grade. Arsenopyrite from hydrothermal occurrences may not have attained equilibrium.

CONCLUSIONS

At Elder Creek, a limited amount of the upper part of the porphyry system appears to have been removed by erosion such that quartz stockworks are well preserved. If these quartz stockworks owe their genesis to crystallization of magma deep within the Elder Creek system—somewhat analogous to the concentration of silica-rich caps at the tops of Climax-type molybdenum systems (Carten and others, 1988; Shinohara and others, 1995)—then porphyritic monzogranite,

which hosts much of the quartz stockworks at Elder Creek, must form the outermost shell of the magma column associated with the porphyry system. Although we have demonstrated the presence of significant amounts of calcium in the fluids associated with the Elder Creek system, potassium silicate alteration is the predominant prograde alteration associated with the quartz stockwork veins. In some other porphyry systems, such as Yerington, Nev., where widespread sodic-calcic alteration is present in the intrusive rocks (Dilles and others, 1995), it has been suggested that much of the sodium and calcium has its source in the surrounding evaporite-bearing wallrocks. There are no evaporite-bearing strata known in the Harmony Formation, and the rocks of the Harmony Formation are notably low in calcareous minerals in this part of the mining district. It seems that the most logical source for the calcium in the fluid-inclusion waters is the magma associated with the Elder Creek system, although it could be argued that calcium could have been derived from reactions involving calcium-bearing wallrocks, possibly basaltic rocks of the Devonian Scott Canyon Formation or the Ordovician Valmy Formation, at significant depths in the system. Calcium-rich fluids, indicated by widespread anhydrite, appear to be common in many gold-rich porphyry systems in the Maricunga belt, northern Chile (Vila and Sillitoe, 1991), a relation that is true, as well, at the Park Premier stock, Utah, which contains early actinolite+magnetite±quartz±K–feldspar veins (John, 1989). At the Marte copper-poor, porphyry gold deposit, northern Chile, gold appears to have been introduced during emplacement of quartz-magnetite±anhydrite veins contemporaneous with K–silicate alteration of the host diorite porphyry (Vila and others, 1991). These veins are generally sulfide mineral poor, a characteristic they have in common with the veins at Elder Creek.

The porphyry system at Elder Creek includes significantly more quartz veins, as stockworks, than the similarly-aged system at Copper Canyon, possibly as a reflection of the absence of carbonate replacement strata to interact with fluids associated with mineralization. Although economic metal concentrations have not been discovered during recent exploration, the possibility remains that gravel-covered quartz stockworks in the central part of the Elder Creek system could provide a target worthy of earnest exploration efforts. These quartz stockworks probably are at the apex of the system, and, as presently exposed, they are probably near the base of a zone of stockworks draped across the intrusive core of the system. Silver-gold ratios of production data from polymetallic veins across the system are favorable for occurrence of a gold target near the Morning Star Mine in the central part of the system (Theodore, 1996). Such a target would be somewhat analogous to gold-bearing quartz stockworks present locally in the Copper Canyon area of the mining district—albeit probably in a much higher temperature environment at Elder Creek than in the Copper Canyon area, which could depress the overall amount of gold remaining for exploitation in this part of the hydrothermal system. In a summary model for development of quartz stockworks in porphyry copper systems in the Former Soviet Union, Zvezdov and others (1993) assign quartz stockwork veins including potassium silicate alteration assemblages to an early paragenetic stage that is (1) typically barren of gold and chalcopyrite; (2) commonly includes minor amounts of magnetite, molybdenum, and pyrite; and (3) confined tightly to the apical parts of the magmatic column associated with the system. Zvezdov and others (1993) infer that most of the gold in such systems is introduced during intermediate stages when the volume of the veins amounted to 20–50 times that of the preceding one, and when phyllic and propylitic assemblages became dominant.

The fluid-inclusion temperatures recorded in the core of the system at Elder Creek, however, are somewhat comparable with those recorded at some gold-bearing quartz stockworks and quartz vein deposits associated with magmatic-hydrothermal environments elsewhere. In the Endeavour 26 North porphyry copper-gold deposit, New South Wales, Australia, the bulk of the gold was intruduced during a quartz stockwork stage which includes bornite, chalcopyrite, and anhydrite, and which has median fluid-inclusion filling temperatures of approximately 600 °C (Heithersay and Walshe, 1995). The Cosmopolitan Howley, Australia, deposit—a quartz vein-hosted gold deposit associated with I–type granite—apparently also formed at high temperatures that were in the 550 to 620 °C range (Matthäi and others, 1995). The Tirad porphyry copper, Philippines, has potassic alteration assemblages, free gold in quartz veins that also contain chalcopyrite and hematite, and average filling temperatures of about 376 to 413 °C (Trudu and Bloom, 1988). The Mt. Estelle pluton of Crowe and others (1990), central Alaska Range, contains concentric gold-bearing fractures and quartz-cored pegmatites along structures which apparently channeled hypersaline fluids (total salinities in the range 73 to 75 weight percent NaCl equivalent), and along which fluids were trapped in fluid inclusions that homogenize at temperatures near 500 °C. These may have been the gold-mineralizing fluids associated with the mineralized structures. In the Fort Knox, Alaska, gold deposit, which contains approximately 4 million oz Au in mostly sulfide-mineral-poor, stockwork veins near the apex of a presumably

genetically associated Late Cretaceous biotite granite, moderate salinity (2 to 8 weight percent NaCl equivalent) fluid inclusions homogenize at somewhat lower temperatures (271 to 328 °C) than at Elder Creek (McCoy and others, 1996). Nonetheless, these veins are remarkably similar in overall appearance to those at Elder Creek, although the alteration at Fort Knox is albitic rather than potassic as at Elder Creek. However, Goldfarb and others (1996) further suggest that the gold veins at Fort Knox are coeval with widespread contact metamorphism during the latter phases of extension of the surrounding Yukon-Tanama terrane. The Battle Mountain Mining District has shown remarkable resilience with respect to changing market conditions and metal prices, and only time, as well as a serious commitment of exploration resources to determine what commercial concentration of metal is concealed by the unconsolidated gravels near the Morning Star Mine, if any, will resolve the implications of our data.

REFERENCES CITED

Barres, O., Burneau, A., Dubessy, J., and Pagel, M., 1987, Application of micro–FT–IR spectroscopy to individual fluid inclusion analysis: Applied Spectroscopy, v. 41, no. 6, p. 1,000–1,008.

Beane, R.E., 1982, Hydrothermal alteration in silicate rocks, *in* Titley, S.R., ed., Advances in geology of the porphyry copper deposits: Tucson, Arizona, The University of Arizona press, p. 117–137.

Belkin, H.E., 1994, Microthermometric investigations: Th and Tm. Practical and theoretical aspects, *in* DeVivo, Benedetto, and Frezzotti, M.L., eds., Fluid inclusions in minerals: methods and applications: Blacksburg, Virginia, Virginia Polytechnic Institute and State University, Short Course of the International Mineralogical Association Working Group "Inclusions in Minerals," Pontignano-Siena, Pisa, Italy, September, 1994, p. 7–23.

Blake, D.W., 1992, Supergene copper deposits at Copper Basin, *in* Theodore, T.G., Blake, D.W., Loucks, T.A., and Johnson, C.A., Geology of the Buckingham stockwork molybdenum deposit and surrounding area, Lander County, Nevada: U.S. Geological Survey Professional Paper 798-D, p. D154–D167.

Blakely, R.J., Potential theory in gravity and magnetic applications: New York, Cambridge University Press, 441 p.

Bloomstein, E.I., Braginton, B., Owen, R., Parratt, R, Rabbe, K., and Thompson, W., 1993, Geology and geochemistry of the Lone Tree gold deposit, Humboldt County, Nevada: 93rd Annual Meeting Reno Nevada, Society for Mining, Metallurgy, and Exploration, Inc. and Society of Economic Geology, February 15–18, 1993, Preprint 93–205, 23 p.

Bloomstein, E.I., Massingill, G.L., Parratt, R.L., and Peltonen, D.R., 1991, Discovery, geology, and mineralization of the Rabbitt Creek gold deposit, Humboldt County, Nevada, *in* Raines, G.L., Lisle, R.E., Schafer, R.W., and Wilkinson, W.H., eds., Geology and ore deposits of the Great Basin, Symposium Proceedings: Reno, Nevada, Geological Society of Nevada, p. 821–843.

Bodnar, R.J., 1995, Fluid-inclusion evidence for a magmatic source for metals in porphyry copper deposits, *in* Thompson, J.F. H., ed., Magmas, fluids, and ore deposits: Victoria, British Columbia, Mineralogical Association of Canada, Short Course v. 23, p. 139–152.

Bodnar, R.J., Burnham, C.W., and Sterner, S.M., 1985, Synthetic fluid inclusions in natural quartz. III. Determination of phase equilibrium properties in the system H_2O–NaCl to 1,000 °C and 1,500 bars: Geochimica et Cosmochimica Acta, v. 41, p. 1,861–1,873.

Bodnar, R.J., and Vityk, M.O., 1994, Interpretation of microthermometric data for H_2O–NaCl fluid inclusions, *in* DeVivo, Benedetto, and Frezzotti, M.L., eds., Fluid inclusions in minerals: methods and applications: Blacksburg, Virginia, Virginia Polytechnic Institute and State University, Short Course of the International Mineralogical Association Working Group "Inclusions in Minerals," Pontignano-Siena, Pisa, Italy, September, 1994, p. 117–130.

Briggs, I.C., 1974, Machine contouring using minimum curvature: Geophysics, v. 39, p. 39–48.

Brown, P.E., and Hagemann, S.G., 1994, MacFlinCor: a computer program for fluid inclusion data reduction and manipulation, *in* DeVivo, Benedetto, and Frezzotti, M.L., eds., Fluid inclusions in minerals: methods and applications: Blacksburg,

Virginia, Virginia Polytechnic Institute and State University, Short Course of the International Mineralogical Association Working Group "Inclusions in Minerals," Pontignano-Siena, Pisa, Italy, September, 1994, p. 231–250.

Brown, P.E., and Lamb, W.M., 1989, P–V–T properties of fluids in the system $H_2O \pm CO_2 \pm$ NaCl: New graphical presentations and implications for fluid inclusions: Geochimica et Cosmochimica Acta, v. 53, p. 1,209–1,221.

Brown, P.E., and Vry, J.K., 1990, Applications of micro–FTIR spectroscopy to fluid inclusions [abs.]: Toronto, Ontario, Third Biennial Pan-American Conference on Research on Fluid Inclusions (PACROFIL III), May, 1990, v. 3, p. 23–24.

Campbell, A.R., 1995, The evolution of a magmatic fluid: a case history from the Capitan Mountains, New Mexico, *in* Thompson, J.F. H., ed., Magmas, fluids, and ore deposits: Victoria, British Columbia, Mineralogical Association of Canada, Short Course v. 23, p. 291–308.

Carten, R.B., Geraghty, E.P., Walker, B.M., and Shannon, J.R., 1988, Cyclic development of igneous features and their relationship to high-temperature hydrothermal features in the Henderson porphyry molybdenum deposit, Colorado: Economic Geology, v. 83, p. 266–296.

Cheilletz, A., Feraud, G., Giuliani, G., and Rodriguez, C.T., 1994, Time-pressure constraints on the formation of Colombian emeralds: an 40Ar/39Ar laser microprobe and fluid inclusion study: Economic Geology, v. 89, p. 361–380.

Cline, J.S., and Bodnar, R.J., 1990, Magmatic-hydrothermal fluids in the Questa, NM, porphyry molybdenum system: Fluid inclusion evidence [abs.]: Geological Society of America, Abstracts with Programs, v. 22, p. A180.

Cline, J.S., and Vanko, D.A., 1995, Magmatically generated saline brines related to molybdenum at Questa, New Mexico, USA, *in* Thompson, J.F. H., ed., Magmas, fluids, and ore deposits: Victoria, British Columbia, Mineralogical Association of Canada, Short Course v. 23, p. 153–174.

Collins, P.L.F., 1979, Gas hydrates in CO_2–bearing fluid inclusions and the use of freezing data for estimation of salinity: Economic Geology, v. 74, p. 1,435–1,444.

Cox, D.P., and Singer, D.A., 1990, Descriptive and grade-tonnage models for distal disseminated Ag–Au deposits: A supplement to U.S. Geological Survey Bulletin 1693: U.S. Geological Survey Open-File Report 90–282, 7 p.

Crawford, M.L., 1981, Phase equilibria in aqueous fluid inclusions, in Hollister, L.S., and Crawford, M.L., eds., Fluid inclusions: applications to petrology: Calgary, Mineralogical Association of Canada, Short Course, p. 75–100.

Crowe, Douglas, Millholland, Madelyn, and Brown, Philip, 1990, High-grade gold mineralization associated with high salinity hydrothermal fluids, Mt. Estelle pluton, central Alaska Range [abs.]: Geological Society of America, Abstracts with Programs, v. 22, p. A41.

Davis, D.W., Lowenstein, T.K., and Spencer, R.J., 1990, Melting behavior of fluid inclusions in laboratory-grown halite crystals in the system NaCl–H_2O, NaCl–KCl–H_2O, NaCl–$MgCl_2$–H_2O, and NaCl–$CaCl_2$–H_2O: Geochimica et Cosmochimica Acta, v. 54, 591–601.

DeVivo, Benedetto, and Frezzotti, M.L., eds., 1994, Fluid inclusions in minerals: methods and applications: Blacksburg, Virginia, Virginia Polytechnic Institute and State University, Short Course of the International Mineralogical Association Working Group "Inclusions in Minerals," Pontignano-Siena, Pisa, Italy, September, 1994, 377 p.

Dilles, J.H., Farmer, G.L., and Field, C.W., 1995, Sodium-calcium alteration by non-magmatic saline fluids in porphyry copper deposits: Results from Yerington, Nevada, *in* Thompson, J.F. H., ed., Magmas, fluids, and ore deposits: Victoria, British Columbia, Mineralogical Association of Canada, Short Course v. 23, p. 309–.

Doebrich, J.L., Wotruba, P.R., Theodore, T.G., McGibbon, D.H., and Felder, R.P., 1995, Field trip guidebook for geology and ore deposits of the Battle Mountain Mining

District, Humboldt and Lander Counties, Nevada: Reno, Nevada, Geological Society of Nevada and U.S. Geological Survey, Great Basin Symposium III, Geology and ore deposits of the American Cordillera, Trip H, April 14–16, 1995, 92 p.

Doebrich, J.L., and Theodore, T.G., 1996, Geologic history of the Battle Mountain Mining District, Nevada, and regional controls on the distribution of mineral systems, *in* Coyner, A.R., and Fahey, P.L., eds., Geology and ore deposits of the American Cordillera, Symposium Proceedings, Geological Society of Nevada, Reno/Sparks, Nevada, April, 1995 (in press).

Giuliani, G., Cheilletz, A., and Rodriguez, C.T., 1990, Emerald deposits from Columbia: Chemical composition of fluid inclusions and origin [abs.]: Eighth IAGOD Symposium, Ottawa, Canada, August 12–18, 1990, Program with Abstracts, p. A48–A49.

Goldfarb, R.J., Miller, L.D., Leach, D.L., and Snee, L.W., 1996, Gold deposits in metamorphic rocks of Alaska, *in* Goldfarb, R.J., and Miller, L.D., Mineral deposits of Alaska: Economic Geology Monograph (in press).

Graney, J.R., and McGibbon, D.H., 1991, Geological setting and controls on gold mineralization in the Marigold Mine area, Nevada, *in* Raines, G.L., Lisle, R.E., Schafer, R.W., and Wilkinson, W.H., eds., Geology and ore deposits of the Great Basin, Symposium Proceedings: Reno, Nevada, Geological Society of Nevada, p. 865–874.

Graney, J.R., and Wallace, A.B., 1988, Stratigraphic and structural controls of gold mineralization in the Marigold project area, Nevada [abs.]: Geological Society of America Abstracts with Programs, v. 20, no. 7, p. A141.

Guthrie, G.D., Navon, O., and Veblen, D.R., 1989, Analytical and transmission electron microscopy of turbid coated diamonds [abs.]: Eos, v. 70, p. 510.

Hall, D.L., Sterner, S.M., and Bodnar, R.J., 1988, Freezing point depression of NaCl–KCl–H_2O solutions: Economic Geology, v. 83, p. 197–202.

Heithersay, P.S., and Walshe, J.L., 1995, Endeavour 26 North: a porphyry copper-gold deposit in the late Ordovician, shoshonitic Goonumbla volcanic complex, New South Wales, Australia: Economic Geology, v. 90, no. 6, p. 1,506–1,532.

Hollister, L.S., and Crawford, M.L., eds., 1981, Short course in fluid inclusions: Applications to petrology: Mineralogical Association of Canada, Short Course Handbook, v. 6, 304 p.

Howe, S.S., and Theodore, T.G., 1993, Sulfur isotopic composition of vein barite—A guide to the level of exposure of disseminated gold-porphyry copper systems in north-central Nevada? [abs.]: Geological Society of America Abstracts with Programs, v. 25, no. 6, p. A162–A163.

Howe, S.S., Theodore, T.G., and Arehart, G.B., 1995, Sulfur and oxygen isotopic composition of vein barite from the Marigold mine and surrounding area, north-central Nevada: Applications to gold exploration [abs.]: Geology and ore deposits of the American cordillera, Symposium, Reno/Sparks, Nevada, April 10–13, 1995, Program with Abstracts, p. A39.

Ivosevic, S.W., and Theodore, T.G., 1996, Weakly developed porphyry system at upper Paiute Canyon, Battle Mountain Mining District, Nevada, *in* Coyner, A.R., and Fahey, P.L., eds., Geology and ore deposits of the American Cordillera, Symposium Proceedings, Geological Society of Nevada, Reno/Sparks, Nevada, April, 1995 (in press).

John, D.A., 1989, Geologic setting, depths of emplacement, and regional distribution of fluid inclusions in intrusions of the Central Wasatch Mountains: Economic Geology, v. 89, p. 386–409.

Kotlyar, B.B., Theodore, T.G., and Jachens, R.C., 1995, Re-examination of rock geochemistry in the Copper Canyon area, Lander County, Nevada: U.S. Geological Survey Open-File Report 95–816, 47 p.

Kretschmar, Ulrich, and Scott, S.D., 1976, Phase relations involving arsenopyrite in the system Fe–As–S and their application: Canadian Mineralogist, v. 14, p. 364–386.

Linke, W.F., 1965, Solubilities of inorganic and metal-organic compounds; K–Z, 4th edition: Washington, D.C., American Chemical Society, v. 2, 1,914 p.

Lu, Fang-Qiong, Smith, J.V., Sutton, S.R., Rivers, M.L., and Davis, A.M., 1989, Synchrotron X–ray fluorescence analysis of rock-forming minerals—1. Comparison with other techniques; 2. White-beam energy-dispersive procedure for feldspars: Chemical Geology, v. 75, p. 123–143.

Matthäi, S.K., Henley, R.W., Bacigalupo-Rose, Stephen, Binns, R.A., Andrew, A.S., Carr, G.R., French, D.H., McAndrew, John, and Kananagh, M.E., 1995, Intrusion-related, high-temperature gold quartz veining in the Cosmopolitan Howley metasedimentary rock-hosted gold deposit, Northern Territory, Australia: Economic geology, v. 90, no. 5, p. 1,012–1,045.

Mavrogenes, J.A., and Bodnar, R.J., 1992, Experimentally-induced dissolution of chalcopyrite daughter minerals in natural fluid inclusions [abs.]: Lake Arrowhead, California, Fourth Biennial Pan-American Conference on Research on Fluid Inclusions, May 21–25, 1992, Program and Abstracts, p. 58.

———1994, Hydrogen movement into and out of fluid inclusions in quartz: Geochimica et Cosmochimica Acta, v. 58, no. 1, p. 141–148.

Mavrogenes, J.A., Williamson, M.A., and Bodnar, R.J., 1992, Cu, Fe, and S concentrations in magmatic/hydrothermal fluids: Evidence from natural and synthetic fluid inclusions [abs.]: Geological Society of America, Abstracts with Programs, v. 24, no. 7, p. A144.

McCoy, Dan, Newberry, R.J., Layer, Paul, Dimarchi, J.J., Bakke, Arne, Mastermans, J.S., and Minehane, D.L., 1996, Plutonic-related gold deposits of interior Alaska, *in* Goldfarb, R.J., and Miller, L.D., Mineral deposits of Alaska: Economic Geology Monograph (in press).

McKee, E.H., 1994, Cenozoic volcanic rocks and mineral deposits of Nevada: U.S. Geological Survey Miscellaneous Field Investigations Map (in press).

Myers, G.L., 1994, Geology of the Copper Canyon-Fortitude skarn system, Battle Mountain, Nevada: Pullman, Washington, Washington State University, Ph.D. dissertation, 338 p.

Nash, J.T., 1976, Fluid-inclusion petrology—data from porphyry copper deposits and applications to exploration: U.S. Geological Survey Professional Paper 907–D, p. D1–D16.

Pironon, J., and Barres, O., 1990, Semi-quantitative FT–IR microanalysis limits: Evidence from synthetic hydrocarbon fluid inclusions in sylvite: Geochimica et Cosmochimica Acta, v. 54, p. 509–518.

Roberts, R.J., 1964, Stratigraphy and structure of the Antler Peak quadrangle, Humboldt and Lander Counties, Nevada: U.S. Geological Survey Professional Paper 459–A, 93 p.

Roberts, R.J., and Arnold, D.C., 1965, Ore deposits of the Antler Peak quadrangle, Humboldt and Lander Counties, Nevada: U.S. Geological Survey Professional Paper 459–B, 94 p.

Rock, N.M.S., 1991, Lamprophyres: Glasgow, Blackie; New York, Van Nostrand Reinhold, 285 p.

Roedder, Edwin, 1984, Fluid inclusions: Mineralogical Society of America, Reviews in Mineralogy, v. 12, 644 p.

Samoilov, V.S., Kovalenko, V.I., Naumov, V.B., Sandimirova, G.P., and Chuvashova, L.A., 1988, Immiscibility of silicate and salt melts during the formation of the Mushugai-Huduk alkaline complex (southern Mongolia): Geokhimiya, no. 10, 1988, p. 1,447–1,459 (in Russiam, translation in Roedder, Edwin, ed., 1988, Fluid-inclusion research, v. 21, p. 472–484).

Sayers, R.W., Tippett, M.C., and Fields, E.D., 1968, Duval's new copper mines show complex geologic history: Mining Engineering, v. 20, no. 3, p. 55–62.

Seedorff, Eric, Bailey, C.R.G., Kelley, David, and Parks, Wright, 1991, Buffalo Valley Mine: A porphyry-related gold deposit, Lander County, Nevada, *in* Buffa, R.H., and Coyner, A.R., eds., Geology and ore

deposits of the Great Basin, Field Trip Guidebook Compendium volume 2: Geological Society of Nevada, Symposium, April 1–5, 1990, Reno/Sparks, p. 118–145.

Selverstone, J, Franz, G., and Thomas, S., 1990, Fluids at high pressures: Inferences from 20 kbar eclogites and associated veins in the Tauern Window, Austria [abs.]: V. M. Goldschmidt Conference, Baltimore, Maryland, 1990, Program with Abstracts, p. 81.

Sharp, Z.D., Essene, E.J., and Kelly, W.C., 1985, A re-examination of the arsenopyrite geothermometer: pressure considerations andn applications to natural assemblages: Canadian Mineralogist, v. 23, p. 517–534.

Shinohara, Hiroshi, Kazahaya, Kohei, and Lowenstern, J.B., 1995, Volatile transport in a convecting magma column: Implications for porphyry Mo mineralization: Geology, v. 23, no. 12, p. 1,091–1,094.

Theodore, T.G., 1994, Preliminary geologic map of the Snow Gulch quadrangle, Humboldt and Lander Counties, Nevada, *with a section on* Radiolarians in the Ordovician Valmy Formation and Devonian Scott Canyon Formation, by B.L. Murchey, *and a section on Helicoprion* sp. from the Pennsylvanian and Permian Antler Peak Limestone, Lander County, Nevada, by R.A. Hanger, E.E. Strong, and R.T. Ashinhurst: U.S. Geological Survey Open-File Report 94–436, 31 p.

———1996, Geology and implications of silver/gold ratios in the Elder Creek porphyry copper system, Battle Mountain Mining District, Nevada, *in* Coyner, A.R., and Fahey, P.L., eds., Geology and ore deposits of the American Cordillera, Symposium Proceedings, Geological Society of Nevada, Reno/Sparks, Nevada, April, 1995 (in press).

Theodore, T.G., and Blake, D.W., 1975, Geology and geochemistry of the Copper Canyon porphyry copper deposit and surrounding area, Lander County, Nevada: U.S. Geological Survey Professional Paper 798-B, p. B1–B86.

———1978, Geology and geochemistry of the West ore body and associated skarns, Copper Canyon porphyry copper deposits, Lander County, Nevada, *with a section on* Electron microprobe analyses of andradite and diopside by N.G. Banks: U.S. Geological Survey Professional Paper 798-C, p. C1–C85.

Theodore, T.G., Blake, D.W., Loucks, T.A., and Johnson, C.A., 1992, Geology of the Buckingham stockwork molybdenum deposit and surrounding area, Lander County, Nevada, *with a section on:* Potassium-argon and $^{40}Ar/^{39}Ar$ geochronology of selected plutons in the Buckingham area *by* E.H. McKee, *and a section on* Economic geology *by* T.A. Loucks and C.A. Johnson, *and a section on* Supergene copper deposits at Copper Basin *by* D.W. Blake, *and a section on* Mineral chemistry of Late Cretaceous and Tertiary skarns *by* J.M. Hammarstrom: U.S. Geological Survey Professional Paper 798-D, p. D1–D307.

Theodore, T.G., Silberman, M.L., and Blake, D.W., 1973, Geochemistry and K–Ar ages of plutonic rocks in the Battle Mountain mining district, Lander County, Nevada: U.S. Geological Survey Professional Paper 798–A, 24 p.

Trudu, A.G., and Bloom, M.S., 1988, A genetic model for the origin of hypogene gold in porphyry copper systems; The Tirad porphyry copper-gold deposit (Guinaoang, NW Luzon, Philippines) [abs.]: Bicentennial Gold 88, Geological Society of Australia Abstract Series no. 22, p. 211–216.

Trudu, A.G, Mernagh, T.P., and Bloom, M.S., 1990, Laser Raman microprobe studies of fluid inclusions and the definition of "copper windows" in porphyry copper-gold mineralisation (Tirad prospect, NW Luzon, Philippines)[abs.]: Geological Society of Australia Abstracts Number 25, p. 267–268.

Vanko, D.A., Sutton, S.R., Rivers, M.L., and Bodnar, R.J., 1993, Major-element ratios in synthetic fluid inclusions by synchrotron X–ray fluorescence microprobe: Chemical Geology, v. 109, p. 125–134.

Vila, Tomás, and Sillitoe, R.H., 1991, Gold-rich porphyry systems in the Maricunga belt, northern Chile: Economic Geology, v. 86, no. 6, p. 1,238–1,260.

Vila, Tomás, Sillitoe, R.H., Betzhold, Jorge, and Viteri, Enrique, 1991, The porphyry gold deposit at Marte, northern Chile:

Economic Geology, v. 86, no. 6, p. 1,271–1,286.

Wallace, A.R., 1991, Effect of late Miocene Extension on the exposure of gold deposits in north-central Nevada, *in* Raines, G.L., Lisle, R.E., Schafer, R.W., and Wilkinson, W.H., eds., Geology and ore deposits of the Great Basin, Symposium Proceedings: Reno, Nevada, Geological Society of Nevada, p. 179–183.

Werre, R.W., Jr., Bodnar, R.J., Bethke, P.M., and Barton, P.B., Jr., 1979, A novel gas-flow fluid inclusion heating/freezing stage [abs.]: Geological Society of America, Abstracts and Programs, v. 11, p. 539.

Wilson, J.W.J., Kesler, S.E., Cloke, P.L., and Kelly, W.C., 1980, Fluid inclusion geochemistry of the Granisle and Bell porphyry copper deposits, British Columbia: Economic Geology, v. 75, p. 45–61.

Wopenka, Brigitte, Pasteris, J.D., and Freeman, J.J., 1990, Analysis of individual fluid inclusions by Fourier transform infrared and Raman microspectroscopy: Geochimica et Cosmochimica Acta, v. 54, p. 519–533.

Wotruba, P.R., Benson, R.G., and Schmodt, K.W., 1986, Battle Mountain describes the geology of its Fortitude gold-silver deposit at Copper Canyon: Mining Engineering, July 1986, v. 38, no. 7, p. 495–499.

Yanatieva, O.K., 1946, Solubility polytherms in the system CaCl2–NaCl–H2O, and CaCl2–$MgCl_2$–H_2O: Zhurnal Prikladnoi Khimii, v. 19, p. 707–722.

Zvezdov, V.S., Migachev, I.F., and Girfanov, 1993, Porphyry copper deposits of the CIS and the models of their formation: Ore Geology Reviews, v. 7, p. 511–549.

Zwart, E.W., and Touret, J.L.R., 1994, Melting behavior and composition of aqueous fluid inclusions in fluorite and calcite: applications within the system H_2O–$CaCl_2$–NaCl: European Journal of Mineralogy, v. 6, p. 773–786.

Table 1—Summary of temperature data from fluid-inclusions hosted by quartz in the Elder Creek porphyry copper system.

[All data from vein quartz unless indicated otherwise;----do.----, same as above; Porph. monz., porphyritic monzogranite of Elder Creek]

Loc no. (fig. 2)	Sample number	Host rock	Type of fluid inclusion[1]	Liquid-vapor homogenization temp. range (°C)
1	93TT100	[2]Harmony Fm.	I	196–389 (32)[3]
			II	387–416 (2)
			III	265–448 (10)
2	93TT099	----do.----	I	201–382 (26)
			II	379–>500 (2)
			III	313–336 (7)
3	93TT101	----do.----	I	201–382 (13)
			II	423–496 (3)
			III	309–580 (25)
4	93TT081	----do.----	I	120–357 (24)
5	93TT023	[4]Porph. monz.	I	330–376 (2)
			II	408–410 (2)
			III	260–387 (8)
5	[5]93TT023	Porph. monz.	I	298–>505 (10)
			II	318–389 (2)
			III	372–400 (5)
6	93TT102	Harmony Fm.	I	285–>450 (18)
			II	387–406 (5)
			III	276–395 (21)
7	[5]93TT107	Porph. monz.	I	205–330 (33)
			II	448–498 (2)
			III	330–460 (12)
8	93TT109	----do.----	I	182–450 (16)
			II	390–445 (3)
			III	280–410 (12)
9	93TT108	----do.----	I	305–443 (20)
			II	402–483 (4)
			III	360–390 (4)
10	95TT001	Harmony Fm.	I	236–371 (22)
			III	254–304 (4)
10	95TT002	----do.----	I	237–365 (38)
11	93TT089	----do.----	I	114–401 (27)
			II	394–459 (5)
			III	192–444 (9)

Table 1—continued

12	93TT088	----do.----	I	270–454 (20)
			III	234–463 (19)
13	93TT104	Porph. monz.	I	308–368 (27)
			III	230–386 (3)
14	93TT103	----do.----	I	290–326 (9)
14	[5]93TT103	----do.----	I	322–348 (9)
			III	110–338 (5)
15	93TT087	Harmony Fm.	I	274–336 (29)
			III	215–342 (6)
16	93TT083	----do.----	I	251–368 (32)
			III	267–415 (10)

[1]At room temperature: I, low vapor volume+mostly liquid H_2O—may include an opaque mineral as well as some CO_2; II, high vapor volume+mostly liquid H_2O—may include an opaque mineral as well as some CO_2; III, halite bearing+typically containing a number of other translucent daughter minerals, as well as±opaque mineral(s) and some CO_2.

[2]Rocks of Upper Cambrian Harmony Formation typically contact metamorphosed to dense biotite hornfels and show presence of K–feldspar selvages on mineralized quartz veins associated with porphyry copper system.

[3]In parentheses, number of determinations of temperatures of homogenization.

[4]Generally contains abundant quartz phenocrysts.

[5]Fluid-inclusion data obtained from phenocrystic quartz.

Table 2—Representative microprobe analyses of arsenopyrite from quartz-arsenopyrite-stibnite-pyrite vein at 1,090–ft depth at location 10 (fig. 2).

[--, not detected; analyst, R.L. Oscarson, U.S. Geological Survey, Menlo Park]

	Microprobe analyses (weight percent)		
Fe	33.6	33.7	33.9
Co	.04	.04	.04
Ni	.02	--	--
Sb	--	.03	.03
Bi	.09	.03	.07
Au	--	--	--
As	44.8	45.5	44.6
S	20.7	19.9	20.9
Ag	--	--	--
Cu	.01	.02	--
Zn	.01	.01	--
Pb	--	--	--
Total	99.27	99.13	99.54

LIST OF ILLUSTRATIONS

Figure 1—Generalized geologic map of the Antler Peak quadrangle and the Battle Mountain Mining District, Lander and Humboldt Counties, Nev. Geology modified from Roberts (1964), and Theodore (1991, 1994).

Figure 2—Geologic map of the general area of the Elder Creek porphyry copper system showing locations of mined polymetallic veins, alteration zoning, and fluid-inclusion sample locations. Geology modified from Theodore (1994).

Figure 3—Back-scattered electron micrographs of ilmenite-sphene relations in presumably Tertiary biotite-hornblende lamprophyre. Sample 93TT020. S, sphene; ilm, ilmenite; bi, biotite; hb, hornblende; Z, zircon; ap, apatite. *A*, sharp crystal boundary between primary hornblende and primary biotite, which includes a small clot of ilmenite mantled by sphene as well as small grains of apatite. Ilmenite includes small grains of zircon, and even smaller grains of zircon, <1 μm wide, are enclosed in biotite; *B*, clot of ilmenite mantled by sphene intergrown and interstitial to primary biotite which includes zircon.

Figure 4—Photographs showing outcrops of the late Eocene or early Oligocene porphyritic monzogranite of Elder Creek cut by dense networks of quartz stockwork veins near the core of the porphyry copper system. *A*, Relatively coarse-grained porphyritic monzogranite veined by quartz approximately 0.4 km south-southwest of the Morning Star Mine; *B*, biotite hornfels of the Upper Cambrian Harmony Formation approximately 0.9 km west of the Morning Star Mine and near the outer limit of the area intensely veined by quartz in the core of the porphyry system. Gossan at this latter locality suggests a relatively high Fe/Cu ratio.

Figure 5—Photomicrographs showing aplitic groundmass of the porphyritic monzogranite of Elder Creek. G, quartz plus K–feldspar groundmass; Q, quartz; P, plagioclase; A, amphibole; B, biotite. *A*, Relatively small-scale view of textural relations among groundmass and phenocrysts. Sample 93TT107, crossed nicols. *B*, Close-up view of textural relations among groundmass and phenocrysts. Sample 93TT091, partially-crossed nicols.

Figure 6—Photomicrographs of type I fluid inclusions in vein quartz (Q) from quartz-arsenopyrite vein at 1,090–ft depth at locality 10 (fig. 2). Sample 95TT002. *A*, isolated primary or pseudosecondary fluid inclusion showing liquid-vapor phase proportion typical in sample. Most type I fluid inclusions from this locality show homogenization temperatures near 300 °C. *B*, secondary or pseudosecondary type I fluid inclusions; *C*, relatively isolated primary or pseudosecondary type I and type II (at head of arrow) fluid inclusions. Type II fluid inclusion completely filled by vapor. *D*, closeup of type I fluid inclusion shown in C. The apparent daughter mineral in left side of fluid inclusion results from irregularities in wall of fluid-inclusion cavity.

Figure 7—Infrared spectra of absorbance versus wavenumber for a two-phase type I fluid inclusion and a type II fluid inclusion, both of which contain CO_2. Sketches of approximate phase proportions of fluid inclusions at room temperature also shown—both fluid inclusions also contain an opaque mineral. *A*, type I fluid inclusion showing broad absorbance band for liquid water. The sharp peak at 2,350 cm^{-1} is superimposed on a slightly broader peak, the latter which is likely to be the doublet due to CO_2 gas. The sharp singlet appears to be caused by liquid CO_2, even though there was no second liquid phase

observed under the microscope. Sample 93TT107. *B*, type II fluid inclusion also shows the broad band for liquid water, though the peak is small due to the lesser size of the fluid inclusion. At 2,350 cm^{-1}, only a doublet is observed, indicating gaseous CO_2, fluid notwithstanding the obvious presence of liquid CO_2 visible within the fluid inclusion. This result could be due to the small size of the inclusion and the geometry of the beam path through the sample. Sample 93TT100.

Figure 8—Photomicrograph of primary or pseudosecondary type II fluid inclusions (at heads of arrows). Q, vein quartz in 1–cm-wide quartz vein that cuts porphyritic monzogranite of Elder Creek. Sample 93TT091.

Figure 9—Secondary scanning electron micrographs of artificially broken and polished surfaces showing minerals in and around type III fluid-inclusion cavities. Q, quartz; H, halite; S, sylvite; IC, iron chloride; FX, iron±manganese oxide (magnetite). *A*, Halite, sylvite, and iron-manganese oxide. Sample 93TT023. *B*, iron oxide (magnetite?), iron chloride, iron-potassium chloride (FK), halite, and a clot of several minerals that, in all, may include sylvite and iron±manganese oxide (magnetite) (UNK). Sample 93TT085. *C*, a number of small euhedral sylvite crystals that apparently have fallen out of a train of aligned fluid inclusion cavities. Sample 93TT029. *D*, halite grain probably masking an underlying grain of iron chloride, both of which protrude from a fluid-inclusion cavity from which a number of extremely small ovoid grains of halite have formed as dessication products when fluid-inclusion waters dried on the surrounding broken surface as the fluid-inclusion cavity was opened. Sample 93TT081. *E*, triangular-shaped iron-manganese oxide resting on calcium chloride (CC) and possibly sylvite, as well as a clot of unknown mineral(s) that include Fe, Ca, Mn, Ti, K, and Cl (UNK). Sample 93TT104. *F*, iron chloride, calcium chloride (CC), and sylvite. Sample 93TT023. *G*, ilmenite (ILM). Sample 93TT085. *H*, probable erythrosiderite ($K_2FeCl_5 \cdot H_2O$) (ER). Sample 93TT021. *I*, barite (BA). Sample 93TT023. *J*, polished surface showing a number of apatite (AP) crystals in fluid-inclusion cavities. Sample 93TT109.

Figure 10—Secondary scanning electron micrographs of artificially broken surfaces showing iron-molybdenum minerals in some fluid-inclusion cavities. Sample 93TT087. *A*, Relatively small-scale view of broken surface. Minerals at heads of arrows are iron-molybdenum-oxide minerals that probably resulted from hydrogen diffusion out of fluid-inclusion cavities late in paragenesis of the system. *B*, closeup of probable ferrimolybdite (ideally $Fe_2O_3 \cdot 3MoO_3 \cdot 8H_2O$) (FB). There also may be some powellite ($Ca(Mo,W)O_4$) in with the larger of the two minerals.

Figure 11—Photomicrographs showing textural relations of apatite to fluid inclusions in vein quartz. Q, quartz; AP, apatite; OP, unknown opaque mineral. Sample 93TT109. *A*, fluid inclusion completely containing opaque mineral and partly containing elongate crystal of apatite which projects well into the surrounding vein quartz. Homogenization by vapor disappearance occurs at 374 °C, and eutectic temperature is –40.2 °C suggesting a significant calcium component in the fluid-inclusion waters. Out of focus along apatite crystal near top of photomicrograph (at head of arrow) is a similar relation between fluid-inclusion waters and apatite. *B*, apparently hypersaline fluid inclusion containing two crystals of apatite and a halite crystal (H). Homogenization by vapor disappearance occurs at 406 °C (apatite does not dissolve), and eutectic temperature is –74.2 °C suggesting a significant number of components in the fluid-inclusion waters. Halite dissolves at 208 °C, and fluid inclusion also contains some CO_2. *C*, fluid inclusion similar to that shown in *A* next to two elongate crystals of apatite that terminate with an opaque mineral between them. We infer that a fluid inclusion was at one time enclosed the opaque mineral. *D*,

calcium-bearing type I fluid inclusions (I) near fluid inclusion containing apatite (at head of arrow).

Figure 12—Summary diagrams showing homogenization temperature versus eutectic temperature. *A*, fluid inclusions from within area of quartz stockwork veins that are probably complex NaCl–KCl–$CaCl_2$–($FeCl_3$)–(CO_2)–H_2O saline to hypersaline brines enriched with various base metals (including copper, lead, and zinc), as well as barium and other minor anions; *B*, fluid inclusions from within area of quartz stockwork veins that are probably $CaCl_2$–(NaCl)–(KCl)–H_2O moderate salinity brines; *C*, fluid inclusions from within area of quartz stockwork veins that are NaCl–KCl–$CaCl_2$–H_2O moderate salinity brines, or NaCl–(KCl)–H_2O–CO_2 relatively low salinity fluids; *D*, fluid inclusions, which are in vein quartz associated with quartz-arsenopyrite veins at 1,090–ft depths at locality 10 (fig. 2), that are NaCl–KCl–$CaCl_2$–H_2O saline brines and moderate salinity brines.

Figure 13—Summary diagrams showing homogenization temperature versus weight percent NaCl equivalent. *A*, data from within area of quartz stockwork veins; *B*, data from vein quartz associated with quartz-arsenopyrite veins at 1,090–ft depths at locality 10 (fig. 2).

Figure 14—Pressure-temperature diagram showing trapping conditions (shaded) possible for type III fluid inclusions at Elder Creek that homogenize by halite dissolution. H, halite; L, liquid; V, vapor; ISO, isochore dividing high-temperature field that shows final homogenization of type III fluid inclusions to liquid (ThL) and low-temperature field that shows final homogenization of type III fluid inclusions by halite dissolution (TmH). Modified from Cline and Vanko (1995).

Figure 15—Fluid-inclusion data at Elder Creek contoured by interpolating to a square grid (using approximately a 100–m grid value) by means of a routine based on the principal of minimum curvature (Briggs, 1974). Explanation same as figure 2. *A*, highest temperature of filling by vapor disappearance of most saline fluid inclusion measured from each locality; *B*, highest salinities (weight percent NaCl equivalent) determined from each locality; *C*, mean temperature of all homogenization temperatures measured at each locality.

Figure 16—Back-scattered electron micrographs showing arsenopyrite-galena textural relations in polished surfaces of quartz-arsenopyrite veins at locality 10. Q, quartz; ASP, arsenopyrite; GN, galena. *A*, large clot of arsenopyrite including microcracks filled by galena. Sample 95TT001. *B*, large clot of arsenopyrite showing most galena present as minute blebs in surrounding quartz. Sample 95TT002. *C*, blebs of galena totally engulfed by well-formed arsenopyrite crystal that has typical kite-shaped form. Sample 95TT002.

Figure 17—Back-scattered electron micrographs showing textural relations of sulfosalt minerals in polished surfaces of quartz-arsenopyrite veins at locality 10. *A*, boulangerite (B) (ideally $5PbS \cdot 2Sb_2S_3$) cutting argentiferous tetrahedrite (T) (ideally $5Cu_2S \cdot 2(Cu,Fe,Zn)S \cdot 2Sb_2S_3$) in quartz (Q). Sample 95TT001. *B*, boulangerite (B) and stibnite (S) in carbonate mineral (C).

Figure 18—X–ray intensity maps showing distribution of elements in a select arsenopyrite crystal from quartz-arsenopyrite vein at locality 10. Sample 95TT002. *A*, iron; *B*, cobalt; *C*, arsenic (hook-shaped pattern in central part of grain is result of plotting problem); *D*, copper (none detected); *E*, sulfur.

Figure 19—X–ray intensity maps showing distribution of elements in a select pyrite crystal from quartz-arsenopyrite vein at locality 10. Sample 95TT002. *A*, iron; *B*, cobalt; *C*, arsenic, demonstrating presence of small crystals of arsenopyrite near margins of pyrite and also demonstrating apparent compatibility between arsenopyrite and pyrite; *D*, copper, only traces detected; *E*, sulfur.

Figure 20—Basal quadrilateral of ternary Fe–As–S diagram showing 82 microprobe analyses of arsenopyrite from a select sample of quartz-arsenopyrite vein from locality 10 plotted using atomic percent of end-member elements. Sample 95TT001.

Figure 1

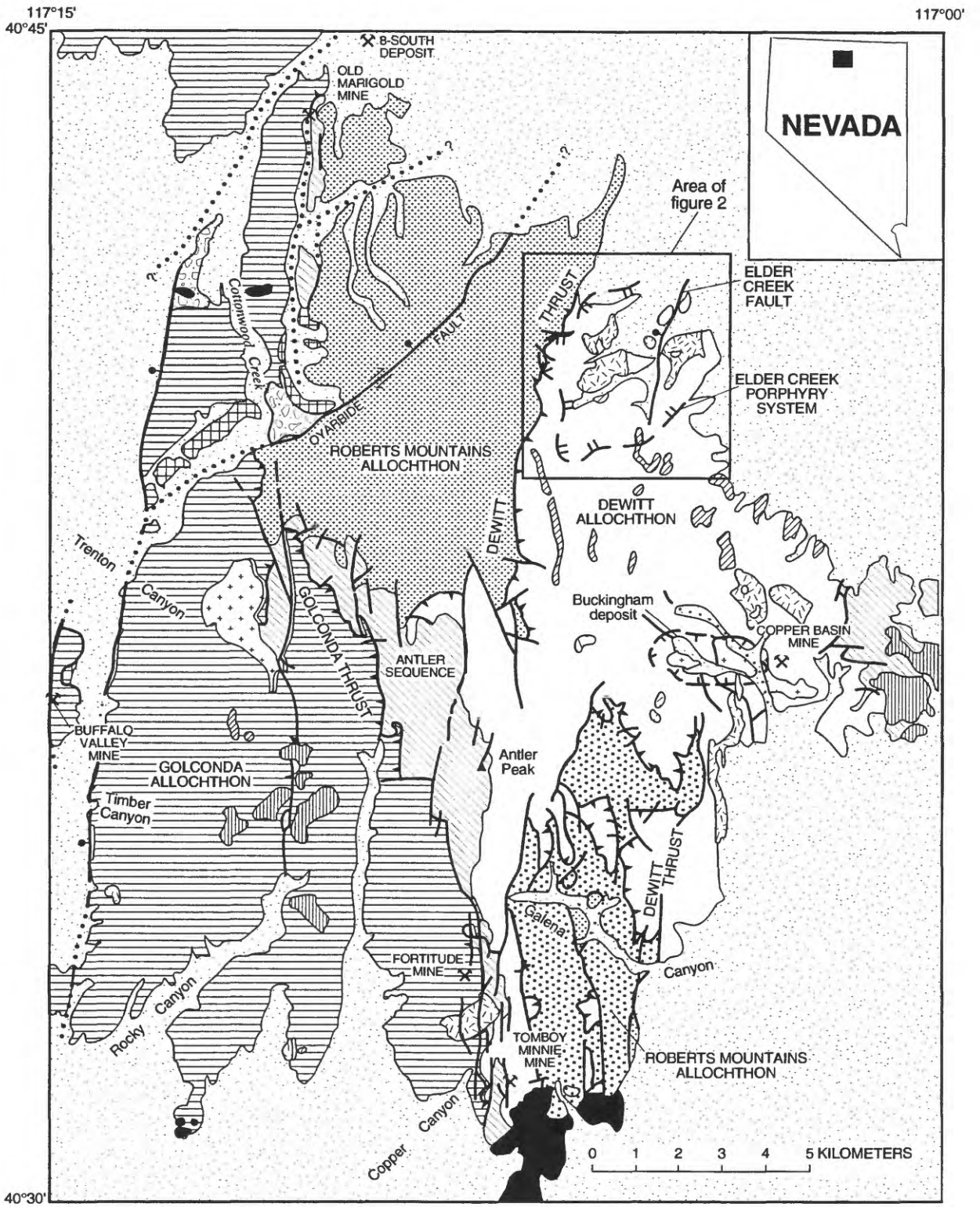
117°15'
117°00'
40°45'
40°30'
B-SOUTH DEPOSIT
OLD MARIGOLD MINE
NEVADA
Area of figure 2
ELDER CREEK FAULT
THRUST
ELDER CREEK PORPHYRY SYSTEM
Cottonwood Creek
FAULT
OVERTHRUST
ROBERTS MOUNTAINS ALLOCHTHON
DEWITT
DEWITT ALLOCHTHON
Trenton Canyon
GOLCONDA THRUST
ANTLER SEQUENCE
Buckingham deposit
COPPER BASIN MINE
BUFFALO VALLEY MINE
GOLCONDA ALLOCHTHON
Antler Peak
Timber Canyon
DEWITT THRUST
Galena Canyon
FORTITUDE MINE
Rocky Canyon
TOMBOY MINNIE MINE
ROBERTS MOUNTAINS ALLOCHTHON
Copper Canyon
0 1 2 3 4 5 KILOMETERS

Figure 1—continued

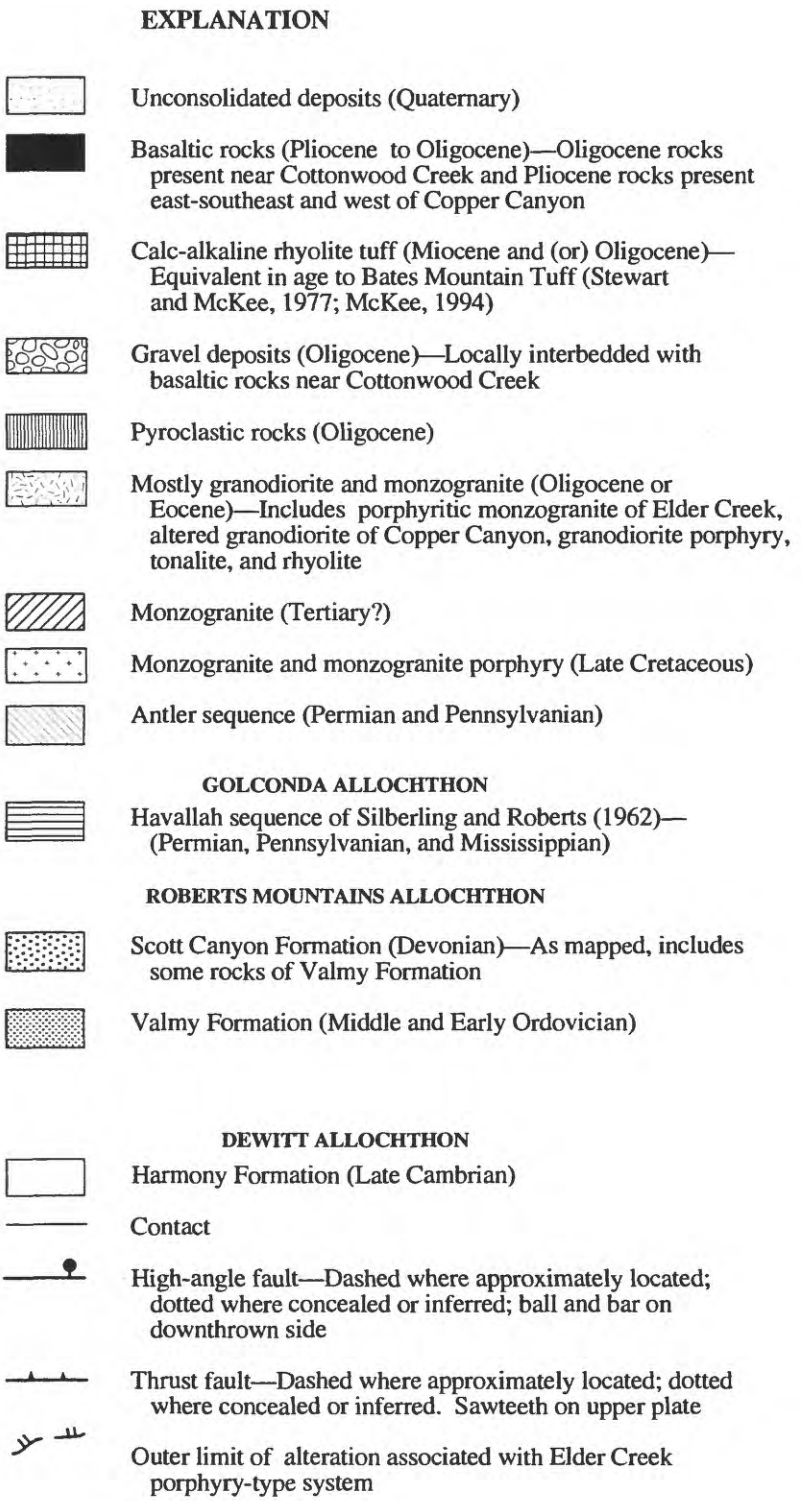

Figure 2

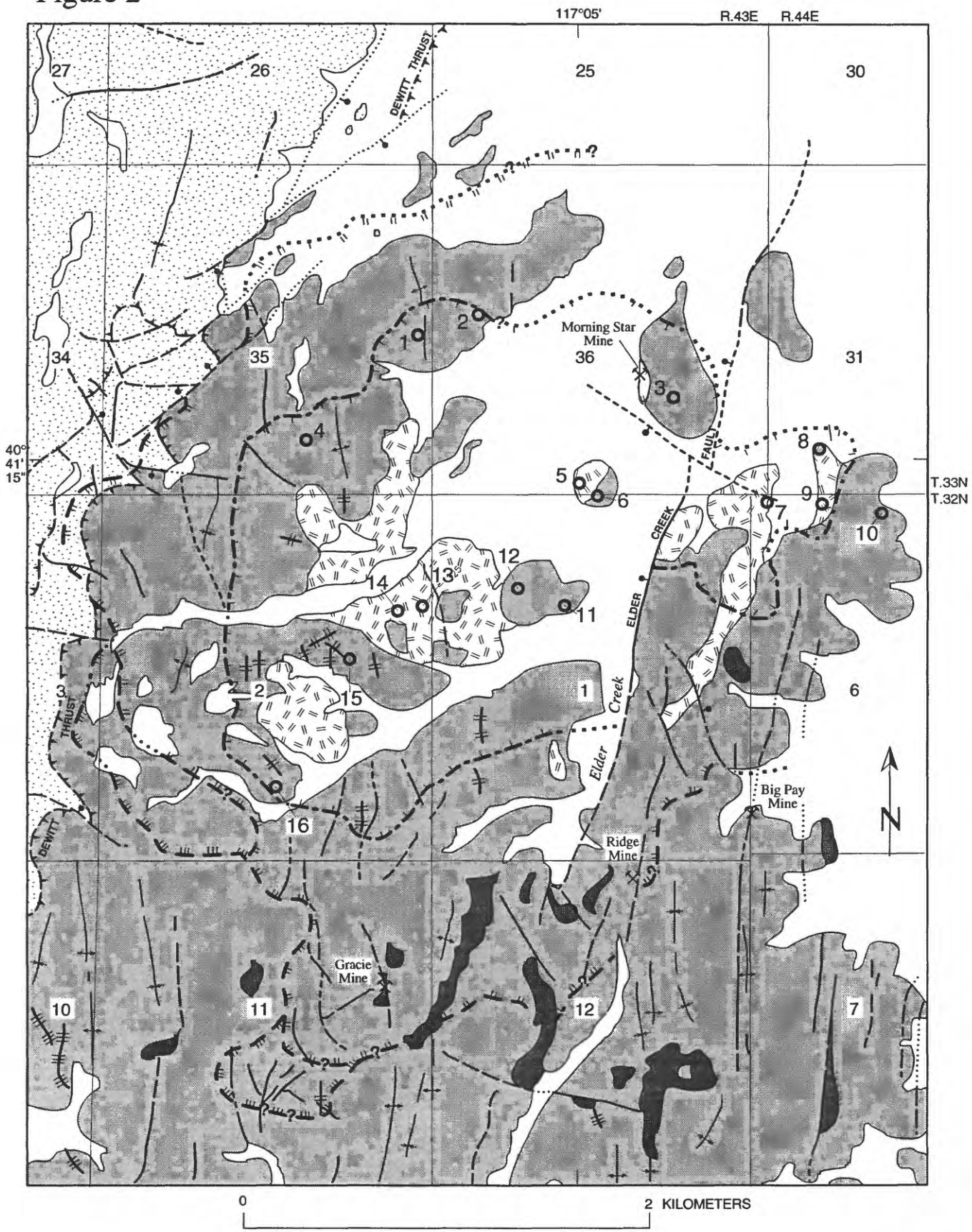
117°05'
R.43E
R.44E
DEWITT THRUST
27
26
25
30
Morning Star Mine
36
31
34
35
40° 41' 15"
FAULT
T.33N
T.32N
ELDER CREEK
Elder Creek
3 THRUST
DEWITT
Big Pay Mine
Ridge Mine
Gracie Mine
N
0
2 KILOMETERS

Figure 2—continued

EXPLANATION

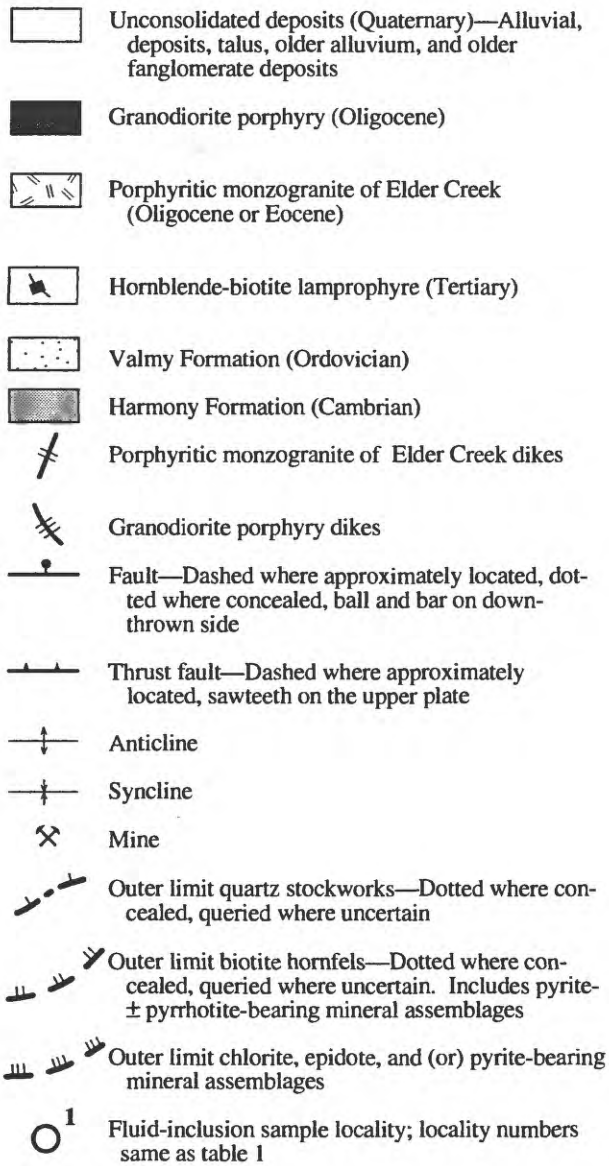

Unconsolidated deposits (Quaternary)—Alluvial, deposits, talus, older alluvium, and older fanglomerate deposits

Granodiorite porphyry (Oligocene)

Porphyritic monzogranite of Elder Creek (Oligocene or Eocene)

Hornblende-biotite lamprophyre (Tertiary)

Valmy Formation (Ordovician)

Harmony Formation (Cambrian)

Porphyritic monzogranite of Elder Creek dikes

Granodiorite porphyry dikes

Fault—Dashed where approximately located, dotted where concealed, ball and bar on downthrown side

Thrust fault—Dashed where approximately located, sawteeth on the upper plate

Anticline

Syncline

Mine

Outer limit quartz stockworks—Dotted where concealed, queried where uncertain

Outer limit biotite hornfels—Dotted where concealed, queried where uncertain. Includes pyrite-± pyrrhotite-bearing mineral assemblages

Outer limit chlorite, epidote, and (or) pyrite-bearing mineral assemblages

Fluid-inclusion sample locality; locality numbers same as table 1

Figure 3

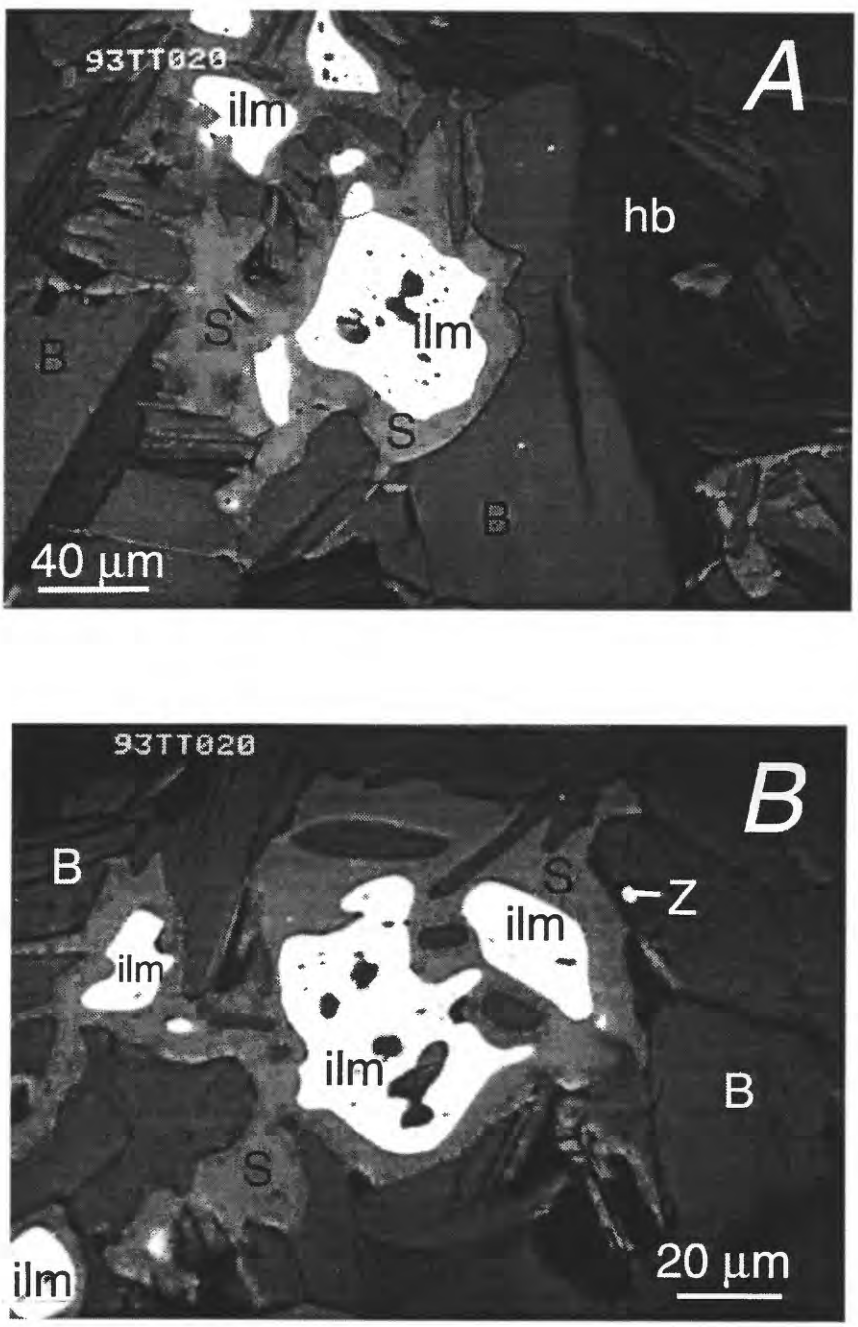
93TT020
A
ilm
hb
S
ilm
B
S
B
40 µm
93TT020
B
B
S
Z
ilm
ilm
ilm
B
S
ilm
20 µm

Figure 4

Figure 5

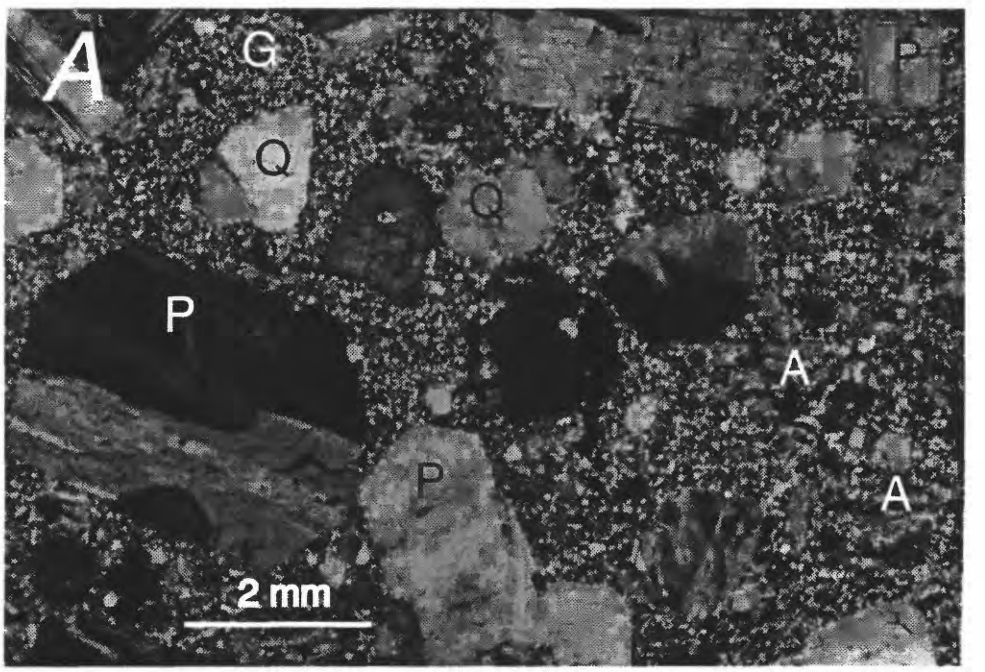

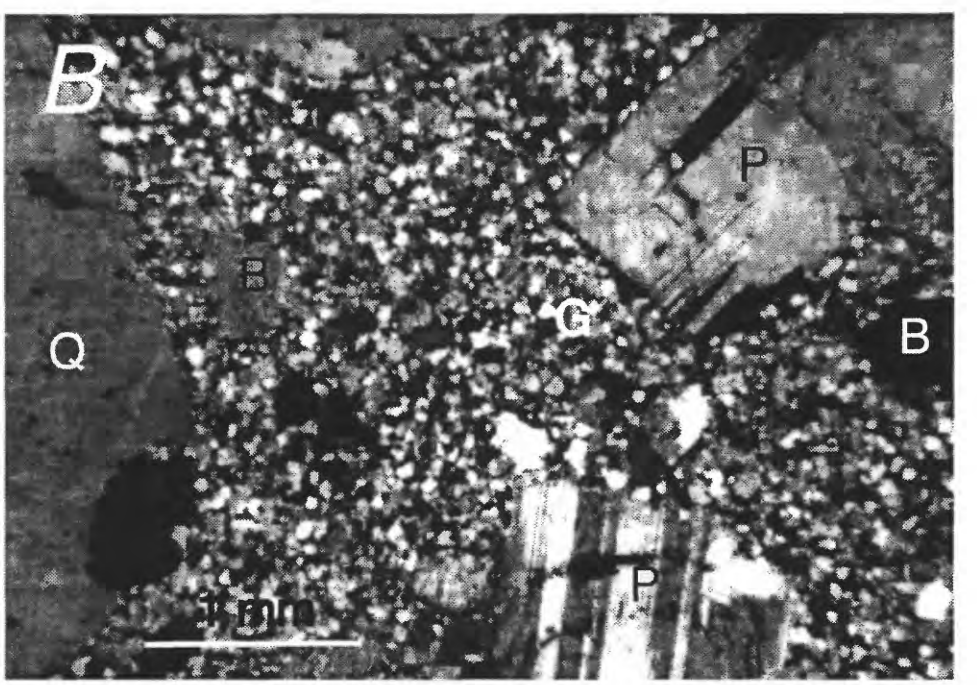

Figure 6

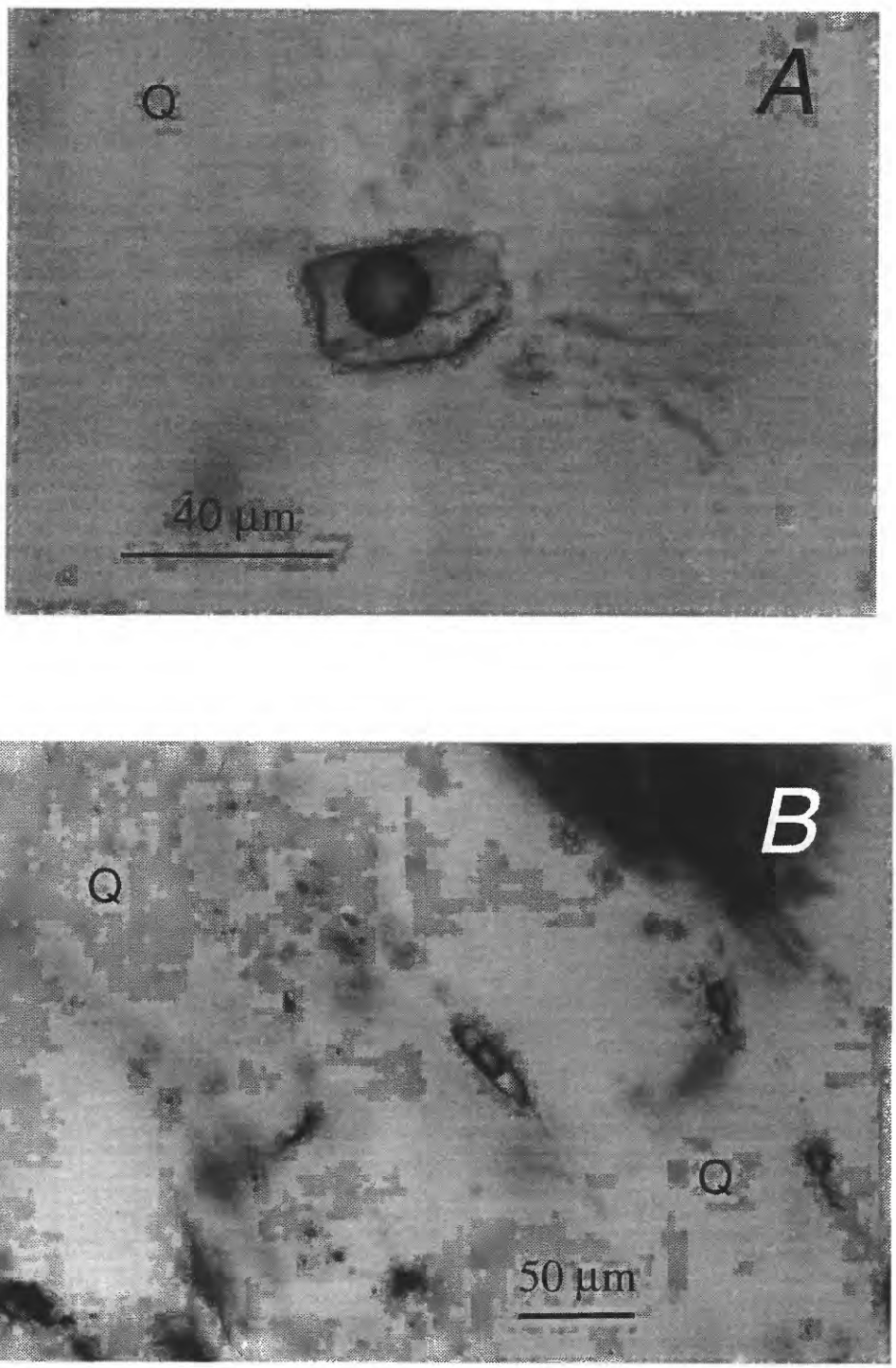

Figure 6—continued

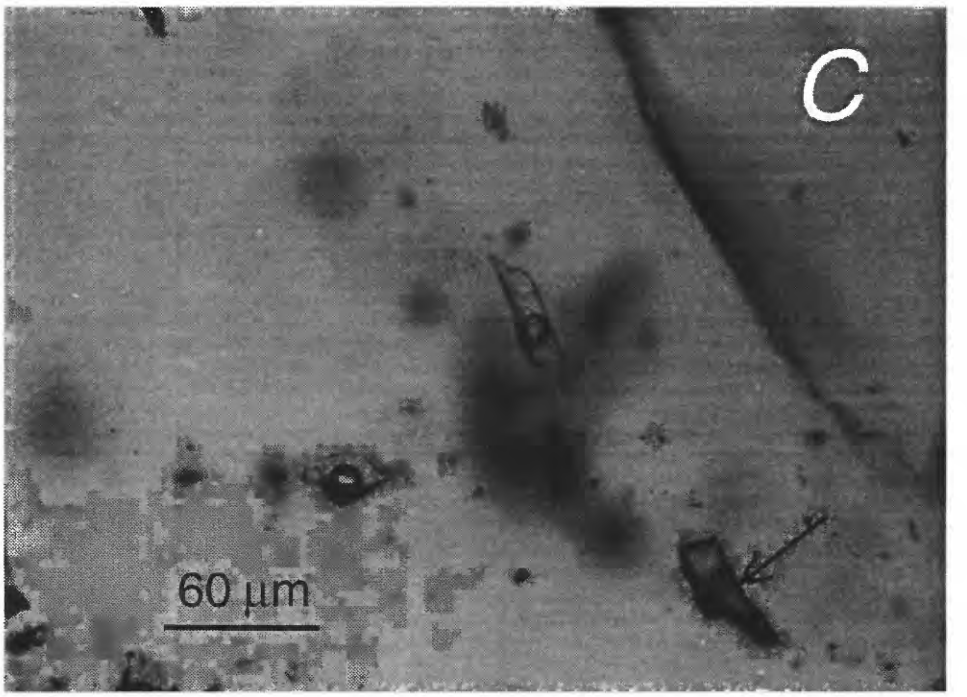

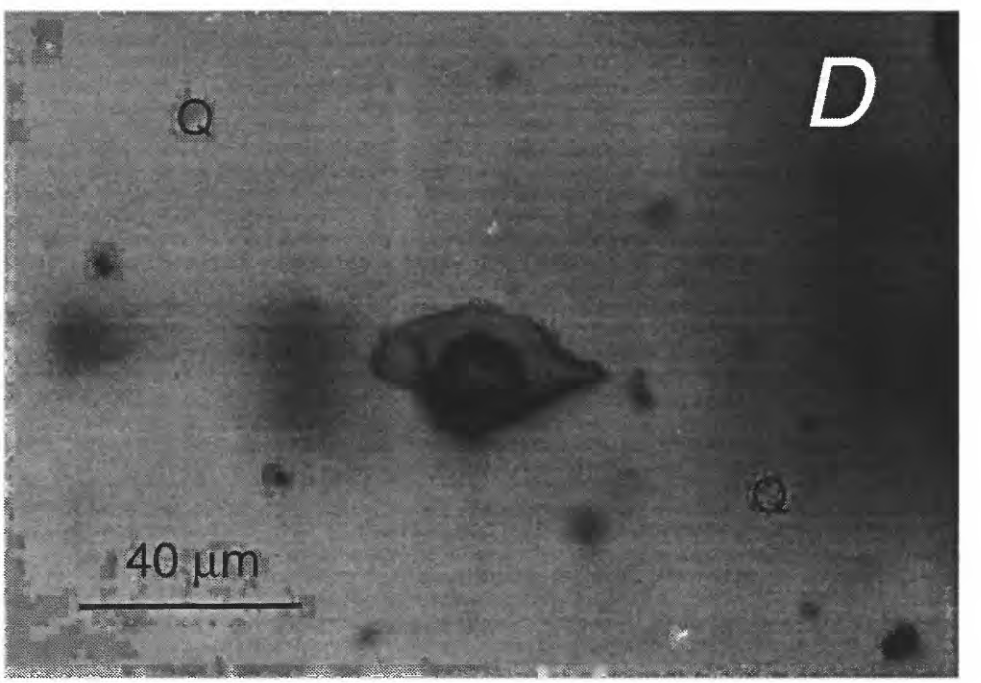

Figure 7

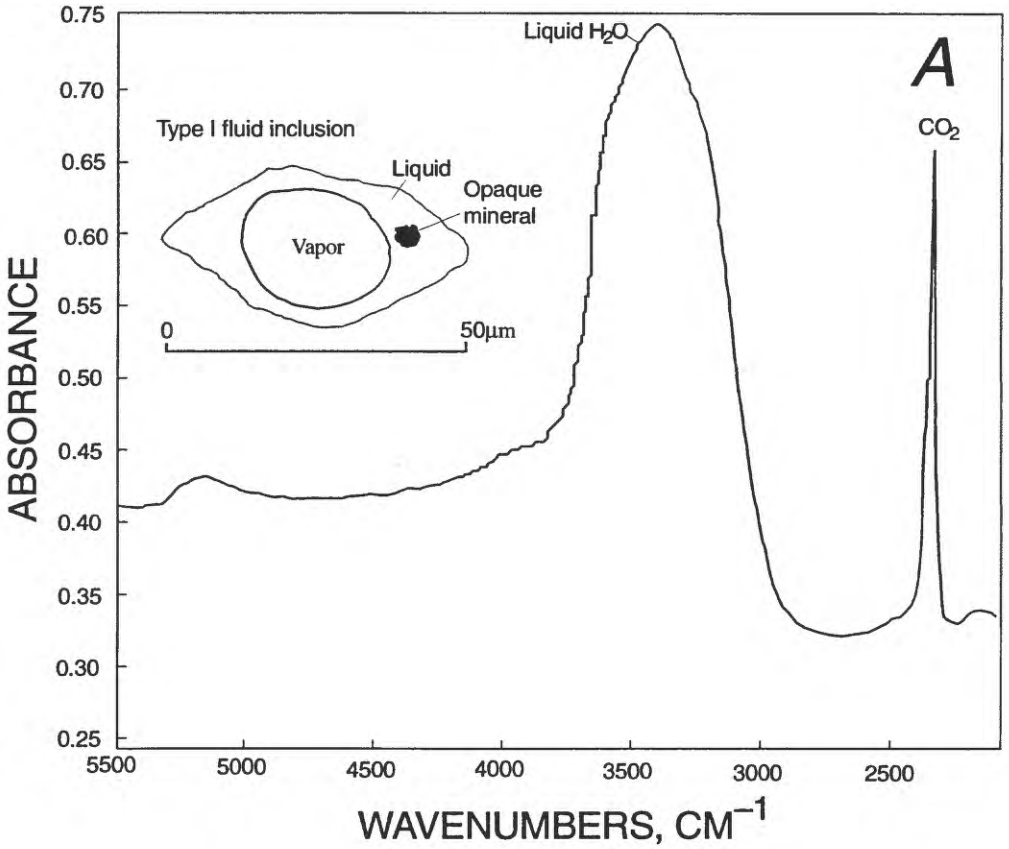
A
Liquid H_2O
CO_2
Type I fluid inclusion
Liquid
Opaque mineral
Vapor
0
50µm
ABSORBANCE
0.75
0.70
0.65
0.60
0.55
0.50
0.45
0.40
0.35
0.30
0.25
5500
5000
4500
4000
3500
3000
2500
WAVENUMBERS, CM^{-1}

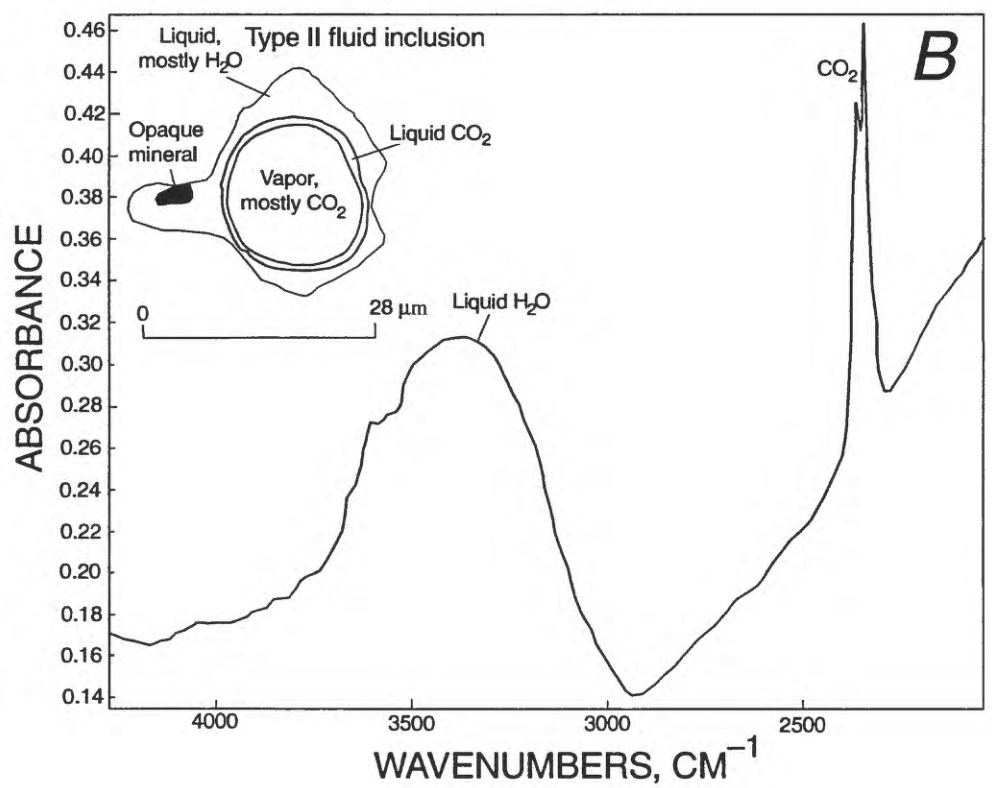
B
Liquid, mostly H_2O
Type II fluid inclusion
CO_2
Opaque mineral
Liquid CO_2
Vapor, mostly CO_2
0
28 µm
Liquid H_2O
ABSORBANCE
0.46
0.44
0.42
0.40
0.38
0.36
0.34
0.32
0.30
0.28
0.26
0.24
0.22
0.20
0.18
0.16
0.14
4000
3500
3000
2500
WAVENUMBERS, CM^{-1}

Figure 8

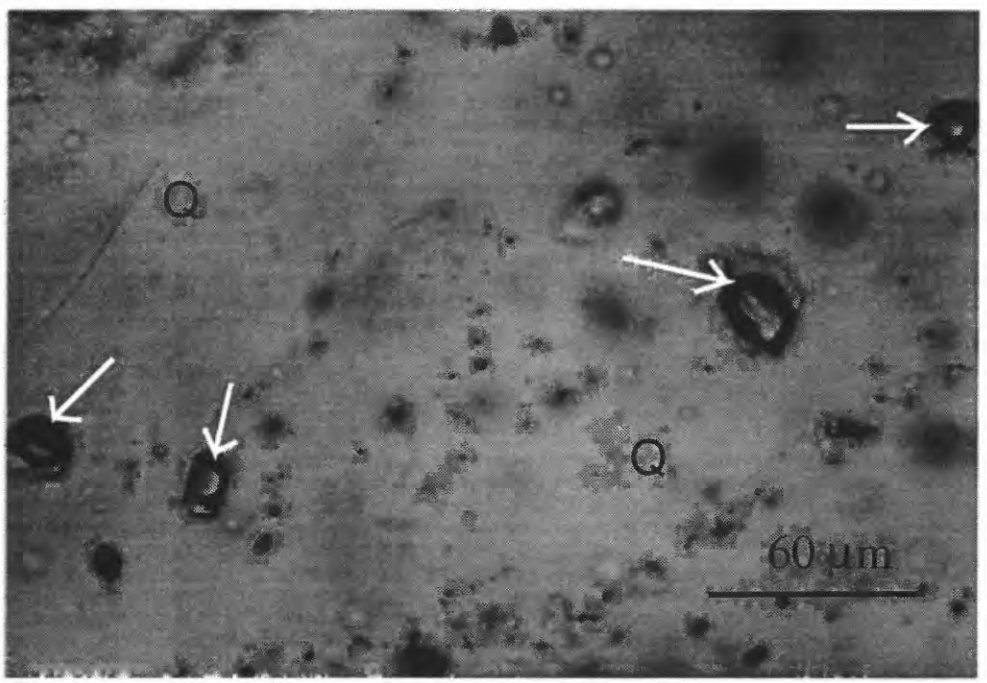

Figure 9

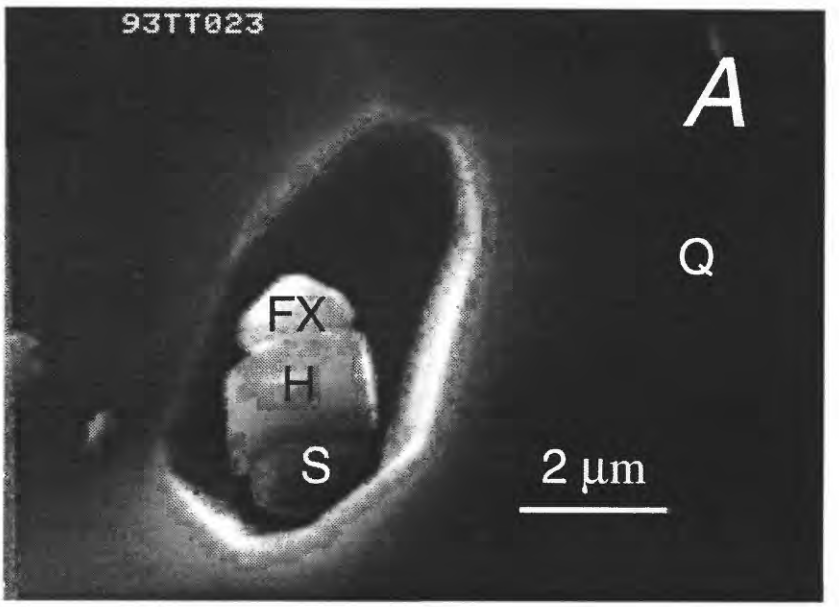

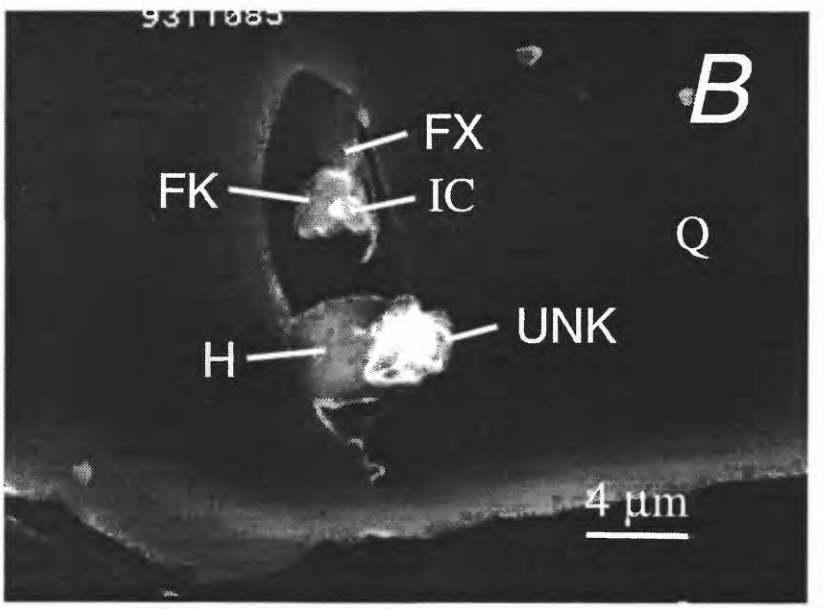

Figure 9—continued

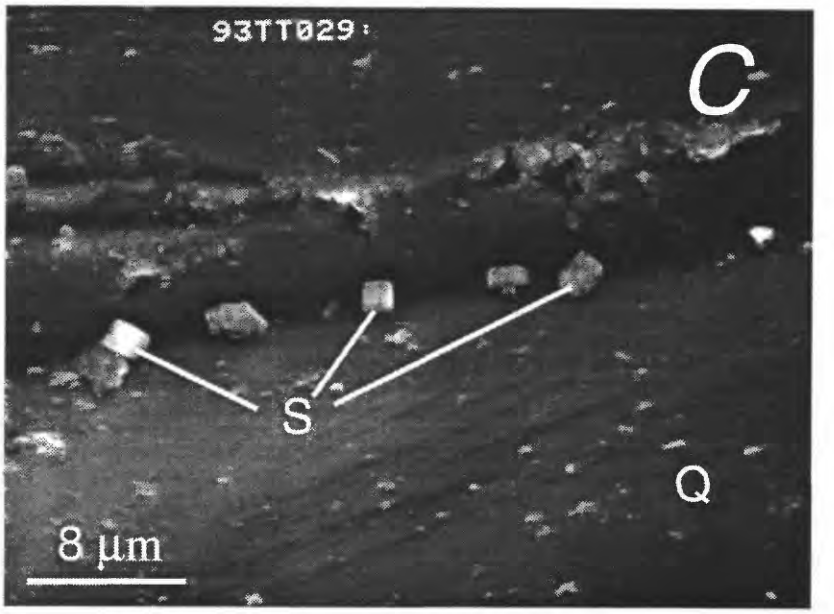

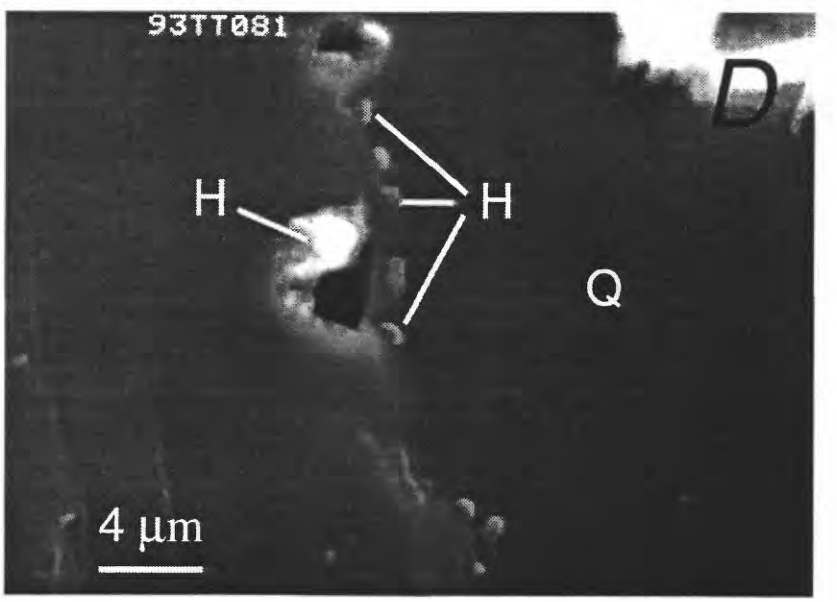

Figure 9—continued

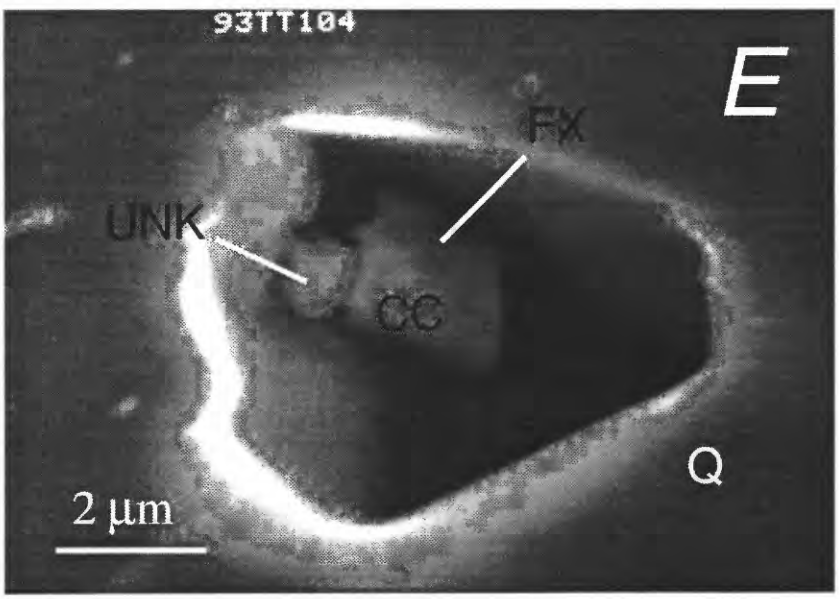

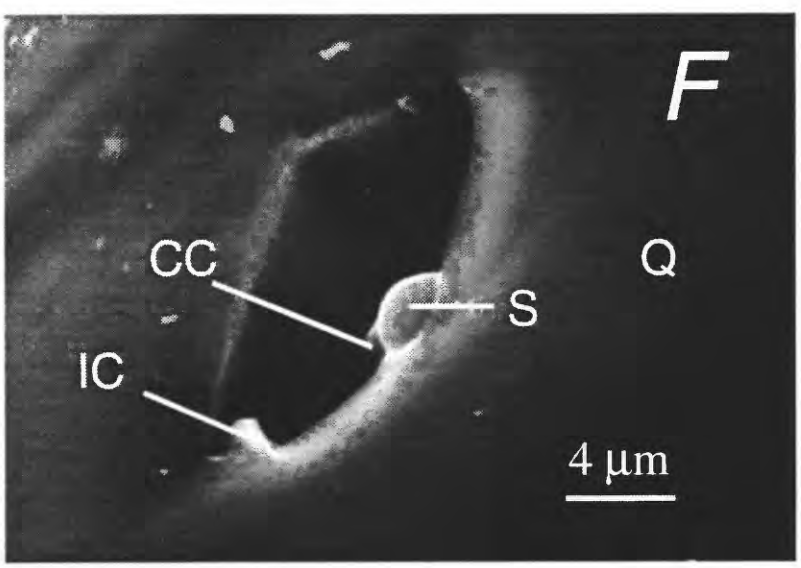

Figure 9—continued

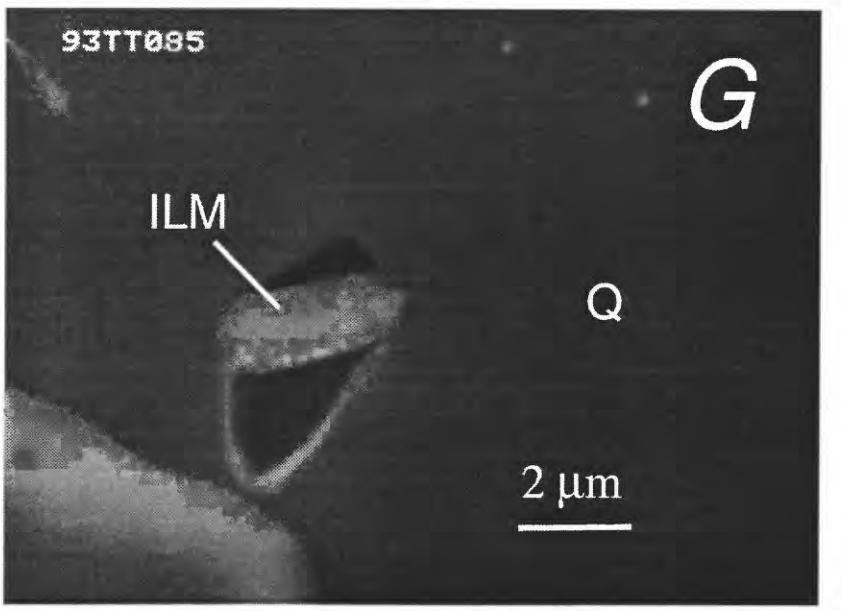

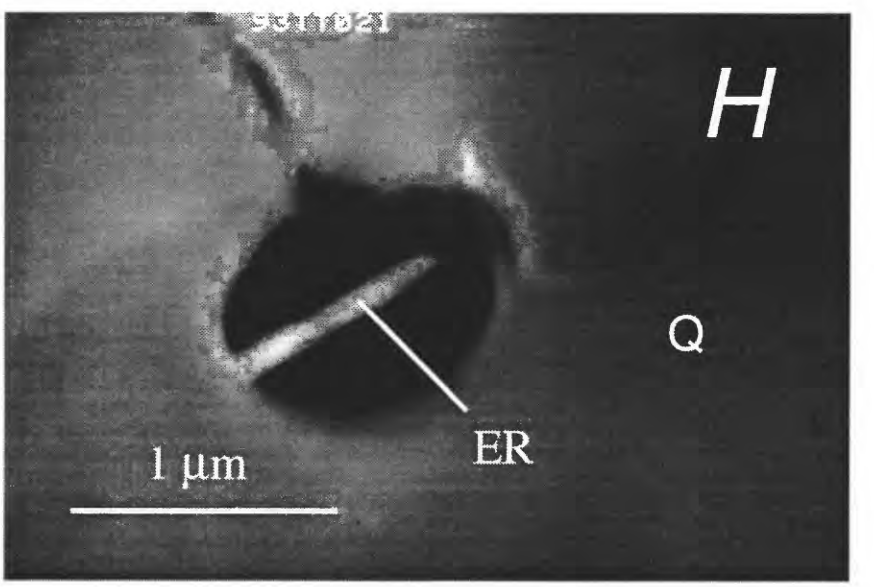

Figure 9—continued

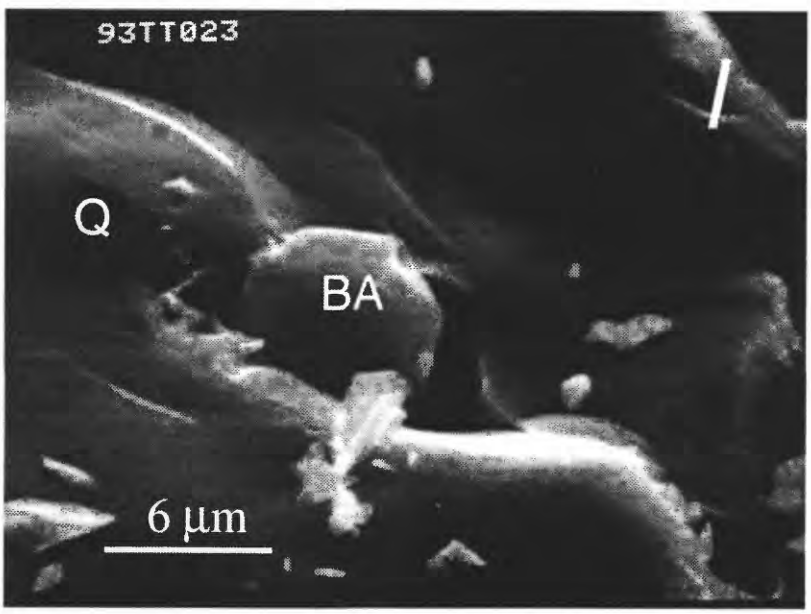

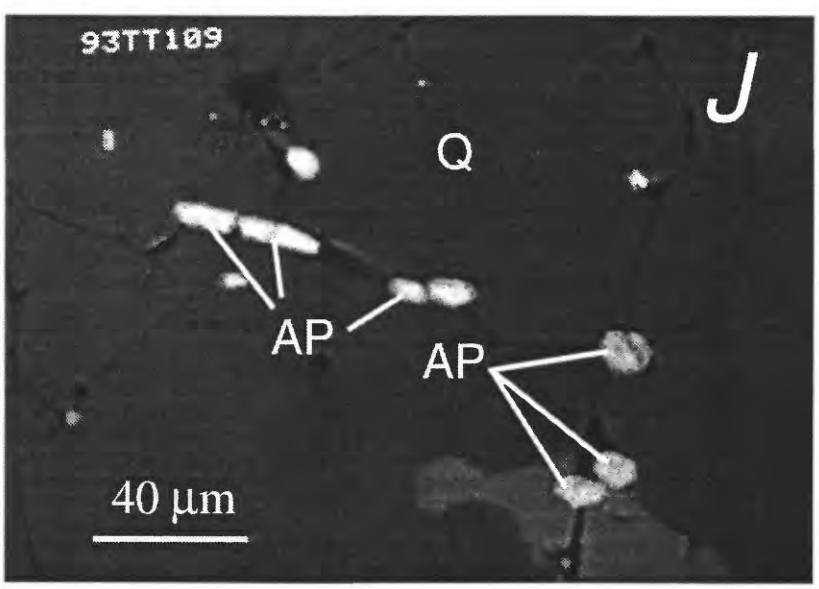

Figure 10

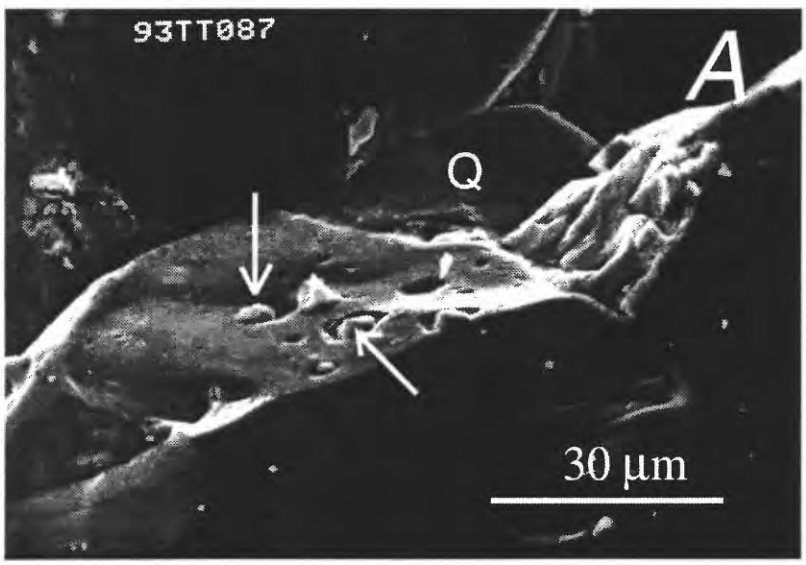

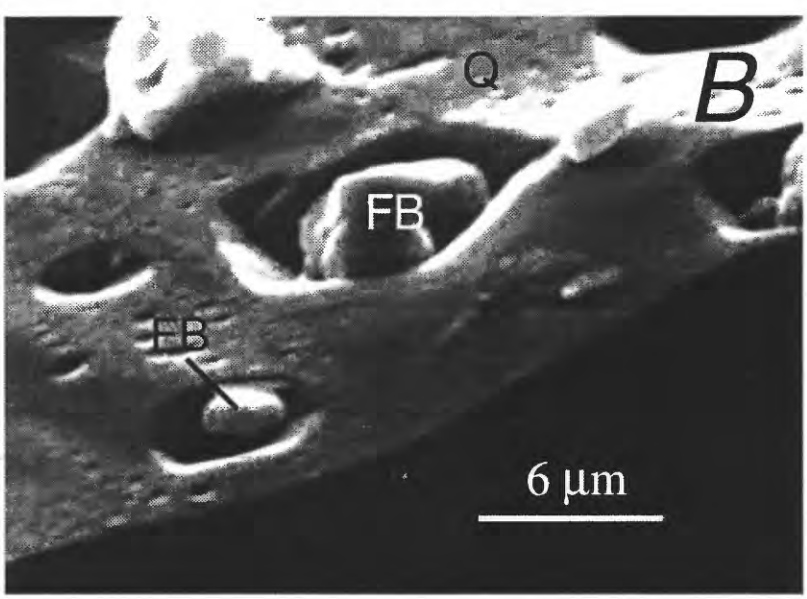

Figure 11

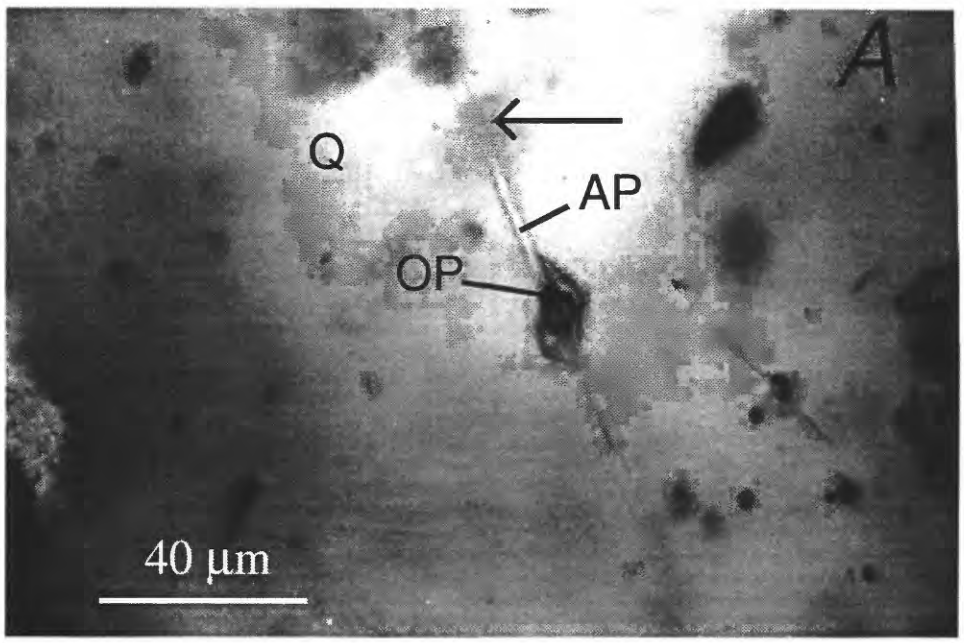

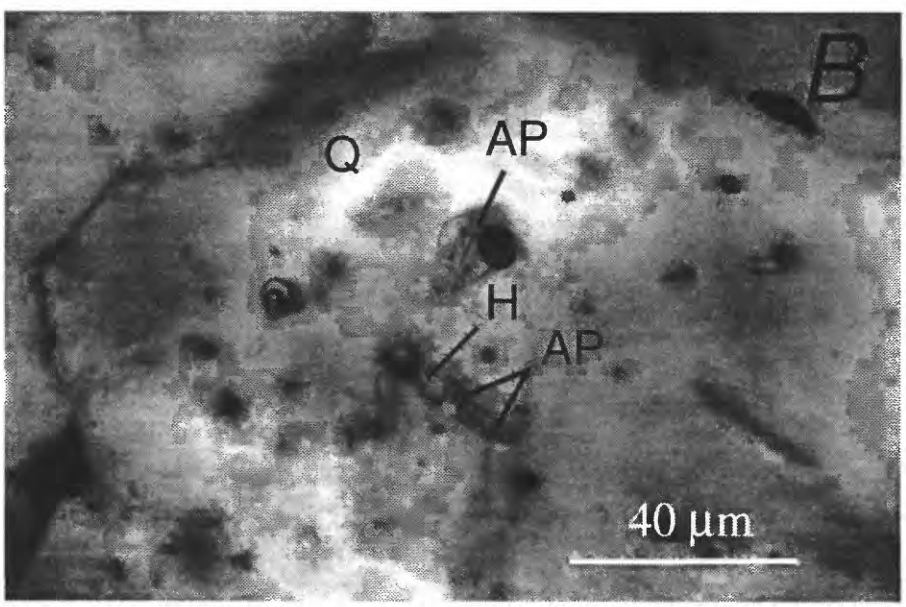

Figure 11—continued

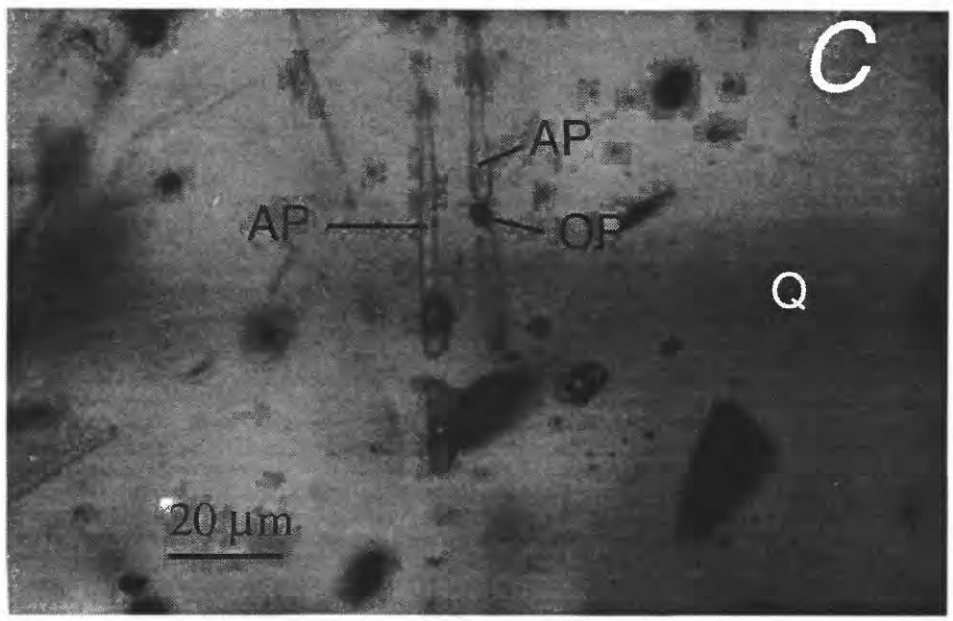

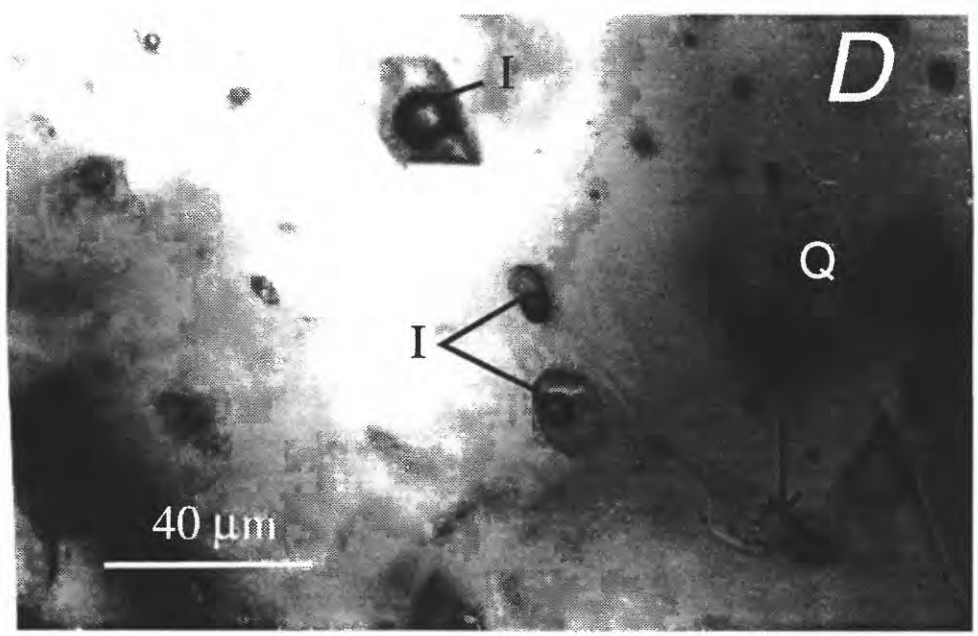

Figure 12

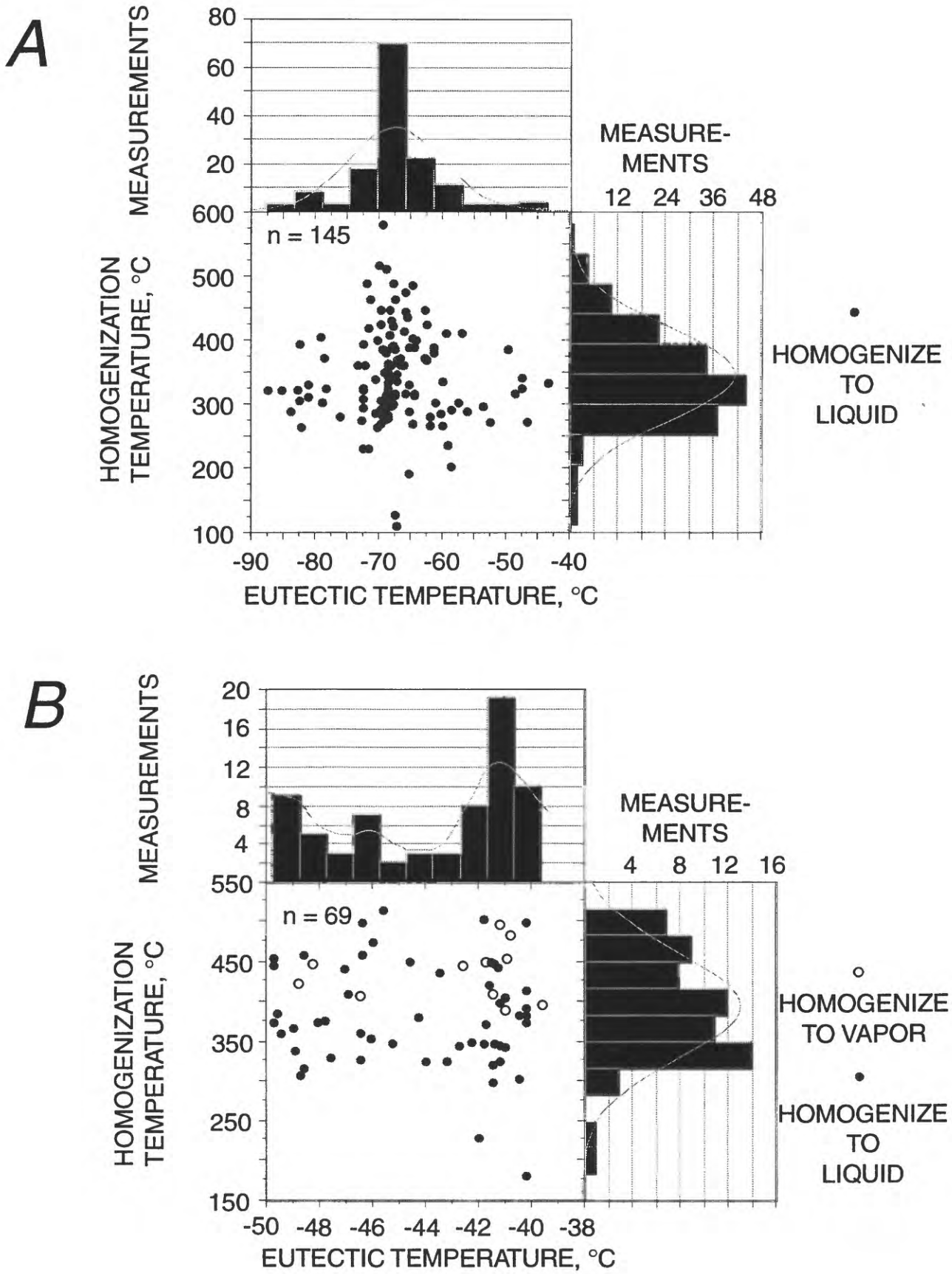
A
MEASUREMENTS
80
60
40
20
MEASURE-
MENTS
12 24 36 48
600
n = 145
500
400
300
200
100
HOMOGENIZATION
TEMPERATURE, °C
HOMOGENIZE
TO
LIQUID
-90 -80 -70 -60 -50 -40
EUTECTIC TEMPERATURE, °C
B
MEASUREMENTS
20
16
12
8
4
MEASURE-
MENTS
4 8 12 16
550
n = 69
450
350
250
150
HOMOGENIZATION
TEMPERATURE, °C
HOMOGENIZE
TO VAPOR
HOMOGENIZE
TO
LIQUID
-50 -48 -46 -44 -42 -40 -38
EUTECTIC TEMPERATURE, °C

Figure 12—continued

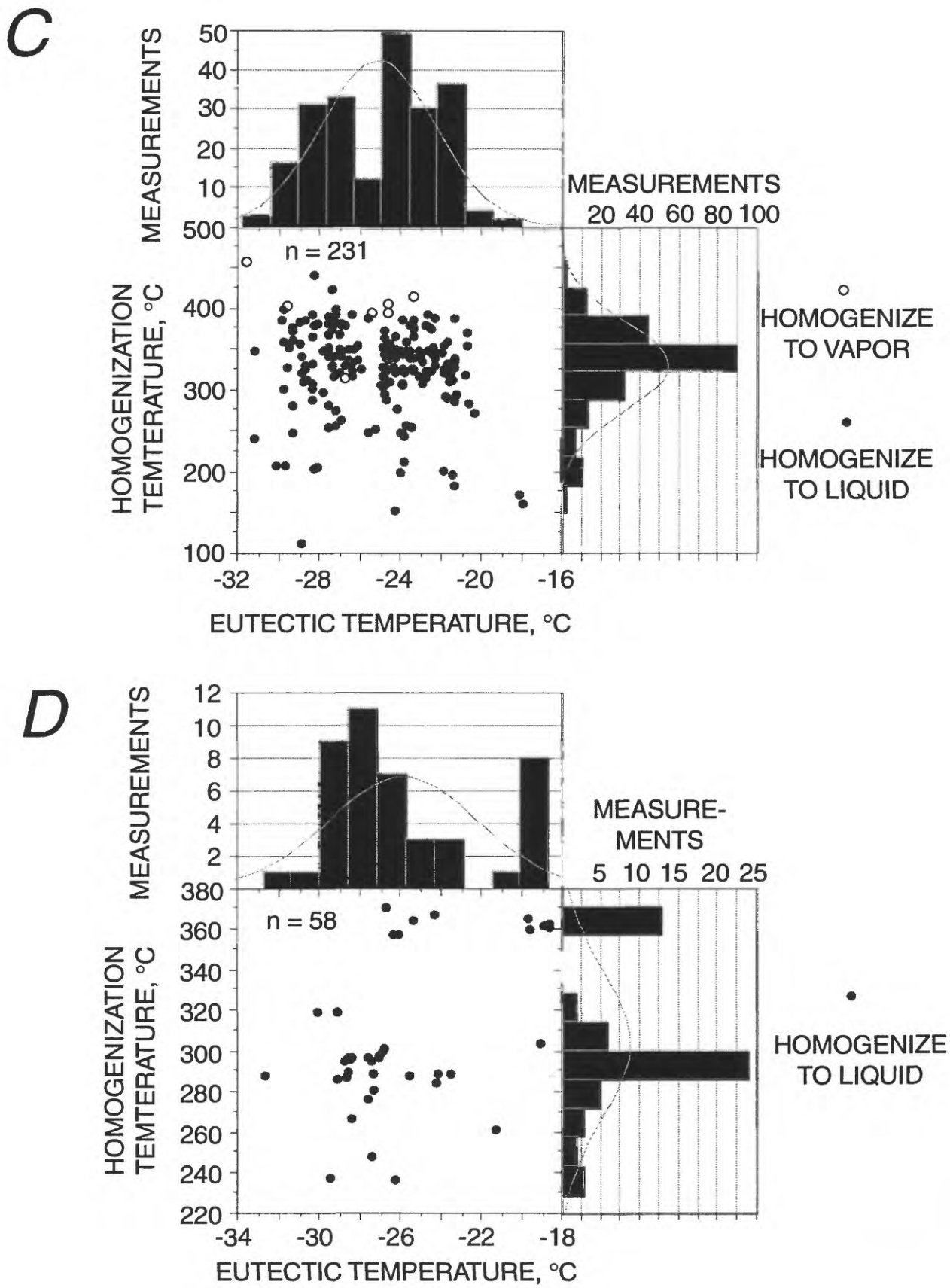

Figure 13

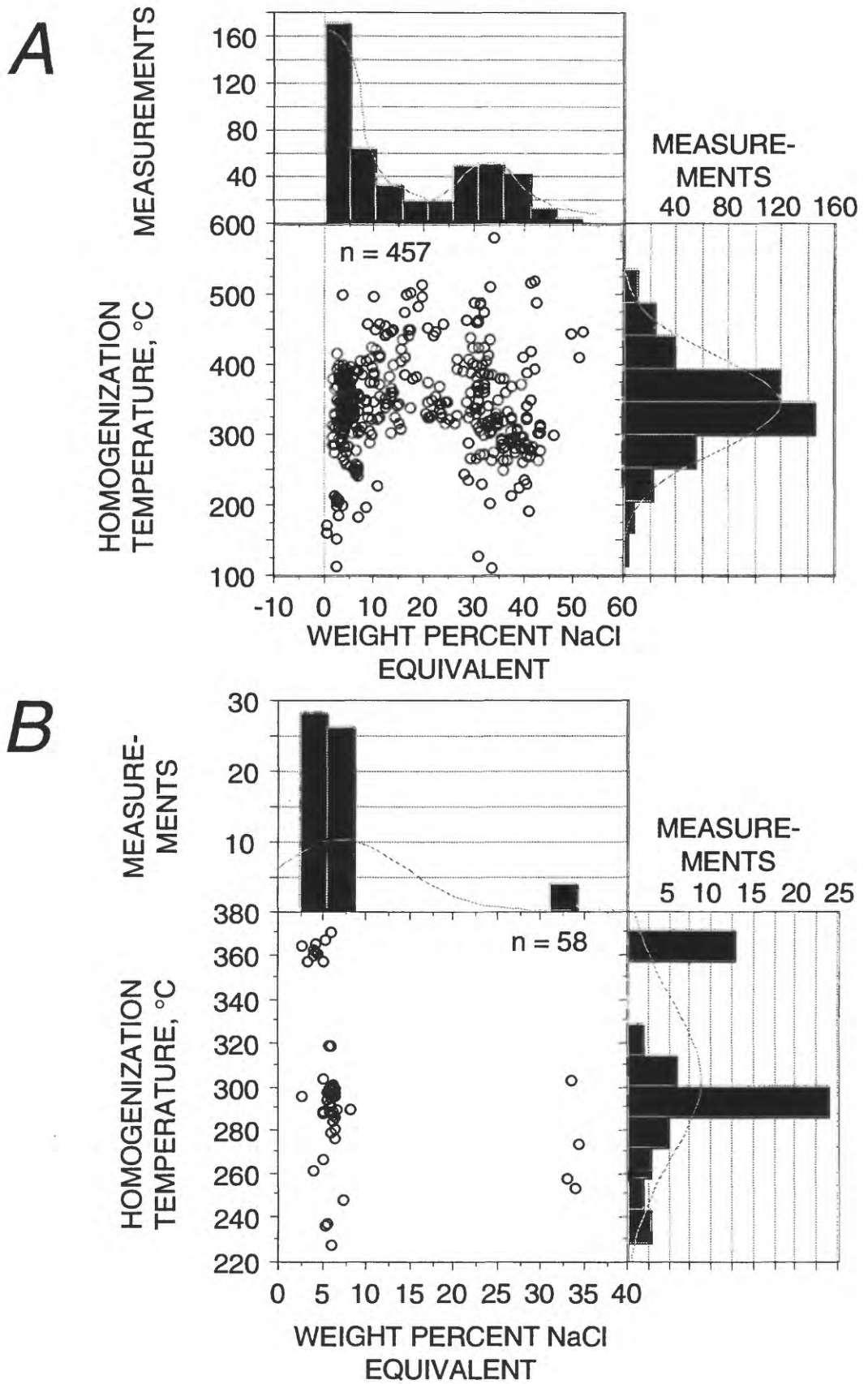
A
MEASUREMENTS
160
120
80
40
MEASURE-
MENTS
40 80 120 160
600
n = 457
500
400
300
200
100
HOMOGENIZATION
TEMPERATURE, °C
-10 0 10 20 30 40 50 60
WEIGHT PERCENT NaCl
EQUIVALENT
B
30
20
10
MEASURE-
MENTS
MEASURE-
MENTS
5 10 15 20 25
380
360
340
320
300
280
260
240
220
n = 58
HOMOGENIZATION
TEMPERATURE, °C
0 5 10 15 20 25 30 35 40
WEIGHT PERCENT NaCl
EQUIVALENT

Figure 14

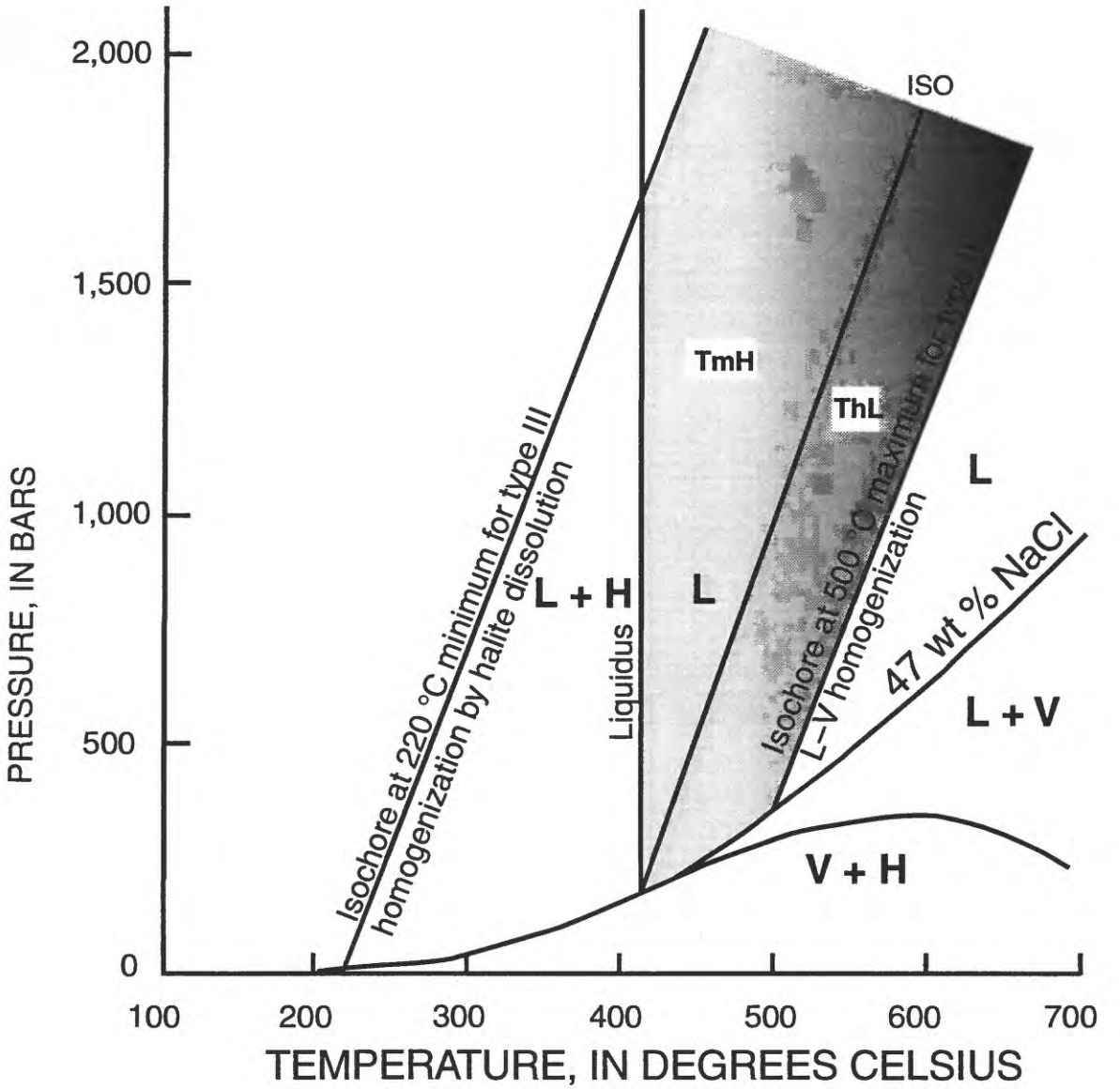
2,000
1,500
1,000
500
0
PRESSURE, IN BARS
100
200
300
400
500
600
700
TEMPERATURE, IN DEGREES CELSIUS
ISO
TmH
ThL
L
L + H
L
Liquidus
Isochore at 220 °C minimum for type III homogenization by halite dissolution
Isochore at 500 °C maximum for type II L–V homogenization
47 wt % NaCl
L + V
V + H

Figure 15

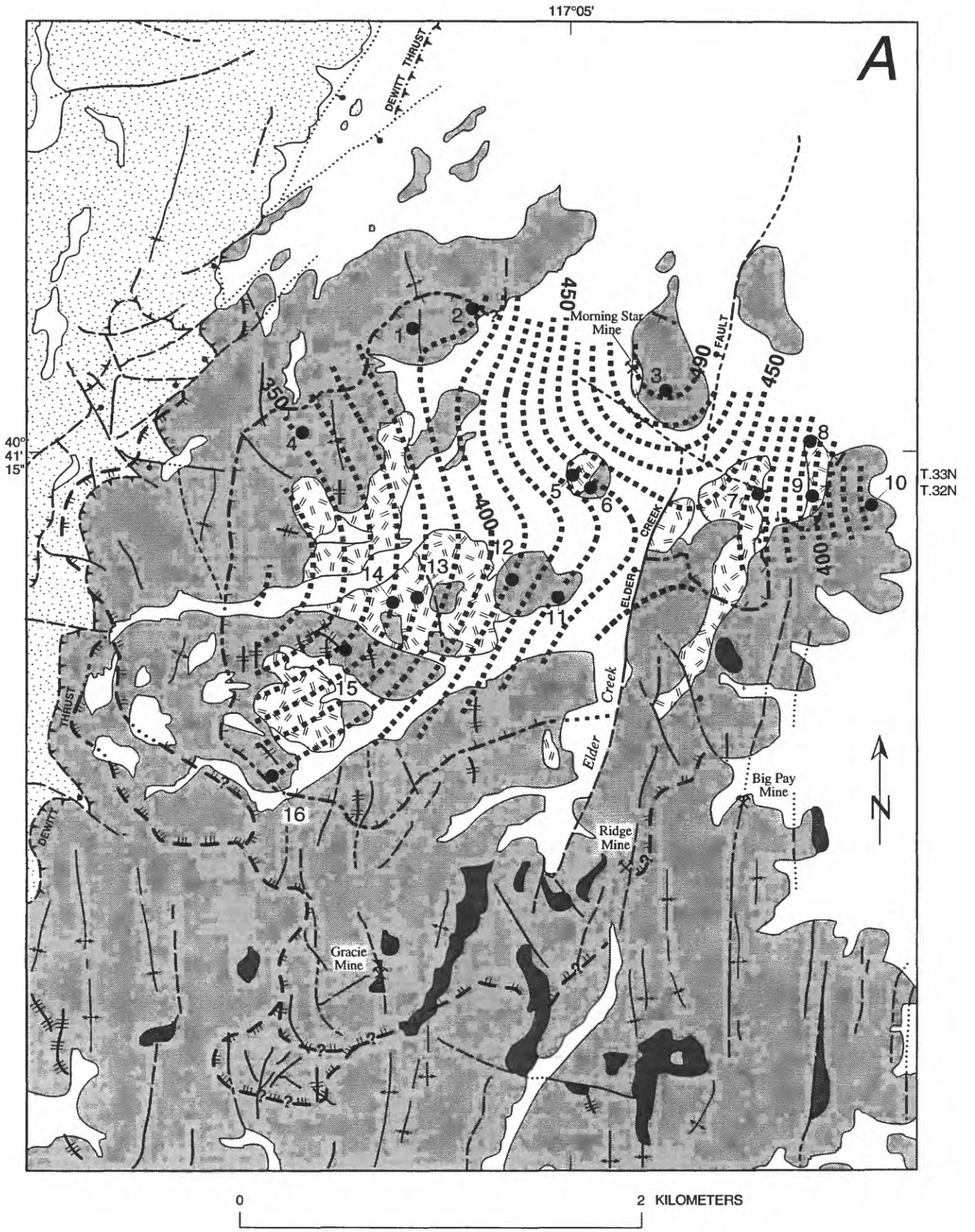
117°05'
A
DEWITT THRUST
Morning Star Mine
FAULT
450
490
450
350
400
400
400
40° 41' 15"
T.33N
T.32N
ELDER CREEK
Elder Creek
THRUST
DEWITT
Big Pay Mine
Ridge Mine
Gracie Mine
N
1
2
3
4
5
6
7
8
9
10
11
12
13
14
15
16
0
2 KILOMETERS

Figure 15—continued

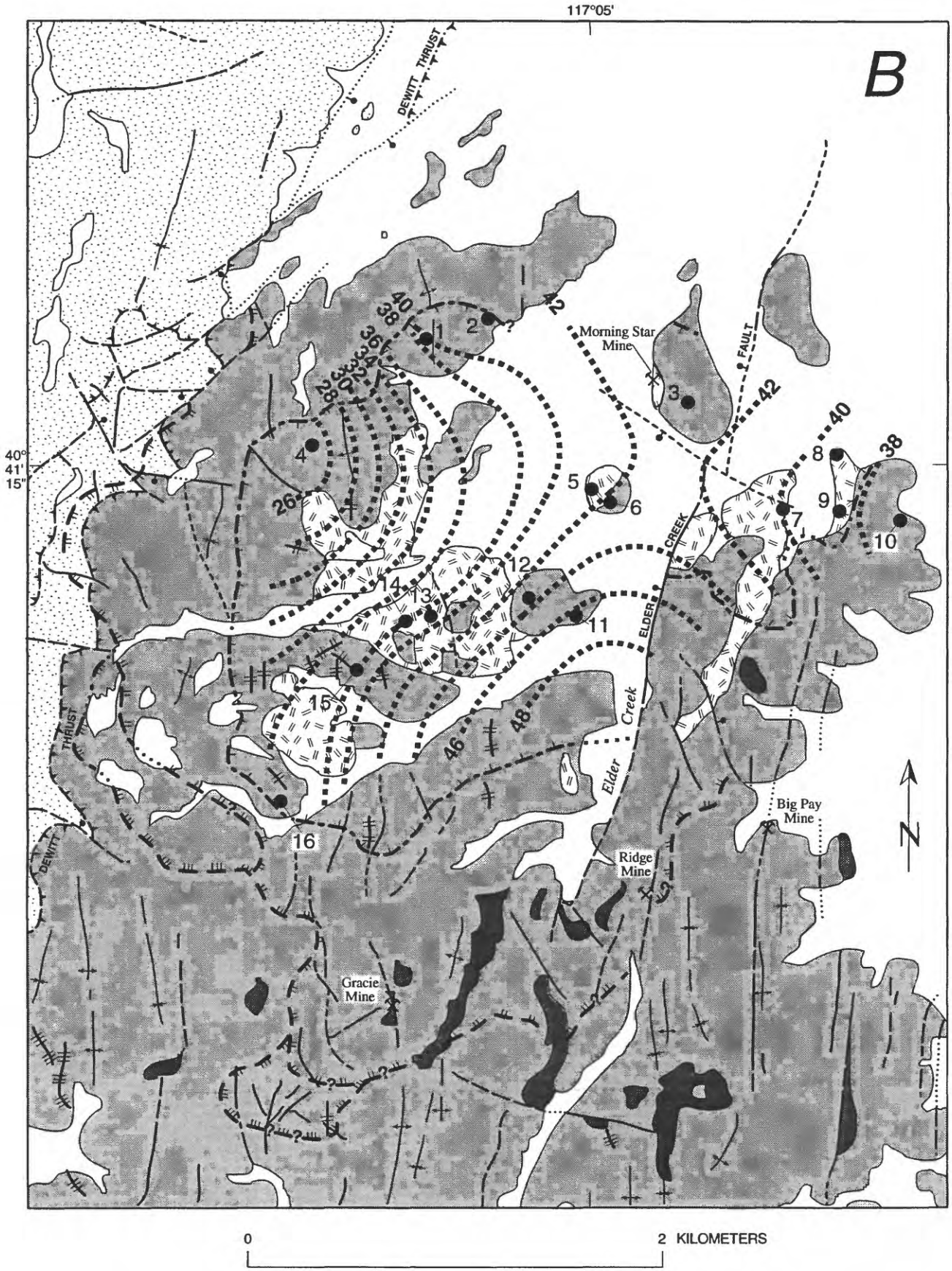

Figure 15—continued

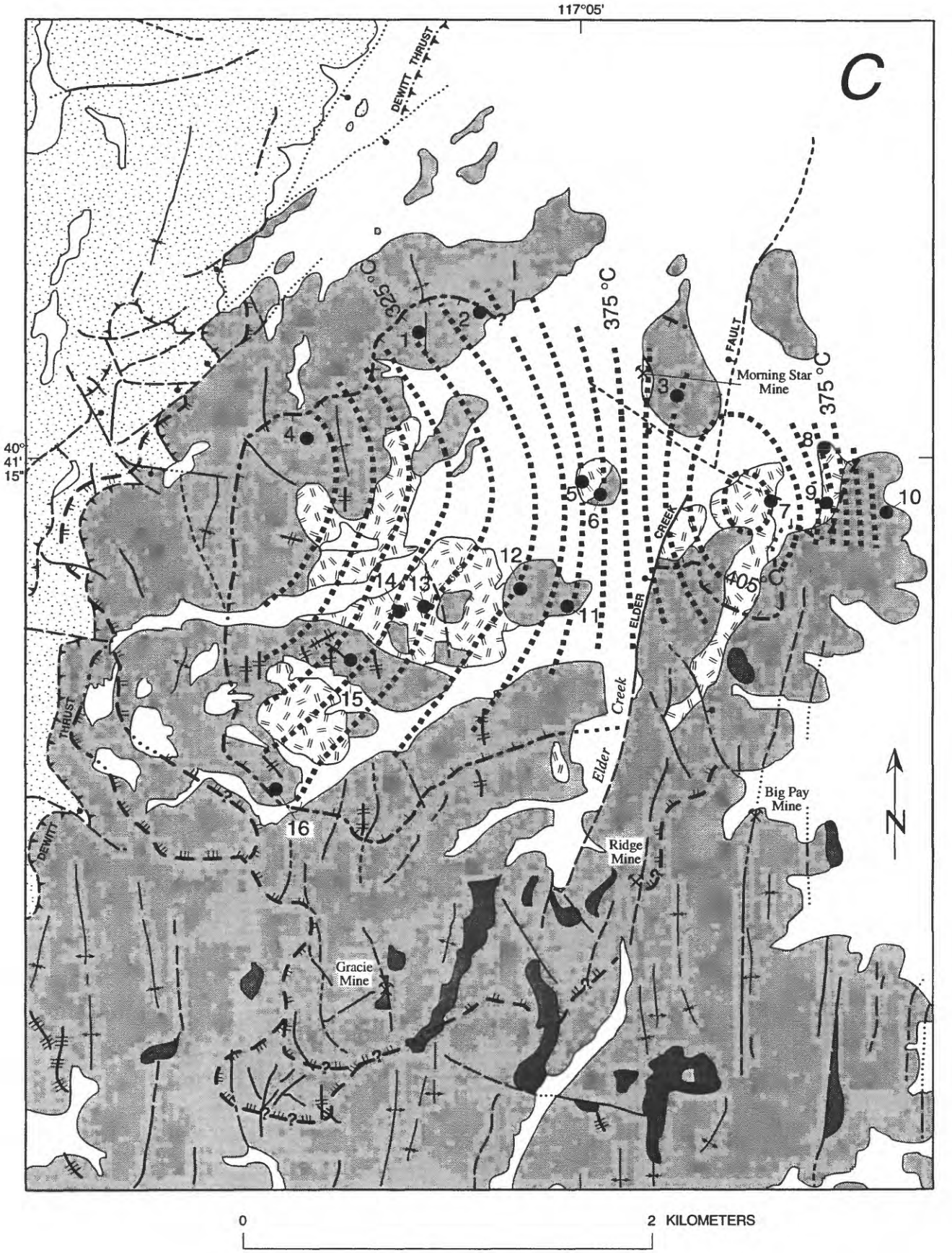

Figure 16

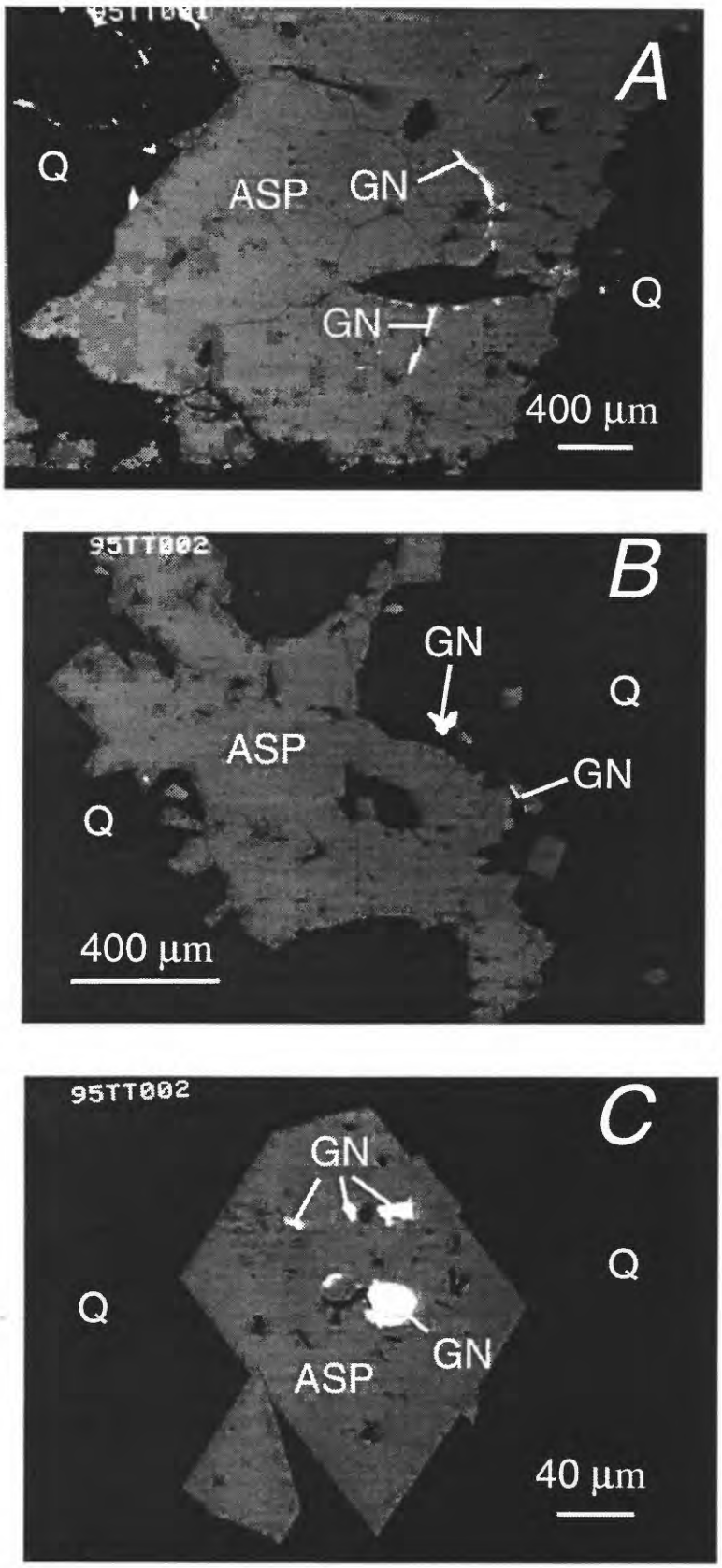
A
Q
ASP
GN
GN
Q
400 µm
95TT002
B
GN
Q
ASP
GN
Q
400 µm
95TT002
C
GN
Q
Q
GN
ASP
40 µm

Figure 17

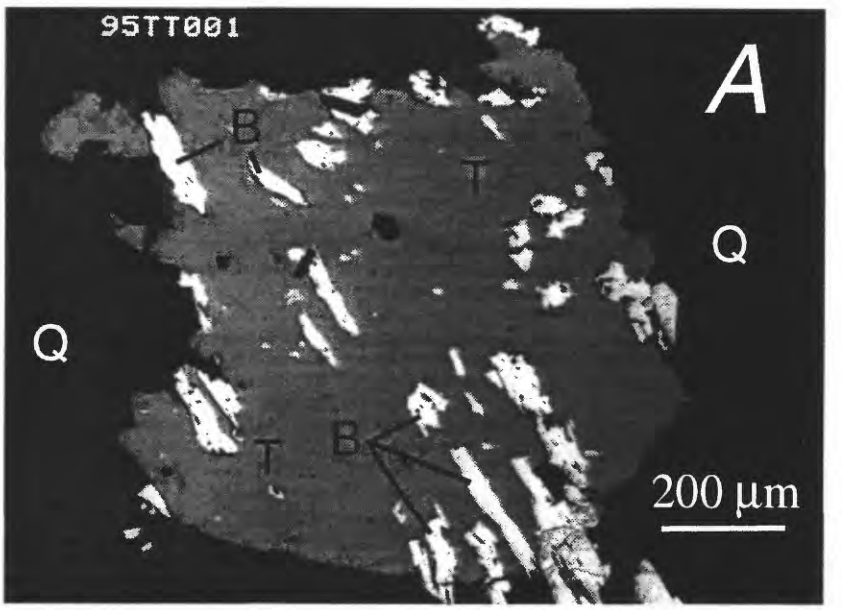

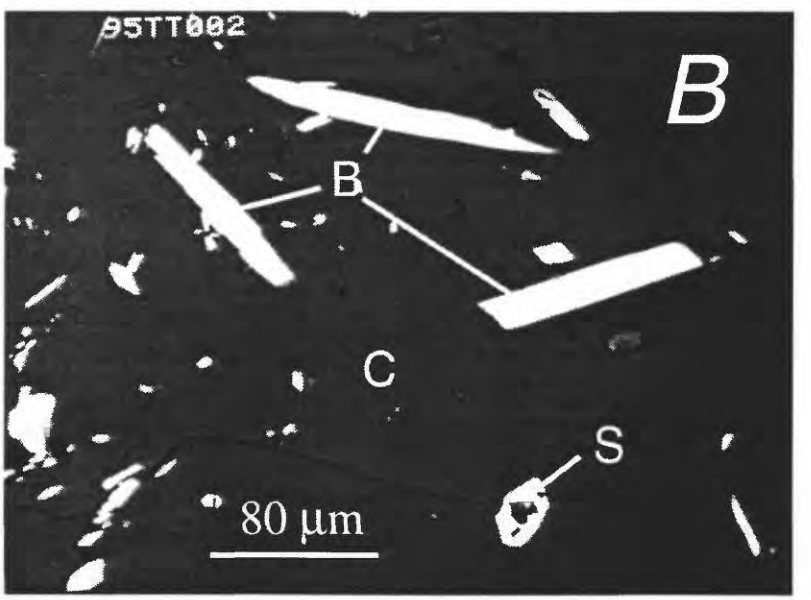

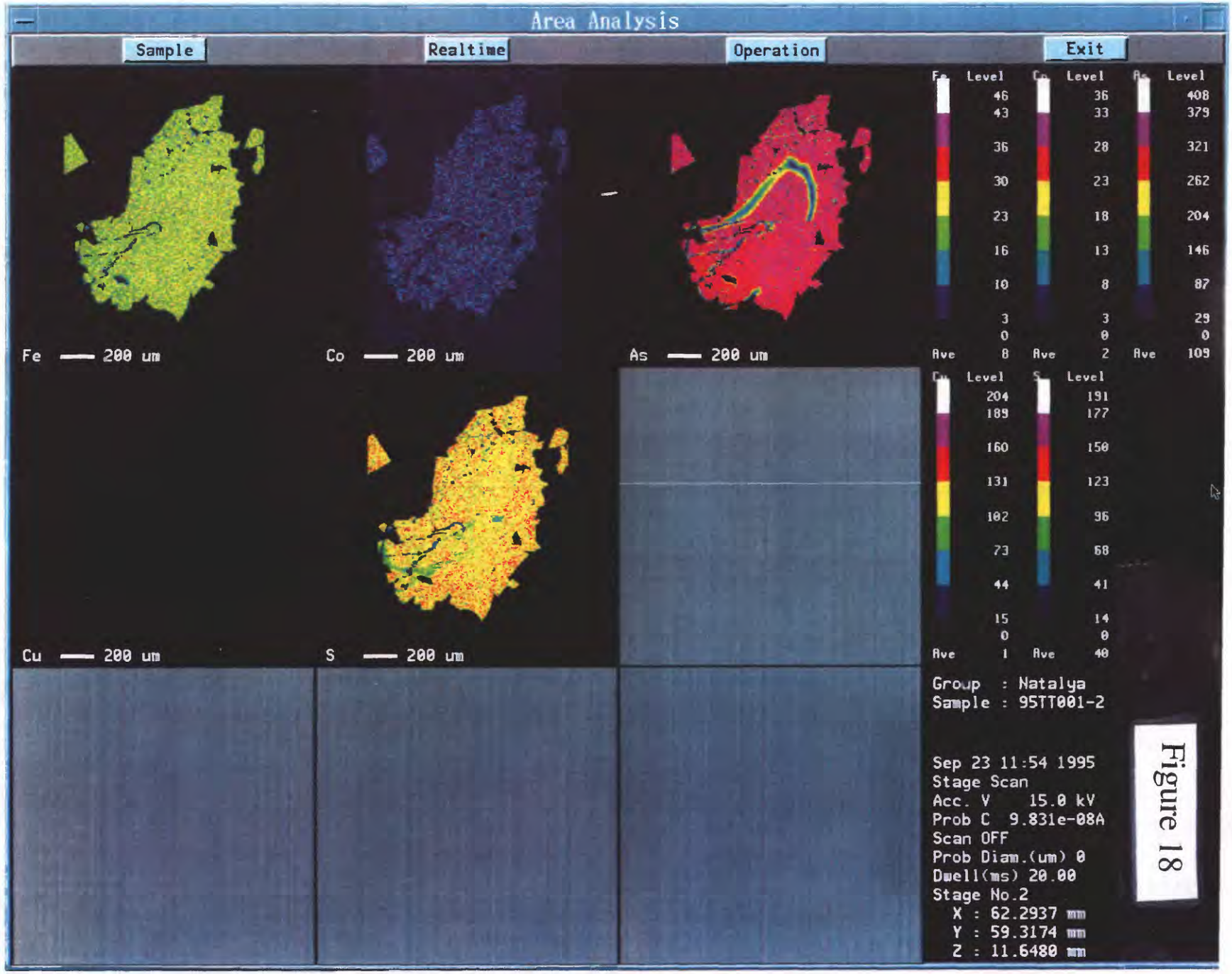
Area Analysis
Sample
Realtime
Operation
Exit
Fe Level
46
43
36
30
23
16
10
3
0
Ave 8
Co Level
36
33
28
23
18
13
8
3
0
Ave 2
As Level
408
379
321
262
204
146
87
29
0
Ave 109
Fe — 200 um
Co — 200 um
As — 200 um
Cu Level
204
189
160
131
102
73
44
15
0
Ave 1
S Level
191
177
150
123
96
68
41
14
0
Ave 40
Cu — 200 um
S — 200 um
Group : Natalya
Sample : 95TT001-2
Sep 23 11:54 1995
Stage Scan
Acc. V 15.0 kV
Prob C 9.831e-08A
Scan OFF
Prob Diam.(um) 0
Dwell(ms) 20.00
Stage No.2
X : 62.2937 mm
Y : 59.3174 mm
Z : 11.6480 mm

Figure 18

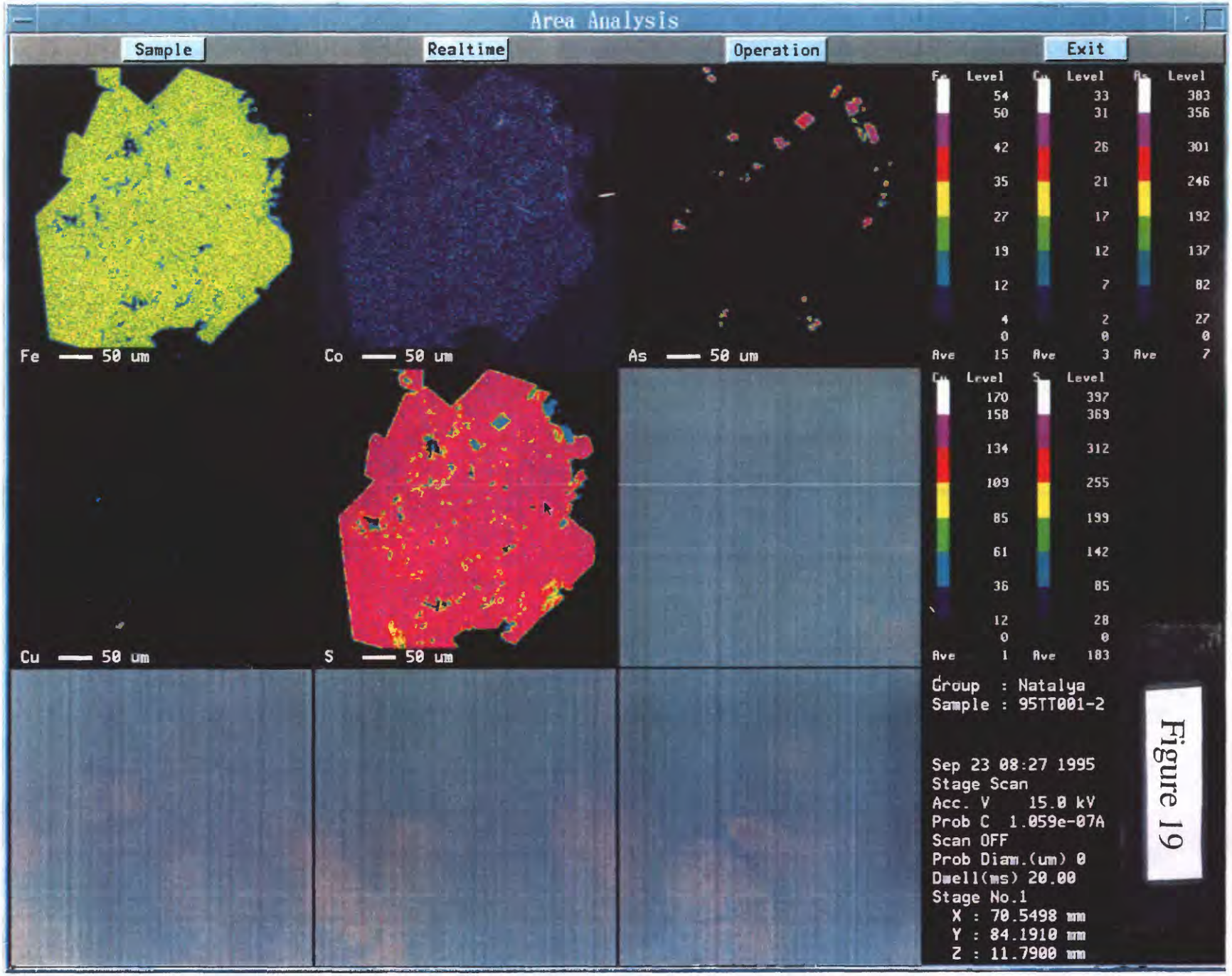
Area Analysis
Sample
Realtime
Operation
Exit
Fe — 50 um
Co — 50 um
As — 50 um
Cu — 50 um
S — 50 um
Level
54
50
42
35
27
19
12
4
0
Ave 15
Level
33
31
26
21
17
12
7
2
0
Ave 3
Level
383
356
301
246
192
137
82
27
0
Ave 7
Level
170
158
134
109
85
61
36
12
0
Ave 1
Level
397
369
312
255
199
142
85
28
0
Ave 183
Group : Natalya
Sample : 95TT001-2
Sep 23 08:27 1995
Stage Scan
Acc. V 15.0 kV
Prob C 1.059e-07A
Scan OFF
Prob Diam.(um) 0
Dwell(ms) 20.00
Stage No.1
X : 70.5498 mm
Y : 84.1910 mm
Z : 11.7900 mm

Figure 19

Figure 20